Geotechnics and hydrology of landslides in Thompson River Valley, near Ashcroft, British Columba

by

Nicholas Franklin Bishop

A thesis

presented to the University of Waterloo

in fulfillment of the

thesis requirement for the degree of

Master of Science

in

Earth Sciences

Waterloo, Ontario, Canada, 2008

Author's Declaration

I hereby declare that I am the sole author of this thesis. This is a true copy of the thesis, including any required final revisions, as accepted by my examiners. I understand that my thesis may be made electronically available to the public.

Abstract

Landslides in Pleistocene sediments along the Thompson River, south of Ashcroft, British Columbia have been known since before the Canadian Pacific (CP) railway was built through the valley in the 1880s. The Canadian National (CN) mainline railway, built in the early twentieth century, also follows the valley. Since the CP mainline was open to traffic in 1886, landslides have occurred along both sides of the Thompson valley and have resulted in derailments and traffic disruption along this strategic railway corridor.

Past work identified a critical interbedded glaciolacustrine silt and clay unit at the base of the valley fill in which the sliding planes of the landslides were located. In our geotechnical characterization of this unit we identify the clay as the main contributing factor towards the instability of slopes in the Thompson River Valley due to its low residual strength parameters. Ring shear testing of this unit indicate residual friction angles between 10^{o} and 15^{o}. The use of residual shear strength parameters is necessitated by the presence of pre-sheared surfaces in the valley fill material caused by historical landsliding and glacial overriding.

An additional contributing factor to slope instability in Thompson River Valley is the presence of artesian pore water pressures located below the failure surfaces of landslides in the valley. Previously suggested explanations for development of the elevated pore pressures include dynamic change in the Thompson River stage, and over irrigation of upslope farm lands. Groundwater models of Thompson River Valley were constructed using the advanced modeling tool HydroGeoSphere in order to determine the origin of these elevated pressures, and to explore additional influences on the regional groundwater flow system, including irrigation and river stage. Analysis of groundwater simulations showed that due to its low permeability, the

glaciolacustrine silt and clay unit is important in controlling groundwater flow patterns, and explains the development of artesian pressures in the valley bottom. Further, it was shown that fluctuation in river stage and additional infiltration due to irrigation of upslope farm lands had minimal impact on pore water pressures, and cannot explain the development of landslides in the study area.

Groundwater simulations were coupled with slope stability analyses in order to assess the slope Factor of Safety associated with certain groundwater conditions. This was achieved by using SLOPE/W and SEEP/W. Slopes were found to be unstable under natural conditions with a Factor of Safety close to unity. Significant changes to the Factor of Safety were noted for scenarios where precipitation was doubled and halved, but irrigation was again shown to have a minimal effect on the stability of Thompson Valley slopes.

Acknowledgements

I would like to thank my supervisors, Professor Steve Evans and Professor Andre Unger, for their exceptional guidance and support throughout my undergraduate and graduate careers.

Without the help of my sponsors, Canadian Pacific and Canadian National, this work would not have been possible. Funding from these companies was secured through NSERC's Industrial Postgraduate Scholarship program. Special thanks go to Chris Bunce (Canadian Pacific), who provided valuable insight and information critical to my research. I would also like to thank Professor Derek Petley (Warwick University, UK) and Professor David Petley (Durham University, UK) for their helpful ideas, and for their great hospitality. Rod Burt and Richard Link (U.S. Bureau of Reclamation) cooperatively provided data and information used in my work regarding valley fill sediments in northeast Washington.

Rob McLaren and Young-Jin Park provided outstanding technical assistance throughout the development of HydroGeoSphere models.

I am forever grateful to my family and friends who have always given me tremendous support and to Melissa for her undying encouragement in all my endeavours.

Table of Contents

List of Figures ix

List of Tables xi

Chapter 1 - Introduction 1

1.1 Overview 1

1.2 Objectives 4

Chapter 2 - Geotechnical characterization of glaciolacustrine materials in Pleistocene valley fills .. 11

2.1 Introduction 11

2.2 Geology of Pleistocene valley fill deposits 12

2.2.1 Valley fill architecture 12

2.2.2 Nature of interbedding in glaciolacustrine deposits 14

2.2.3 Role of glaciolacustrine deposits contributing to slope instability 15

2.3 Geotechnical properties 16

2.3.1 Overview 16

2.3.2 Grain size 17

2.3.3 Index properties 18

2.3.4 Residual strength 19

2.4 Summary and conclusions 20

Chapter 3 - Effects of regional groundwater flow systems 30

3.1 Problem setting 30

3.1.1 Historical landslides 30

3.1.2 Water use 32

3.1.3 Land use 32

3.1.4 Bedrock geology 33

3.1.5 Structural geology and physiography 34

3.1.6 Surficial geology 34

3.2 Groundwater data sources 35
3.2.1 Boreholes 35
3.2.2 Hydraulic data 37
3.2.3 Precipitation and infiltration 39
3.2.4 Irrigation 41
3.2.5 Thompson River data 43
3.3 Groundwater models 43
3.3.1 Reasons for modeling 43
3.3.2 Notes on HydroGeoSphere 45
3.4 Generalized cross-section hydrogeological model 46
3.4.1 Overview 46
3.4.2 Hydrogeological parameter selection 47
3.4.3 Boundary conditions for steady state (base case) analysis 47
3.4.4 Boundary conditions for transient analysis 48
3.5 South Slide (regional scale) hydrogeological model 49
3.5.1 Reasons for selection 49
3.5.2 Cross-section 49
3.5.3 Hydrogeological parameter selection 50
3.5.4 Boundary conditions 51
3.6 Results 52
3.6.1 Overview 52
3.6.2 Generalized cross-section, steady state simulations 52
3.6.3 Generalized cross-section, transient simulation 54
3.6.4 Generalized flow system cross-section, sensitivity analysis 56
3.6.5 South Slide model, steady-state simulations 60
3.6.6 South Slide model sensitivity analysis 61

3.7 Discussion and conclusions 64

Chapter 4 - Slope stability analysis 85

4.1 Introduction 85

4.2 Stability analysis setup 86

4.2.1 Notes on SEEP/W and SLOPE/W 86

4.2.2 Cross-sections 86

4.2.3 Geotechnical material properties 88

4.2.5 Other considerations 90

4.3 Results 91

4.3.1 Overview 91

4.3.2 SLOPE/W results 92

4.4 Discussion and conclusions 94

Chapter 5 - Summary and discussion 99

References 102

Appendices 108

List of Figures

Figure 1 - 1. Map showing landslide locations 7

Figure 1 - 2. Topographic cross-section of Thompson River Valley at 1:1 scale 8

Figure 1 - 3. Photograph showing destruction of CP rail lines caused by the movement of the 1982 Goddard landslide. 9

Figure 1 - 4. Photograph looking northwest above the present-day South Slide 10

Figure 2 - 1. Sequence of valley fill deposits near Ashcroft, BC. 22

Figure 2 - 2. Stratigraphic cross-section of the Columbia River at the Grand Coulee Dam site 23

Figure 2 - 3. Photographs of undisturbed interbedded silt and clay (above), and disturbed silt and clay (below), Thompson River Valley, near Ashcroft, British Columbia 24

Figure 2 - 4. Grain size distribution envelopes for Ashcroft silt (red) and clay (blue) 25

Figure 2 - 5. Plasticity chart for Ashcroft and Grand Coulee silt and clay. 26

Figure 2 - 6. Typical failure envelope for glaciolacustrine clay interbed (sample 18-AU-2B). 27

Figure 2 - 7. Relation between residual friction angle and plasticity index 28

Figure 2 - 8. Relation between residual friction angle and liquid limit. 29

Figure 3 - 1. Photograph taken from atop the North Slide (shown in Figure 1-1). 68

Figure 3 - 2. Aerial photograph showing physical setting of landslides and irrigated fields.. 69

Figure 3 - 3. Average monthly precipitation and Thompson River flow compared to 2005 values. 70

Figure 3 - 4. Generalized cross-section of Thompson River Valley 71

Figure 3 - 5. Annual variation in river level, infiltration, and irrigation used in the transient simulation. 72

Figure 3 - 6. Geological cross-section of South Slide 73

Figure 3 - 7. Steady state saturation distribution of the generalized cross-section neglecting irrigation... 74

Figure 3 - 8. Steady state saturation distribution of the generalized cross-section neglecting irrigation... 75

Figure 3 - 9. Seepage face in Thompson valley, June, 2007 76

Figure 3 - 10. Pressure head distribuation of the slope scale generalized cross-section 77

Figure 3 - 11. Saturation profiles of the generalized cross-section for various precipitation and irrigation scenarios 78

Figure 3 - 12. Progression of pressure head differences between the transient simulation and the base case along a slice taken adjacent Thompson River throughout a one year simulation.. 79

Figure 3 - 13. Steady state saturation distribution of the South Slide cross-section neglecting irrigation. 80

Figure 3 - 14. Steady state saturation distribution of the South Slide cross-section including irrigation .. 81

Figure 3 - 15. Steady state pressure head conditions at South Slide for the case neglecting irrigation. 82

Figure 3 - 16. Saturation distribution for South Slide sensitivity scenarios..... 83

Figure 3 - 17. Slope-scale groundwater flow paths..... 84

Figure 4 - 1. Generalized (Ryder, 1976) cross-section used in slope stability analysis.....96

Figure 4 - 2. South slide cross-section as used in the slope stability analysis. 97

Figure 4 - 3. Pore pressures along the generalized (above) and South Slide (below) cross-section failure surfaces for all scenarios. 98

List of Tables

Table 1 - 1. Known landslides in Thompson River Valley. 2

Table 3 - 1. Hydraulic Conductivity Estimates From Slug Test Data 38

Table 3 - 2. Hydrogeological properties of valley fill materials 39

Table 3 - 3. Environment Canada Climate Stations in the Ashcroft Area 40

Table 3 - 4. Watering Schedule for Hayfield. 41

Table 3 - 5. South Slide hydraulic parameters. 51

Table 3 - 6. Infiltration scenarios for generalized cross-section. 57

Table 3 - 7. Normalized model sensitivity to precipitation and irrigation. 60

Table 3 - 8. Infiltration scenarios for South Slide. 62

Table 3 - 9. Results of pressure head sensitivity analysis. 63

Table 4 - 1. Slope stability analysis parameters for various units 90

Table 4 - 2. Factors of safety and relative percent changes from SLOPE/W analysis for generalized cross-section for all scenarios. 94

Table 4 - 3. Factors of safety and relative percent changes from SLOPE/W analysis for South Slide cross-section for all scenarios. 94

List of Appendices

Appendix A: Summary of geotechnical analysis of Ashcroft silt and clay. 108

Appendix B: Pressures calculated based on drill records of water supply wells near Ashcroft 113

Appendix C: Formulation of HydroGeoSphere 114

Chapter 1

Introduction

1.1 Overview

As many as thirteen major landslides have occurred in Thompson River Valley, immediately south of Ashcroft, British Columbia from the time the area was settled in the 1880's (Figure 1 - 1, Table 1 - 1) (Stanton, 1898; Evans, 1984; Porter et al, 2002; Clague and Evans, 2003; Eshraghian et al, 2006). The landslides occur within thick Quaternary valley fill deposits along a 10 km reach of the Thompson River. An important transportation corridor occupied by Canadian Pacific (CP) and Canadian National (CN) rail lines traverses the valley bottom (shown in cross-section A-A' in Figure 1 - 2). These rail lines are vital to the North American shipping network, as they provide a strategic connection between the Canadian west coast and points further east. In many places the rail lines rest directly on top of mobile slides where gradual, continuous slope movements and occasional catastrophic failures are impacting their alignment resulting in the need for continuous and expensive track repairs (Eshraghian et al., 2008).

The main cause of the landslides has been debated for some time. One contributing factor that has been identified relates to elevated pore pressures along failure surfaces within the valley side slopes (Porter et al, 2002). Over-irrigation of upslope farmlands was originally suggested as the explanation for elevated pore pressures by Robert Stanton (1898), and was later cited as the cause of a major landslide in 1982 by CP during a court hearing (Wallace, 1987). After suing the owner of the upslope farmland for damages that were incurred during the seven days their track was out of service (Figure 1 - 3), CP failed to prove that water had infiltrated in sufficient quantities to trigger the landslide and the court case was closed (Wallace, 1987).

Table 1 - 1. Known landslides in Thompson River Valley, south of Ashcroft, BC.

Number[1]	Landslide Name	Date(s)	Description	Approximate Volume (m^3)
1	Basque Slide	Up to several thousand YBP	Translational	1.8×10^6
2	Ripley Slide	Up to several thousand YBP	Slow moving translational	15×10^3 (active region)
3	Nepa Slide	Between 1877 and 1898; Feb. 1977; Fall 1997	Rapid flowslide	No data
4	Barnard Slide	Up to several thousand YBP; Between 1877 and 1895	Most likely rapid flowslide (joins Nepa)	No data
5	Red Hill (1921) Slide	Aug. 1921	Rapid flowslide	No data
6	South Slide	Between 1865 and 1877; Winter 1977; Fall 1997	Translational and rotational	3.2×10^6
7	North (1880) Slide	Oct. 1880; Oct. 2000	Rapid flowslide	15×10^6
8	Ashcroft (CN 53.4) Slide	Possibly 1880	No data	No data
9	Goddard Slide	Oct. 1886; Oct. 1976; Sept. 1982	Rapid flowslide	3×10^6 (1982)
10	Unnamed	No data	No data	No data
11	CN51 Slide	1897; Fall 1972; Winter 1977; Fall 2000	Translational and rotational	3.4×10^6 (active region)
12	1897 Slide	Sept. 1897	Translational and rotational	No data
13	Spence's Bridge (not shown in figure 1-1)	Aug. 1880 Dec. 1899 Aug. 1905	Rapid flowslide	No data

Data sources: Evans (1984); Porter et al. (2002); Clague and Evans (2003); BGC Engineering (2007); Eshraghian (2007).

[1]Number refers to location in Figure 1-1.

Regional groundwater flow dynamics may also explain the elevated pore pressures, but insufficient data exists to draw any conclusion. Computer simulations of regional groundwater flow fields in mountainous areas were produced by Hodge and Freeze (1977), which showed that the regional groundwater flow system can be critical to the stability of terraced sediments, such as those found in Thompson River Valley. Further, they demonstrated that elevated pore pressures can occur where sharp contrast in hydraulic conductivity exists between adjacent stratigraphic units.

A weak unit consisting of glaciolacustrine interbedded silt and clay located at the base of the valley fill sequence has been shown to be a contributing factor towards the instability of slopes in Thompson River Valley (Porter et al., 2002; Clague and Evans, 2003). The clay component is highly plastic, and exhibits very low residual strength properties. This unit may contribute to elevated pore water pressures as it is much less permeable than other sediments in Thompson River Valley (Eshraghian et al., 2006).

Eshraghian et al. (2005) suggest that fluctuation in the stage of Thompson River is the main trigger for landslides in Thompson River Valley. When the river level is sustained at a seasonal high stage, pore pressure is thought to increase along the river-proximal portion of the failure surface. Elevated pore pressures remain in the subsurface material following a drop in river levels, leading to unstable conditions (Eshraghian et al., 2005).

It is our hypothesis that the regional groundwater flow system is contributing to artesian pressures within low permeability sediments. This combined with the very low strengths of these materials explains the extent of landsliding in Thompson River Valley. The role of the regional groundwater flow system has not yet been evaluated as a factor controlling slope

stability. Further, the extent to which irrigation and fluctuation in Thompson River level contribute to slope instability have not yet been quantified as a part of the regional groundwater flow system.

1.2 Objectives

The first objective of this work is to establish the geotechnical properties of the key units in the geological succession. This will be accomplished through extensive testing of materials. Characteristic grain size, index properties, and residual strength parameters will be established. The importance of residual strength will be evaluated.

The second objective of this work is to establish the groundwater flow regimes in Thompson River Valley. This will be accomplished using HydroGeoSphere, a fully coupled surface-subsurface water model capable of simulating three-dimensional, variably saturated flow and transport problems (Therrien et al., 2005). The fully-coupled surface-subsurface groundwater model will account for the effects of seepage faces, which are known to occur in the valley. A balance of probabilities approach will be used to simulate the model boundary conditions, as limited field information is available.

The valley's flow dynamics will be simulated at two scales using two cross-sections. The first cross-section (the generalized cross-section) is a non-specific interpretation of the topographic and geological composition of the valley and was selected to explore the behavior of groundwater flow dynamics in the general sense. The second cross-section (the South Slide cross-section, B-B'-B'', shown in Figure 1-1), is over 10 km in length and passes through the South Slide in its lower reaches (Figure 1 - 4). Although this cross-section is more encompassing

than the generalized cross-section, it was selected to capture the specific behavior of regional groundwater flow within Thompson River Valley as it is based on specific topography and geology.

The groundwater flow system at the two scales cross-sections will be explored under a variety of conditions. First, the cross-sectional models will be run to a steady state condition to establish the base-case groundwater setting. Second, transient analyses will help gauge the response of the groundwater flow regime to variability in input parameters such as river level and irrigation. Third, a sensitivity analysis will be performed to determine the relative sensitivity of each input parameter and to account for data uncertainty and climatic uncertainty.

Through this process we will establish our third and fourth objectives: (3) to determine the degree to which irrigation of upslope benchlands may increase pore pressures in the lower units of the valley fill, and (4) to evaluate the effects of variation in river level on the pore pressure distribution in those sediments proximal to Thompson River.

The fifth and final objective of this work is to explore the role of groundwater flow systems on slope stability. This will be accomplished by combining results from all previous objectives described above. Specifically, by coupling the groundwater flow models with slope stability analyses we will assess the effects of various groundwater conditions on slope stability.

A major contribution of this work is the increased understanding of regional groundwater flow dynamics in Thompson River Valley, which have not been previously studied in detail. Furthermore, this work establishes the extent to which the occurrence and movement of the landslides are controlled by antropogenic influences (irrigation), and seasonal variability in the Thompson River stage. Through analysis of laboratory data this work contributes to the

understanding of the geotechnical behaviour of Quaternary valley fill sediments. To our knowledge this work represents the first time where a fully coupled surface-subsurface groundwater model (HydroGeoSphere) was used to assess the impact of groundwater flow systems on slope stability.

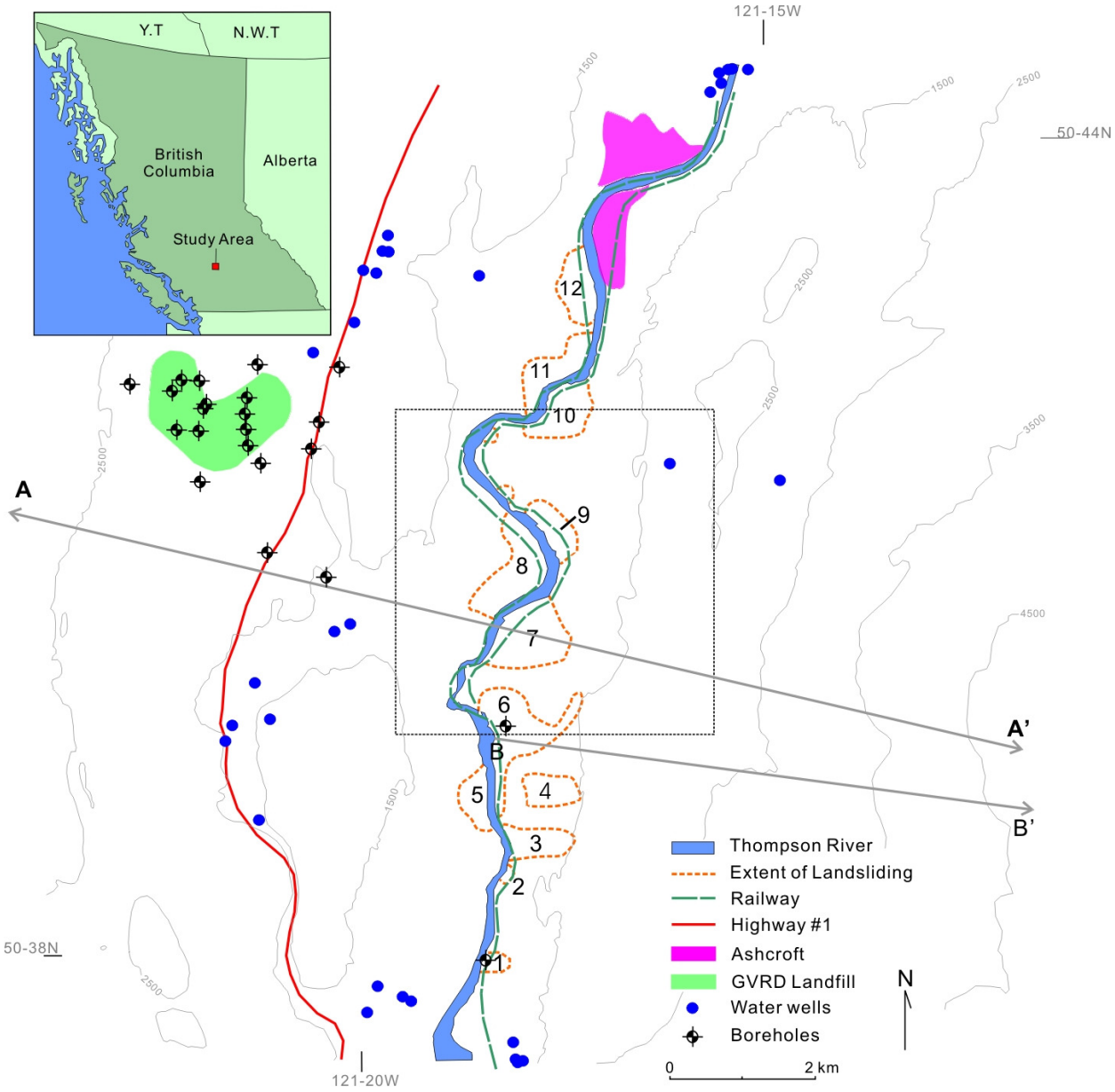

Figure 1 - 1. Map showing landslide locations, boreholes, water wells, Greater Vancouver Regional District (GVRD) landfill, railways, highways, and the town of Ashcroft. Contours are given in feet above sea level. Landslide names associated with the numerical labels are provided in Table 1-1. Cross-section A-A' is shown in Figure 1-2. Cross-section B-B' is given in a subsequent chapter. The dashed box shows the boundary of Figure 3 - 2.

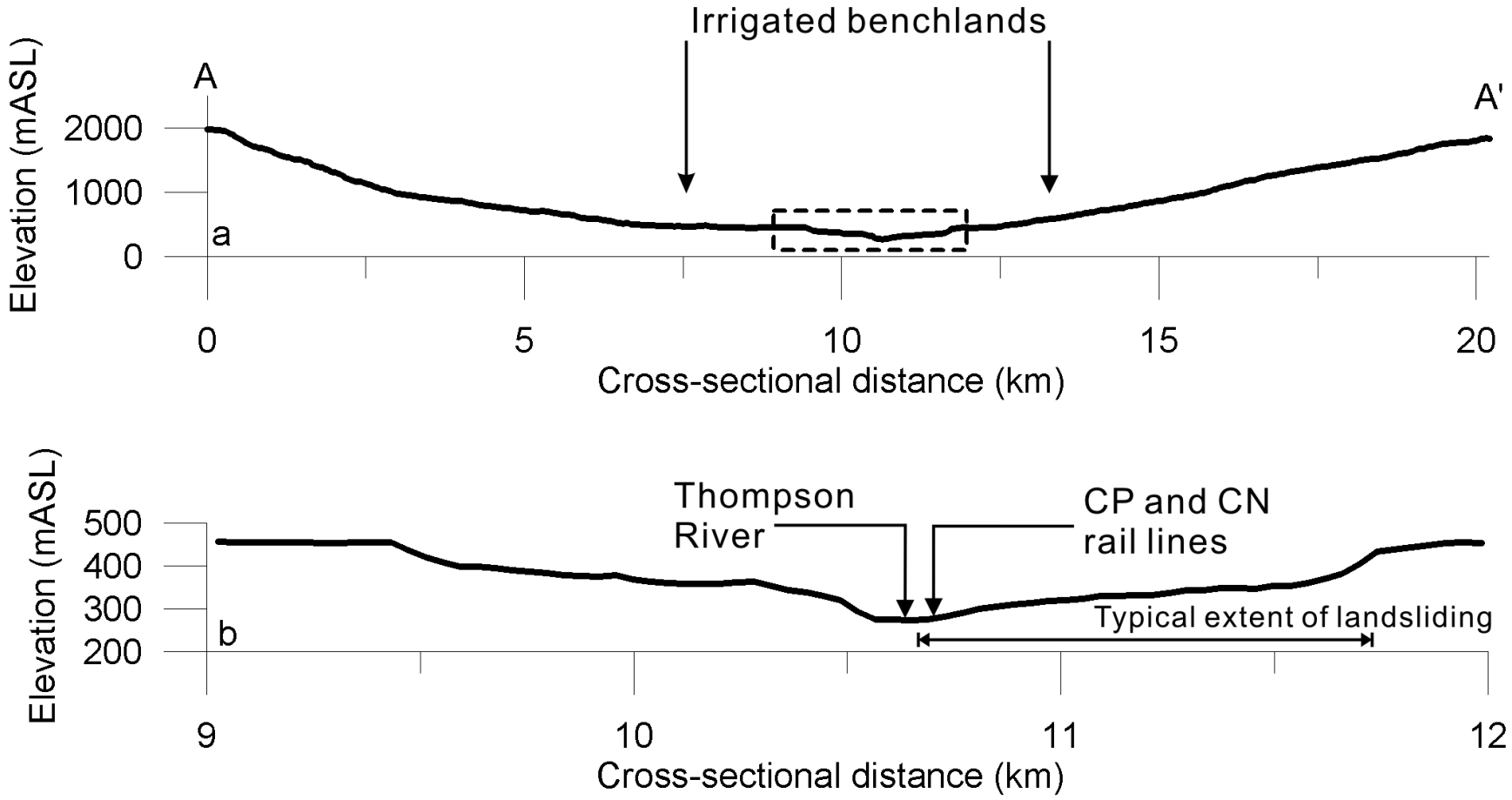

Figure 1 - 2. a) Topographic cross-section of Thompson River Valley at 1:1 scale showing the location of irrigated benches and local peaks, shown at A and A'. Dashed inset box gives location of b): detailed cross-section showing slopes directly adjacent to Thompson River, CP and CN rail lines, and extent of landsliding.

Figure 1 - 3. Photograph showing destruction of CP rail lines caused by the movement of the 1982 Goddard landslide. Top: deformation in the rail along the eastern edge of the landslide. Bottom: severance of the rail line caused by differential landslide movement. Photos used with permission from Chris Bunce, CP.

Figure 1 - 4. Photograph looking northwest above the present-day South Slide. Dashed lines show the approximate extent of the landslide debris. Movement is towards the river (to the left).

Chapter 2

Geotechnical characterization of glaciolacustrine materials in Pleistocene valley fills

2.1 Introduction

Pleistocene valley fills containing glaciolacustrine sediments are commonly found throughout western Canada and the northwestern United States (Flint and Irwin, 1939; Milligan *et al.*, 1962; Evans, 1982; George, 1986). Landsliding and other stability issues are commonly associated with sequences of valley fill deposits and have been continuously problematic since the advent of settlement and the beginnings of infrastructural development in these areas (Stanton, 1898; Flint and Irwin, 1939; Evans, 1982). Given the ever increasing rate of development of the urban landscape and infrastructure in western North America the risk associated with potentially hazardous valley fill deposits is high and increasing. It is therefore important to establish an understanding of the geotechnical behaviour of these materials.

The fills contain multiple glaciolacustrine units separated by glacial tills and outwash gravels reflecting multiple episodes of glacial lake formation, glaciation onset and glacial retreat (Clague and Evans, 2003; Johnsen and Brennand, 2004). Rhythmically bedded silt and highly plastic clay units are an important feature of the glaciolacustrine deposits, which contribute to the instability of the stratigraphical unit. This is especially the case where glacial overriding and landsliding during the formation of the deposits has created pre-sheared surfaces which may effectively reduce the strength of these materials to residual values (Clague and Evans, 2003).

This study reviews the results of geotechnical tests from southern British Columbia and northern Washington glaciolacustrine valley fill deposits. The behaviour of these sediments is examined with an emphasis on the relationship between geology, geotechnical index properties, and residual strength parameters.

2.2 Geology of Pleistocene valley fill deposits

2.2.1 Valley fill architecture

The majority of Quaternary deposition in the non-coastal regions of the western Cordillera occurred within valleys and lowlands during the time when they formed part of proglacial and ice-contact environments (Clague, 1991). Sedimentation in these areas occurred rapidly during brief glacial periods. During interglacial periods sedimentation was restricted, leading to the formation of unconformities in the Quaternary record (Clague, 1991). These factors in addition the incision of valley fill materials by river action has contributed to the development of complex sequences of distinct geological units in valley fills.

The valley fill deposits found in the areas of Thompson River Valley, Ashcroft, British Columbia and Grand Coulee, Columbia River valley, Washington are strikingly similar in terms of their geological setting (Flint and Irwin, 1939; Milligan *et al.*, 1962; Evans, 1982; George, 1986). The Ashcroft deposits, which are composed of eight distinct geological units, were formed as the result of three glacial episodes separated by interglacial melt periods, indicated by unconformities noted in the geological record (Figure 2 - 1) (Fulton, 1975; Clague, 1991; Clague and Evans, 2003).

The lowermost part of the sequence (Figure 2 - 1), formed during the advance and retreat of an older glacial episode, consists of Early Pleistocene glacial till (unit 1) overlain by interbedded glaciolacustrine silt and clay (unit 2). The central geological unit of the sequence (Figure 2 - 1) was formed during the advance and retreat of a second (penultimate) glacial episode that occurred approximately 40,000 years before present (Fulton, 1975; Bradley, 1999). Included here is sand and gravel till overlain by silt and clay (unit 3), and other sediments from the previous interglacial period (Fulton, 1975).

The uppermost sequence of deposits (Figure 2 - 1), formed during the advance and retreat of the Fraser glaciation, represent the thickest of the surficial units in the area. This sequence is composed of four discernable stratigraphic units, described below from bottom to top (units 4 through 7). Unit 4 is defined by horizontally bedded pebble-cobble gravel, approximately 30 m thick in total, deposited by braided river channel meltwater that formed as glaciers advanced into Thompson River Valley during the early Fraser Glaciation (Clague and Evans, 2003). Unit 5 is defined by horizontally bedded, glaciolacustrine silt and sand containing some isolated stones, which likely formed as the result of ice damming that blocked regional drainage and formed a lake within Thompson River Valley. Unit 6 is defined by a matrix-supported diamicton. Unit 7 is defined by poorly sorted, weakly stratified gravel, grading up into sand and silt (Figure 2 - 1).

The uppermost deposit in Thompson River Valley, which overlies the Fraser glacial sequence, is composed of horizontally bedded, pebble-cobble gravel (unit 8, Figure 2 - 1). This unit was deposited by Thompson River during the Pleistocene-Holocene transition (Clague and Evans, 2003).

The valley fill deposits found in the Grand Coulee, within Columbia River valley, Washington exhibit a similar geological architecture to the Ashcroft deposits, indicating similarity in the depositional environments of the two sequences. Flint and Irwin (1939) describe the glacial history of three groups of sediments in the Grand Coulee area deposited during the Fraser glaciation: (1) a basal sequence composed of glacial interbedded silt and clay, overlain by (2) a poorly stratified silt, sand and gravel till, overlain by (3) stratified glaciolacustrine silt, sand and gravel. The basal sequence is composed of massive silt layers, ranging in thickness from several centimeters to 3 m, and interbedded silt and clay, ranging in thickness from 10 cm to 4 m. Several discontinuous seams of fine and coarse sand are found throughout the basal sequence, which reaches a maximum thickness of 60 m. A continuous layer of till composed of poorly sorted silt, sand and gravel overlies the basal sequence. The thickness of this unit is highly variable due to its inter-fingered configuration. The uppermost deposits are composed of stratified lacustrine silt, which in places is interbedded with layers of sand and gravel. This unit is described as a late glacial valley fill deposit that makes up the upper portion of flat-topped terraces common to the Columbia River valley (Jones et al., 1961). Figure 2 - 2, adapted from Flint and Irwin (1939, Pl.1), shows the stratigraphic cross-section of the Columbia River valley found at the Grand Coulee Dam site.

2.2.2 Nature of interbedding in glaciolacustrine deposits

Glaciolacustrine sediments within the valley fill sequences vary in composition relative to the nature of their deposition, which depends on their distance from the glacial front during time of deposition, size of the lake basin, proximity to inflowing glacial streams, and contemporaneous mass movement (Evans, 1982). These materials will often exhibit alternating beds of lighter and

darker material, where the lighter material is typically of higher average grain size (silt), and the darker material is typically of lower average grain size (clay) (Figure 2 - 3) (Fulton, 1965). Typical grain size curves for the silt and clay interbeds are provided in Figure 2 - 4. Data used in Figure 2 - 4 was obtained from 13 samples of glaciolacustrine silt and clay South of Ashcroft, British Columbia (Appendix A).

Abrupt changes in grain size usually occur between adjacent bands. This pattern reflects a seasonal variation in the depositional environment. Fulton (1965) describes the coarser material as being deposited during warmer months when glacial melting contributed to increased runoff into glacial lakes. Finer material is transported into glacial lakes when melting slows in the colder months, resulting in the formation of clay beds. Due to the variability in sediment delivery rates during the summer and winter months the bedding thickness is variable within the glaciolacustrine sediment.

Varved sequences may be either silt-bed dominated or clay-bed dominated, indicating the dominant grain size in terms of relative thicknesses of silt or clay for a given succession (Evans, 1982). In the Ashcroft and Grand Coulee areas the deposits are silt-bed dominated. Examples of clay dominated interbedded valley fill deposits are found in north eastern British Columbia (e.g., Thomson and Mekechuk,1982).

2.2.3 Role of glaciolacustrine deposits contributing to slope instability

The occurrence of glaciolacustrine sediments within a valley fill has implications for the overall strength of the deposit and its geotechnical behaviour. In the Ashcroft and Grand Coulee areas it has been determined that the glaciolacustrine sediments included within the surficial deposits are

partially responsible for local slope stability problems, as landslide failure surfaces have been traced to these units (Figure 2 - 2) (EBA, 1983; USBR, 1983; Porter et al., 2002; Clague and Evans, 2003; Eshraghian et al., 2007; Eshraghian, 2007).

Regarding this phenomenon we hypothesize that: (1) periodic glacial overriding and landsliding during interglacial periods has created pre-sheared surfaces within the glaciolacustrine sediments (first suggested by Clague and Evans, 2003), (2) the presence of pre-sheared surfaces has reduced the shear strength of these already weak materials to residual values, (3) instability within the sequence is primarily controlled by the clay portion of the interbedded deposits, which is significantly weaker than the silt portion, and (4) the form of regional groundwater flow patterns influenced by the relatively low permeability of these materials produce elevated pore water pressures at the base of the slopes, further contributing to their instability. Points 2 and 3 in the above list are examined further through the geotechnical testing of these materials. The fourth point in the above list is the subject of later chapters.

2.3 Geotechnical properties

2.3.1 Overview

We explored the geotechnical properties of 41 soil samples collected from the silt and clay deposits of the Thompson River Valley, near Ashcroft, British Columbia. These samples were obtained as a part of a previous Geological Survey of Canada research project examining the landslides in Thompson River Valley, but results are being reported here for the first time. Of the samples collected, 14 samples were extracted in large (approximately 0.02 m^3) intact blocks, hand trimmed, and immediately coated in wax and packed in foam boxes so as to preserve

moisture content, bedding planes, shear surfaces, and other in situ features of the material. This reduces the effects of weathering on testing of the materials, since the samples were cut back into the slopes away from the surface. 16 samples were selected and sent to the University of Warwick soils lab for ring shear and geotechnical index property testing under the supervision of Dr. Derek Petley, and another 26 were analyzed for grain size distribution and index properties. Through this testing it was possible to establish accurate index properties and residual shear strength estimates of the glaciolacustrine interbedded silt and clay from the Ashcroft area. A summary of Ashcroft geotechnical data obtained in this study is provided in Appendix A.

In addition to the testing of Ashcroft soils, geotechnical testing of the Grand Coulee interbedded silt and clay carried out by the United States Bureau of Reclamation was reviewed. This study was completed as a part of a riverbank stabilization study that was initiated when a large historic landslide reactivated within a populated area adjacent to the Grand Coulee dam following a sudden dam-controlled water level fluctuation in the Columbia River on June 4, 1978 (Miedema *et al.*, 1981; USBR, 1983). A six mile reach of the Columbia River Valley downstream of the Grand Coulee dam was studied to identify possible slope stability problems. This study has provided additional information regarding the behaviour of glaciolacustrine soils in valley fills in the Pacific Northwest.

2.3.2 Grain size

Of the samples collected from the Ashcroft area, 26 were analyzed for grain size (Appendix A). The envelope of grain size distributions is shown in Figure 2 - 4. All samples showed very fine grain size distributions, with clay fractions ranging between 8% and 75%. Some samples (e.g.,

17AU-2A) were extremely well sorted, with almost 100% of the grain size being between 0.005 mm and 0.002 mm in diameter. Others (e.g., 18AU-4B) showed a very even distribution of fines. In general clay varves tend to include a narrower range of grain sizes compared to silt varves. Conversely, silt varves are more gradually sorted compared to clay varves. Typical uniformity coefficients (C_u) for the clay and slit components were approximately 2.5 and 6.9 respectively.

2.3.3 Index properties

Figure 2 - 5 shows plasticity data for silt and clay samples from both the Ashcroft, and Grand Coulee areas. Of the 54 samples included in the plasticity chart the classification of soils is as follows: 2 ML, 2 MI, 1 MH, 16 CI, 16 CH, 17 CV. More than half of the samples can be classified as highly or very highly plastic. Two separate groups of materials are noted in Figure 2 - 5, representing distinct properties of the individual clay and silt varves. Clay varve samples have much higher plasticity values, and as such occupy the upper right region of the plot. Liquid limits of the clay samples ranged from 63 to 87, and Plasticity Indices ranged from 38 to 64. Liquid limits of the silt samples ranged from 30 to 59, and Plasticity Indices ranged from 5 to 36. Ranges of values between these maxima and minima were fairly evenly distributed for the clay samples. However, the plot shows a greater number of silt samples collected in the lower left region of the plot. This is likely an indication that several of the samples contained both silt and clay varves. These samples therefore demonstrate properties intermediate between the silt and clay extremes.

2.3.4 Residual strength

Residual shear testing was completed for 9 of the Ashcroft samples using a Bromhead ring shear apparatus at the University of Warwick soils laboratory. The shearing speed was 0.048 deg/min, and vertical loading on each sample was stepped from 50 kN/m^2 to 100 kN/m^2 to 150 kN/m^2, and back to 50 kN/m^2. Results show two distinct groups of residual angles of internal friction, reflecting the residual shear strength characteristics of the silt and clay interbeds respectively. The lower group of data (representing the clay component) indicates residual angles of internal friction between 10^o and 15^o, and the upper group of data (representing the silt component) indicates residual angles of internal friction between 24^o and 33^o. A typical failure envelope of these materials is shown in Figure 2 - 6. When combined with data from the Grand Coulee area the bimodal distribution of residual friction angles becomes even more apparent. Residual angles of internal friction for Grand Coulee clays and silts ranged from 7^o to 14^o, and 28^o to 32^o respectively.

Figure 2-7 shows residual friction angle plotted against plasticity index, and Figure 2 - 8 shows residual friction angle plotted against liquid limit. An inverse relationship exists between these parameters; the residual angle of internal friction decreases as liquid limit and plasticity index increase. These relationships follow those which were identified previously by others. Skempton (1964) identified a relationship between residual friction angle and clay fraction. Numerous others have elaborated on Skempton's work: e.g., Kenney (1977), and Lupini, et al. (1981). Similarly, relationships between residual friction angle and plasticity index were developed by Fleischer (1972), Voight (1973), and Lambe (1985). Haefeli (1951) originally identified the relationship between residual friction angle and liquid limit. Subsequent research on this relationship was completed by Bishop (1971), Mesri and Cepeda-Diaz (1986), and Stark

and Eid (1994). Further to the research described above, Tiwari and Marui (2005) recently estimated residual friction angle given mineralogical composition of the clay.

Residual friction angle is often estimated based on one or more of the above relationships instead of being measured directly. This is likely because the ring shear apparatus is not widely available, and because index properties are frequently measured for routine geotechnical work. Perhaps the most commonly used of all the above relationships is the empirical relationship developed by Stark and Eid (1994) to obtain residual friction angle given the liquid limit, clay fraction, and effective normal stress. Generally the actual residual strength data from Ashcroft and Grand Coulee fall within the Stark and Eid (1994) relationship plotted for a given range of confining stress and clay fraction in Figure 2 - 8.

2.4 Summary and conclusions

Pleistocene valley fill deposits found in the western mountains of Canada and the northwestern United States are composed of a wide variety of materials, including glaciolacustrine interbedded silt and clay subunits. These subunits are most important in controlling local slope stability in any valley fill sequence, especially where they occur lower in the stratigraphic succession. Clay interbeds within these units were found to be highly plastic with clay fractions of up to 75%.

It is important to distinguish between the silt and clay components of interbedded glaciolacustrine deposits. Each unit possesses unique grain size, liquid limit, plasticity, and residual strength characteristics, and therefore must be considered separately in slope stability analyses. Material testing of these units should be carried out after they have been separated to

distinguish between individual properties. The finer-grained, highly plastic clay component of the valley fill will be most important in controlling slope failure, since it is the weaker unit.

If depositional history indicates that glacial overriding or landsliding may have previously occurred then the strength of these deposits may be at residual values. Residual friction angles based on ring shear testing were found to be very low, ranging from 8^{o} to 15^{o} for clay samples from Ashcroft, BC and Grand Coulee, Washington. Silt samples from the same localities yield higher residual friction angles, between 24^{o} and 33^{o}. This indicates that the clay interbeds play a greater role in contributing to slope failure. A correlation between residual friction angle and index properties was noted for these samples and most data did fit well within previously developed empirical relationships, such as those described by Stark and Eid (1994).

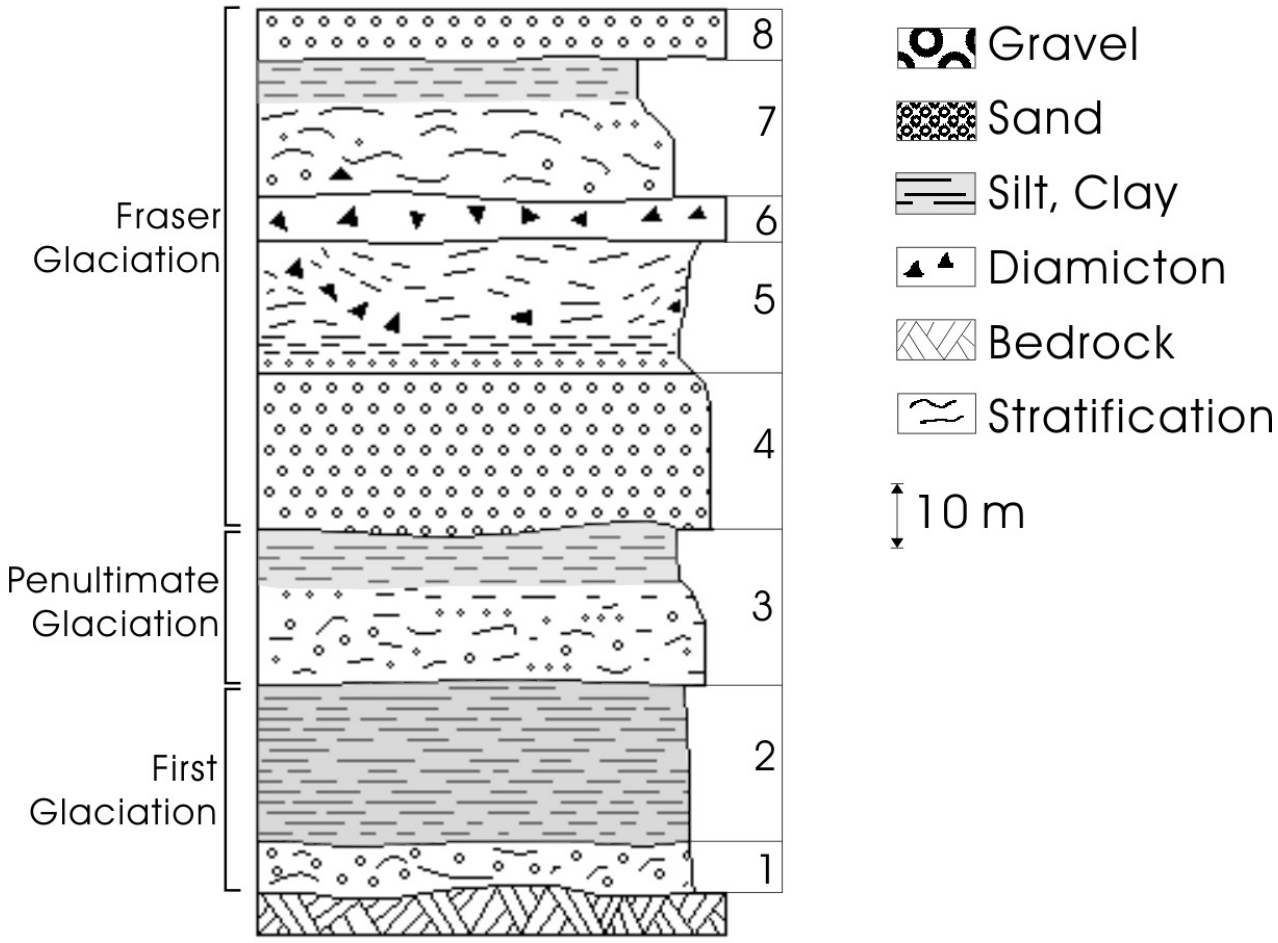

Figure 2 - 1. Sequence of valley fill deposits near Ashcroft, BC. Numerical labels correspond to those listed in the text. Modified after Clague and Evans, 2003.

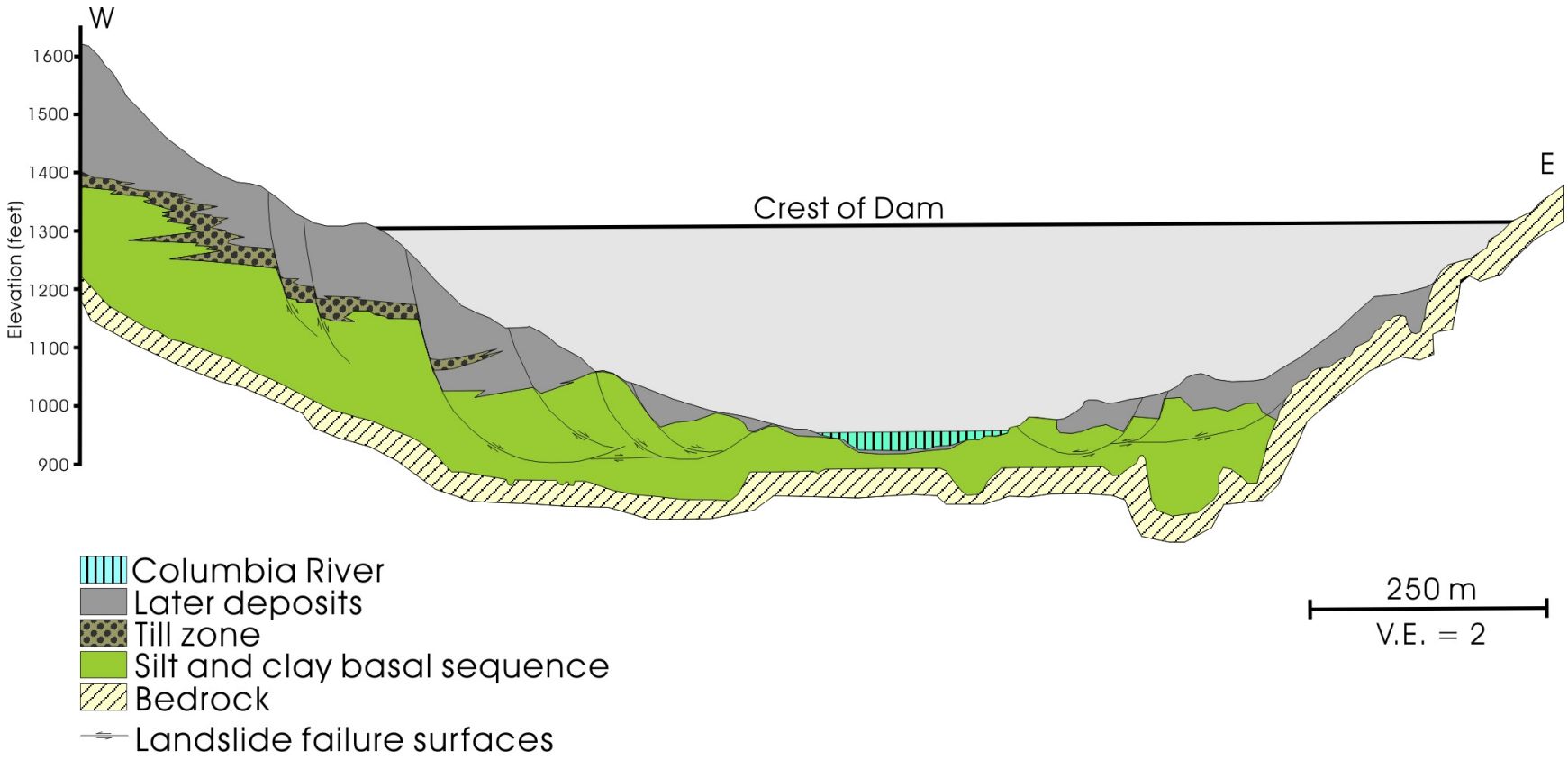

Figure 2 - 2. Stratigraphic cross-section of the Columbia River at the Grand Coulee Dam site (modified after Flint and Irwin, 1939, Pl.1). Landslide failure surfaces are shown developing in the silt and clay basal sequence.

Figure 2 - 3. Photographs of undisturbed interbedded silt and clay (above), and disturbed silt and clay (below), Thompson River Valley, near Ashcroft, British Columbia. Dark layers are clay interbeds, and light layers are silt interbeds. Note the stratigraphic sections are dominated by silt interbeds.

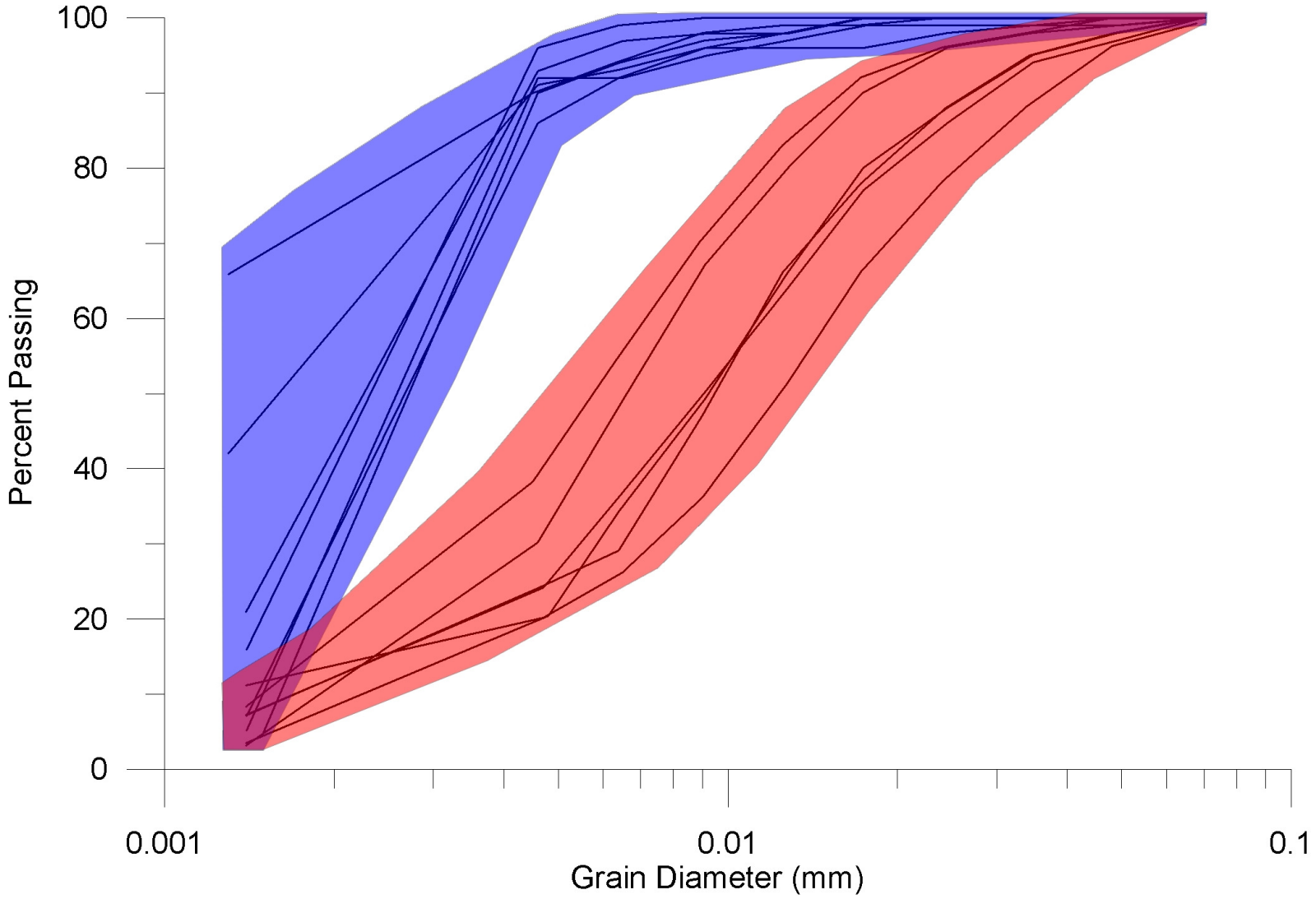

Figure 2 - 4. Grain size distribution envelopes for Ashcroft silt (red) and clay (blue). Data from 13 samples of glaciolacustrine silt and clay collected south of Ashcroft, BC for this study.

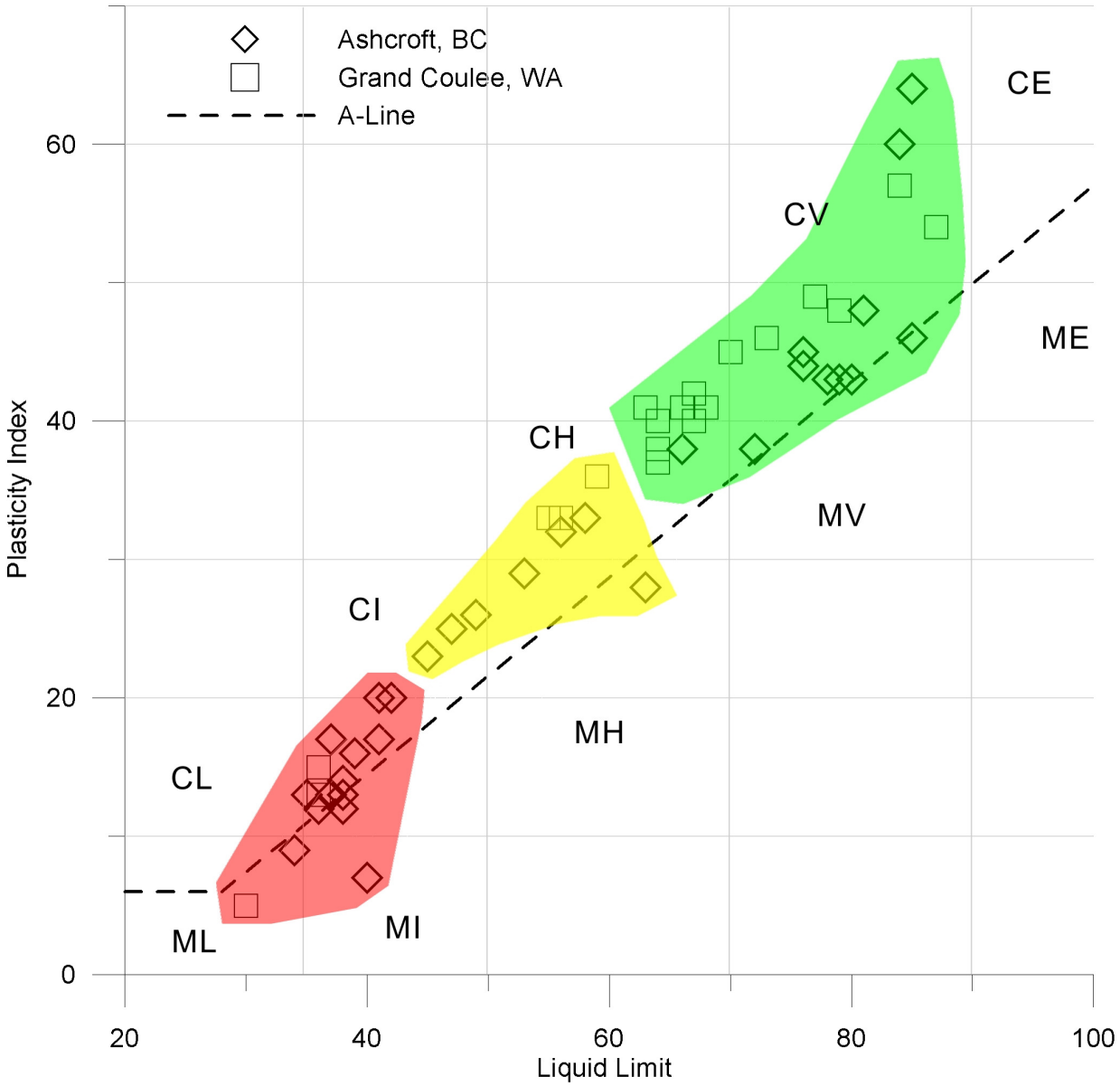

Figure 2 - 5. Plasticity chart for Ashcroft and Grand Coulee silt and clay. Data from clay samples is highlighted in green (furthest to the right); data from silt samples is highlighted in red (furthest to the left); and samples containing both silt and clay are highlighted in yellow (central portion). Data included in this figure from the Grand Coulee area is from Miedema et al. (1981), and USBR (1983).

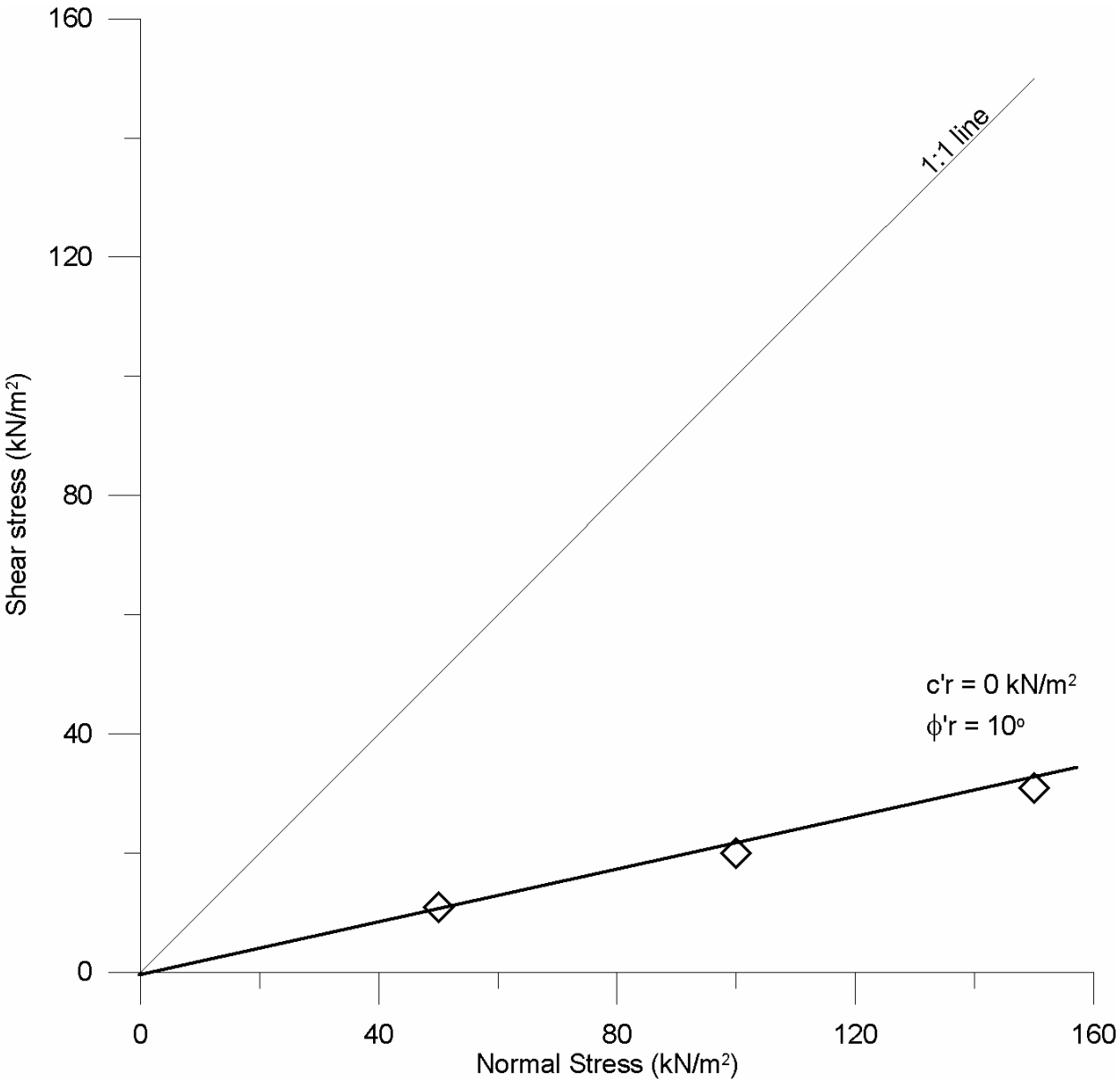

Figure 2 - 6. Typical failure envelope for glaciolacustrine clay interbed (sample 18-AU-2B).

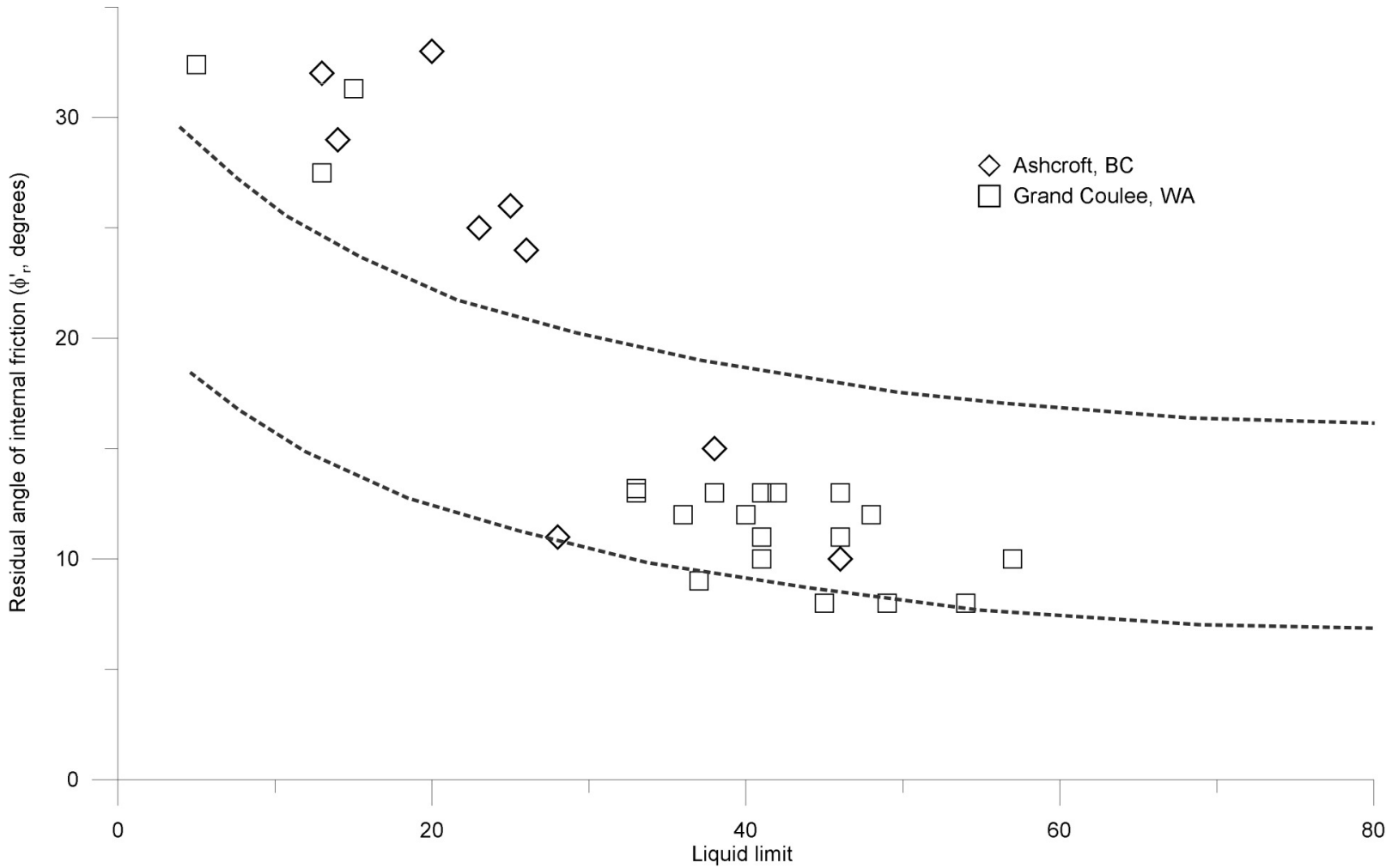

Figure 2 - 7. Relation between residual friction angle and plasticity index. Boundaries of the relationship between these parameters given in Mitchell (1976) are outlined. Values from Ashcroft obtained using a Bromhead ring-shear apparatus, values from Grand Coulee obtained using a repeated direct shear device with reversal. Data from this study from Miedema et al. (1981), and USBR (1983).

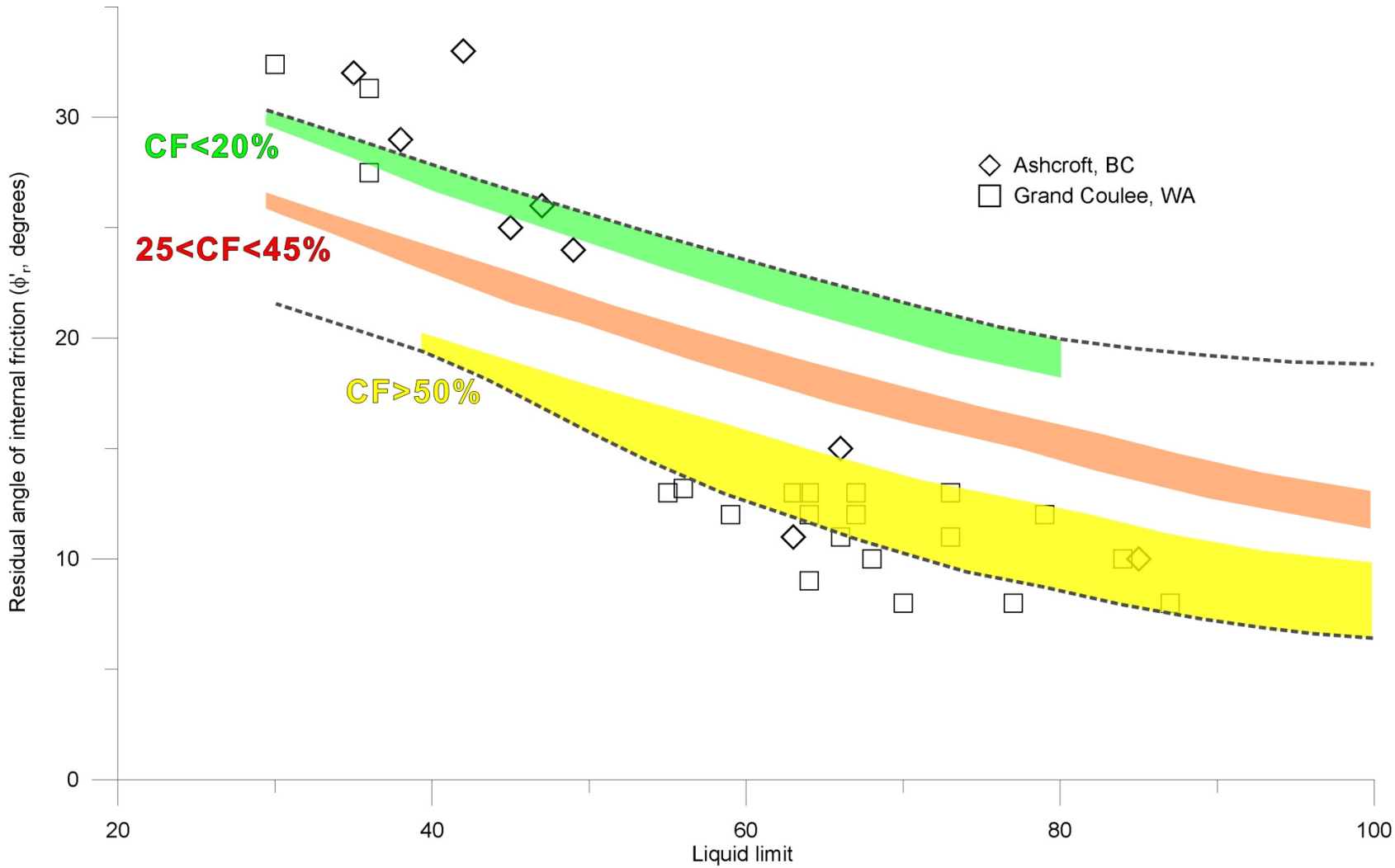

Figure 2 - 8. Relation between residual friction angle and liquid limit. Boundaries for Stark and Eid's (1994) empirical relationship are plotted for a range of clay fractions (CF) and for normal confining stresses ranging between 100 kPa and 700 kPa. The green band gives the range for materials with CF<20%, the orange band gives the range for materials with 25%<CF<45%, and the yellow band gives the range for materials with CF>50%.

Chapter 3

Effects of regional groundwater flow systems

3.1 Problem setting

3.1.1 Historical landslides

As outlined in Chapter 1, thirteen major historical landslides have occurred in Thompson River Valley (Figure 1 - 1) (Table 1 - 1). Damage caused by these landslides has mostly been incurred by the rail companies and not the general public. Although no known deaths have been attributed to these landslides, the potential of landslide dam induced flooding within the town of Ashcroft is high in the event of a future river blockage. The North (1880) Landslide (number 7 in Table 1-1) dammed Thompson River for a period of approximately 44 hours, resulting in flooding to depths of 0.4 m on the terrace where Ashcroft now stands (Evans, 1984).

The main engineering problem associated with the Thompson Valley landslides is their impact on the CP and CN rail lines that traverse the valley bottom. Continuous rail alignment issues arise because several of these landslides, including the North, South, Goddard (Figure 3 - 1), and Ripley slides, currently represent trouble areas for the railway companies (Chris Bunce, CP, personal communication, 2007). In the inner part of the South Slide movement rates have recently been measured at between 8 and 10 mm/yr. The section of rail track under this landslide alone accounts for approximately $10,000 worth of annual maintenance by CP (Chris Bunce, CP, personal communication, 2008).

As indicated in Table 1 - 1, initial formation of some landslides predates nineteenth century human development of the area to several thousand years before present when periods of rapid river incision contributed to river bank erosion (Johsen and Brennand, 2004). However, there appears to be some correlation between the occurrence of first-time landslides, landslide activity, or reactivation of previous landslides and anthropogenic activity. Robert Stanton (1898) first recognized the link between landslides in Thompson River Valley and anthropogenic activity when he suggested that slides were occurring as the result of excessive irrigation on the terraces above Thompson River. In Stanton's time irrigation techniques consisted of contour ditch systems that involved flooding numerous parallel ditches with excessive amounts of water (Government of Canada, 1982). These irrigation systems were inefficient compared to modern sprinkler systems, and would have significantly contributed to increased subsurface water infiltration and groundwater recharge below the root zone.

The visual evidence of the spatial association between irrigation and landslides is still apparent in modern aerial photographs (Figure 3 - 2). The historical initiation of many of the landslides coincides with the timing of original settling of the area (e.g. Nepa, Barnard, South, North, Ashcroft, Goddard, and Spence's Bridge slides), indicating there may be a connection between the landslides and human activity in the area. Further, most of the initial catastrophic slide movements occurred in the late summer and early fall when irrigation of the croplands directly above the slide areas is highest, strongly suggesting anthropogenic impacts on landslide activity (Clague and Evans, 2003).

3.1.2 Water use

Forty water supply wells have been identified in the study area using the British Columbia Ministry of Environment Water Stewardship Division's well database (located in Figure 1 - 1) (BCMWLAP, 2008). Most of the wells were drilled from the mid-1970's to the mid-1980's, and are mostly used for agricultural or residential supply as indicated by the well owner information. Drilling logs are available for all of these wells; however, they cannot be viewed as a completely reliable source of geological information since lithological descriptions in the logs vary considerably depending on the driller. Some of the wells include measurements of static water levels. A list of wells is provided in Appendix B. Almost all wells are drilled low in the valley between river level (280 mASL) and 450 mASL with the majority of these located approximately 2.5 km west of Thompson River (Figure 1 - 1).

3.1.3 Land use

Sagebrush scrubland dominates the landscape at lower elevations throughout most of the study area, although groves of trembling aspen can be found in areas of groundwater springs (Golder Associates, 1999). At higher elevations forests of Ponderosa Pine and Douglas Fir trees are found. The flat tops of benched terraces common to the area are normally used for agriculture or cattle ranges. Alfalfa, orchard grass, barley, and ginseng are the most common locally grown crops (Golder Associates, 1999). Most residential dwellings and commercial properties, with the exception of numerous ranches east of Thompson River, are located within the village of Ashcroft (population: 1,800). Ashcroft Ranch, a 4200-hectare property is located west of Highway 1 on the western side of the river valley, was selected by the Greater Vancouver

Regional District (GVRD) as the location of a major municipal solid waste landfill (Golder Associates, 2004) (Figure 1 - 1).

3.1.4 Bedrock geology

The bedrock composition of the Ashcroft area is defined by early to mid-Jurassic clastic sedimentary rocks of the Ashcroft Formation, which uncomfortably overlie late-Triassic Nicola group volcanic rocks. These rocks have been intruded by the Guichon Creek batholith (Monger and Price, 2000). The Ashcroft Formation is characterized by the occurrence of argillite, siltstone, sandstone, conglomerate, and local carbonate. The bedrock to the east of Thompson River is characterized by the Guichon Creek batholith. The batholith is composed of granodiorite, quartz monzonite, diorite, and amphibolite, is highly fractured, and has abundant features including foliation, joints, shear and fault zones, dikes, veins, and xenoliths (Owsiacki, 1999; Ladd, 1977). Volcanics of the Nicola Group can be found South of Barnard Creek on both the east and west sides of Thompson River. These consist of mafic to felsic pyroclastics, argillite, sandstone, and local carbonates. The bedrock west of Thompson River is composed of mid Permian to late Triassic Cache Creek complex carbonate, argillite, and tuff, with minor basalt and chert. South of Pimainus Creek the mid to late Cretaceous Spences Bridge Group, composed of locally felsic and mafic flows, pyroclastics, sandstone, shale, and conglomerate, are found on both the east and west sides of Thompson River (Monger and McMillan, 1982).

3.1.5 Structural geology and physiography

The Thompson River Valley lies in the southern part of the Interior Plateau of the interior system of the Canadian Cordillera (Fulton, 1975). Many of the valleys within this area trend northwest-southeast, with tributaries running perpendicular to them. This is related to the orientation of the faults and joints within the local bedrock (Fulton, 1975). The occurrence of faults in the Ashcroft area is common along stratigraphic boundaries. One unnamed fault has been inferred by Monger and McMillan (1982) to traverse parallel and to the east of Thompson River from Venables Creek until crossing the river at a point approximately 4 km south of Barnard Creek. Continuing north-northwest, the fault diverges from Thompson River.

3.1.6 Surficial geology

For detailed discussion on the surficial geology of the Thompson River Valley sediments the reader is referred to Chapter 2. Quantitative discussion of the hydrogeological implications of the surficial geology is presented in a later section. A qualitative discussion follows here.

The succession of valley fill sediments in Thompson River Valley exhibits some important characteristics relating to groundwater flow. Two features of the glaciolacustrine silt and clay unit (unit 2 in Figure 2 - 1) indicate the importance of this unit in terms of groundwater dynamics. First, the clay interbeds in this unit are the least permeable of all units in the valley fill sequence, and are less permeable than the silt interbeds of the same unit (Eshraghian et al., 2006). Second, in the undisturbed state this unit is horizontally layered, resulting in strong preferential groundwater flow in the horizontal direction in the groundwater field.

In some places within the Thompson River Valley ancient river gravels are located directly below unit 2 (BGC Engineering, 2005). Permeable fractured bedrock underlies unit 2 in places where river gravels are not found (Golder Associates, 2004). The high permeability of the gravels and fractured bedrock contrasts to the low permeability of unit 2. Hodge and Freeze (1977) conclude that the presence of a low-conductivity unit can be extremely detrimental to slope stability, particularly if it confines a unit of much higher conductivity. Based on this observation, the location of unit 2 in the valley fill sequence may help explain the extent of landsliding within Thompson River Valley.

3.2 Groundwater data sources

3.2.1 Boreholes

Several piezometers installed near the Thompson River have encountered flowing artesian conditions in the basal units of the valley fill (Figure 1 - 1). However, very little groundwater data exists for the area. During drilling flowing artesian conditions were encountered in a gravel zone at a depth of approximately 50 m in boreholes DH04-04 (290.7 mASL; all values are ground surface elevation) at the South slide, DH04-14 (274.4 mASL) at the Basque Slide, as well as in glaciolacustrine silt and clay at approximately 45 m in depth in boreholes DH04-10 (276.0 mASL) and DH04-13 (276.0 mASL) at the South Slide (BGC, 2005). For reference, the stage of Thompson River at the South Slide ranges between 272 mASL and 277 mASL.

Given the well screen dimensions and the properties of materials adjacent the well screen artesian flow rates can be related to pressure heads. Flow rates were determined for some of the

wells (BGC, 2005). However, insufficient information is provided in all cases to determine pressure head.

It is thus possible that artesian pressure is a major driving force responsible for ongoing landslide movement within Thompson River Valley but its origin remains unknown. It is probable that these artesian conditions are a product of the regional groundwater flow system in the valley. The extent to which irrigation of upslope fields contributes to increased pore pressures at the valley bottom is unknown.

As previously mentioned, Golder Associates (2004) investigated the subsurface near the area of the Greater Vancouver Regional District landfill, on the western side of Thompson River Valley (Figure 1-1). In addition to geophysical investigations boreholes were advanced to determine the depth to bedrock, as well as the degree of fracturing within the bedrock. During drilling bedrock was encountered at depths ranging from 0 to 134 m (Golder Associates, 2004). Depth to bedrock was found to increase from west to east towards Thompson River. On the western side of Thompson River the buried bedrock surface slopes approximately 13 to 15 degrees towards the east (Golder Associates, 2004). Buried Nicola group volcanic rocks were found to have a fractured surface ranging from 2 m to 20 m in thickness. Depth of fracturing was found to be related to depth of bedrock, where fracturing depth increases as bedrock depth decreases (Golder Associates, 2004). Based on borehole information, RQD values were typically on the order of 50%, but ranged from 2% to 100% within any given borehole. Bedrock was typically slightly weathered, but the degree of weathering was highly variable.

3.2.2 Hydraulic data

Aside from the limited borehole information very little hydrogeological information exists for the surface deposits found in Thompson River Valley. Eshraghian et al. (2005) give estimates of saturated hydraulic conductivity and water content for five geological units located near the river level. Their estimates, which are based on laboratory experiments, range from 2.31×10^{-3} m/s for saturated hydraulic conductivity in sand and gravel to 1.16×10^{-11} m/s in clay. Comparatively, the values of saturated hydraulic conductivity used in the HydroGeoSphere model ranged from 3.0×10^{-4} m/s for gravel outwash to 5.0×10^{-10} m/s for clay. An explanation of these differences is given below.

Values for hydraulic conductivity, porosity, and specific storage of all units were estimated based on soil type, as found in Freeze and Cherry (1979, p. 29), and supported by previous studies of similar soils (USDA, 2005). Golder Associates (2004) estimated the hydraulic conductivity of two surficial units within the Thompson River Valley, identified only as sand and glacial till. These units are estimated to have hydraulic conductivities of 8×10^{-5} m/s, and 1×10^{-6} m/s, respectively.

Hydraulic conductivity estimates of two other geologic units were confirmed by slug test data obtained during a field site visit in June 2007. Slug tests were performed using the three piezometers (DH04-04, DH05-18, and BGC98-04) installed within the South Slide area. Piezometers DH04-04 and DH05-18 are installed in unit 2 (Figure 2 - 1), glaciolacustrine interbedded silt and clay. The horizontal hydraulic conductivity of unit 2 is calculated to be between 2.13×10^{-8} m/s (DH04-04), and 5.27×10^{-8} m/s (DH05-18). Piezometer BGC98-04 is installed within a sand layer and the upper portions of an adjacent silt layer (BGC Engineering,

1998), which is likely part of unit 3, the pre-Fraser till (Figure 2 - 1). The double straight line method (Bouwer, 1989) was used to calculate hydraulic conductivity of the sand and silt layers separately. Hydraulic conductivity is calculated to be 5.03×10^{-5} m/s for the sand and 1.97×10^{-6} m/s for silt. All calculations were obtained using the Hvorslev method (Hvorslev, 1951). It should be noted that the average hydraulic conductivity of this unit was assumed, since the individual silt and sand beds were not specified individually. A summary of the results of the slug test is provided in Table 3 - 1 below.

Table 3 - 1. Hydraulic Conductivity Estimates From Slug Test Data

Well	Geological Unit	Hydraulic Conductivity (m/s)
DH04-04	Interbedded silt and clay (unit 2)	2.13E-08
DH05-18	Interbedded silt and clay (unit 2)	5.27E-08
BGC 98-04	Sand	5.03E-05
BGC 98-04	Silt	1.97E-06

Using a variety of field and laboratory measurement techniques, Bradbury and Muldoon (1989) estimated the saturated hydraulic conductivity of unlithified glacial material in Wisconsin. They found that estimates of hydraulic conductivity vary greatly with the scale and method of measurement. In some cases, estimates of hydraulic conductivity for the same material varied by four orders of magnitude depending on the method used (Bradbury and Muldoon, 1989). Given the scale and geological complexity of the groundwater model, bulk estimates of hydraulic conductivity are appropriate.

The bedrock within Thompson River Valley is mainly composed of early to middle Jurassic Argillite of the Ashcroft Formation (GSC, 1989). This bedrock unit has been described by Golder Associates (2004) in detail in a hydrogeological study of the Ashcroft Ranch landfill site, mentioned previously. Golder Associates (2004) estimates of the hydraulic conductivity of the

fractured bedrock and competent bedrock to be $9x10^{-7}$ m/s and $5x10^{-8}$ m/s respectively. A complete list of the hydrogeological parameters assigned to bedrock units is provided in Table 3 - 2.

The values for Van Genuchten (1980) parameters and residual saturation were estimated based on grain size, as outlined in the U.S. Salinity lab Class Average Hydraulic Parameter Lookup Table (USDA, 2005). A complete list of these parameters is provided in Table 3 - 2 below.

Table 3 - 2. Hydrogeological properties of valley fill materials

				Hydraulic Conductivity*		Van Genuchten Parameters		
Unit Description	Unit #	Porosity *	Specific Storage [1/m]*	X-direction (m/s)	Z-direction (m/s)	α [m^{-1}] **	β **	Residual Sat. S_r **
Alluvial fans	-	0.35	1.1E-05	5.0E-06	5.0E-06	2.67	1.5	0.039
Terrace gravels	8	0.33	2.4E-06	1.0E-05	1.0E-05	3.52	3.2	0.01
Glaciolacustrine silt and sand	7	0.4	9.8E-04	3.0E-06	3.0E-06	0.506	1.7	0.065
Gravel outwash	-	0.35	1.0E-04	3.0E-04	3.0E-04	2.67	1.5	0.039
Till	5	0.4	9.8E-04	1.0E-08	1.0E-08	0.506	1.7	0.065
Fluvial gravels	4	0.33	2.4E-06	1.0E-05	1.0E-05	3.52	3.2	0.01
Glaciolacustrine silt	3	0.45	9.8E-04	1.0E-07	1.0E-07	0.658	1.7	0.05
Till	3	0.4	9.8E-04	5.0E-07	5.0E-07	0.506	1.7	0.065
Interbedded silt and clay	2	0.45	7.8E-02	5.0E-09	5.0E-10	1.62	1.3	0.111
Fractured bedrock	-	0.1	1.4E-06	9.0E-07	9.0E-07	1	3	0.01
Competent bedrock	-	0.01	9.9E-06	5.0E-08	5.0E-08	1	3	0.05

* indicates values were obtained from Freeze and Cherry (1979, p. 29)

** indicates values were obtained through U.S.D.A. (2005) lookup table

3.2.3 Precipitation and infiltration

Nearly complete precipitation data from the Ashcroft area were available from various Environment Canada climate monitoring stations since 1924 (Environment Canada, 2008). These stations are summarized in Table 3 - 3. Using data from these six monitoring stations the

average annual precipitation was calculated to be 232 mm/yr. Average monthly precipitation data are shown in Figure 3 - 3.

Table 3 - 3. Environment Canada Climate Stations in the Ashcroft Area

Name/Location	Number	Period of Record
Ashcroft	1160510	1924-1969
Ashcroft	1160511	1973-1980
Ashcroft Manor	1160540	1944-1972
Ashcroft North	1160520	1980-1986
Cache Creek	1161215	1982-1998
Spence's Bridge	1167637	1980-2002

Previous hydrogeological modelling of the South Slide area by Eshraghian et al (2006) used an infiltration flux value of 5.5% of the mean annual rainfall. In determining this rate of infiltration, Eshraghian et al. (2006) referenced case studies of infiltration rates in low permeability materials (clays, etc), located in regions that are dissimilar to Thompson River Valley in terms of vegetation and climate (e.g., the east-central Saskatchewan study of Pauls et al., 1999).

It is suggested that applying an infiltration flux of 5.5 % of the mean annual precipitation is unrealistic considering the surface stratum in Thompson River Valley is largely composed of highly permeable sands, gravels, and glacial tills. Furthermore, this infiltration flux contradicts field-measured infiltration rates of 65% of the mean annual precipitation recorded by Eshraghian et al. (2006) at South Slide. It should also be noted that the Eshraghian et al. (2006) analysis focused only on a very localized groundwater flow regime, and not on the regional groundwater flow system.

It is ideal to use accurate measurements of the sources (infiltration from precipitation, infiltration from irrigation) and sinks (evapotranspiration, runoff) of a flow system model's water budget. However, these measurements cannot be made without extensive study over prolonged periods

of time (e.g. Droogers, 2000; Chanasyk et al., 2006). For the purposes of this study we suggest an infiltration rate of about 17% of the mean annual precipitation be used. Reasons for the selection of this value are based on the infiltration rate determined in the 1986 court case, (discussed in the following section), and the relative location of seepage faces in the valley bottom predicted by trial and error testing of groundwater models (discussed in section 3.3).

3.2.4 Irrigation

Estimation of the irrigation rate and resulting infiltration was provided by information disclosed in the 1986 B.C. Supreme Court hearing between CP and Highland Valley Ranch (Wallace, 1987). Dr. Krahn, a witness for the plaintiff, calculated the total irrigation water applied to the field throughout a given year. Dr. Krahn's calculation was based on a 120-day irrigation schedule. The irrigation schedule is composed of three, forty-day periods of watering with seven-day intermittent periods without watering. During the watering periods, a 31.2 hectare field receives approximately 2.59 million litres of water, or approximately 8.3 mm a day via a three-wheeled line irrigation system. This results in approximately 311 million litres or 1.0 m of water applied to the field annually. An example of the watering schedule follows that outlined in Table 3 - 4.

Table 3 - 4. Watering Schedule for Hayfield.

Annual Week #	Rate of water application mm/day	Estimated Evapotranspiration	Infiltration due to Irrigation mm/day
18	8.3	4.2	4.1
24	0	-	0
25	8.3	4.7	3.6
35	0	-	0
37	8.3	5.0	3.3
43	0	-	0

Of course, only a fraction of the water that is applied to the field infiltrates below the surface. Significant losses are attributed to two components of the water budget, evapotranspiration, and runoff (Chanasyk et al., 2006). Estimation of the daily evapotranspiration rate for the Ashcroft area was calculateed by Dr. Chanasyk, a witness for the defendant, for the years 1981 and 1982 (Wallace, 1987). Values ranged from 2.8 mm/d for the month of April 1982 to 5.0 mm/d for the month of June 1982.

Dr. Chanasyk calculated the infiltration rate resulting from irrigation to be 0.114 m/yr (or 11.4% of the total water applied to the field). Dr. Chanasyk identified that the Irrigation Deisgn Manual for Farm Systems in British Columbia revealed that the sprinkler system was only 72% efficient, meaning that 72% of the water supplied to the sprinkler system lands within the target application area, with the remaining water landing outside the target application area or evaporating in transit (Wallace, 1987). However, this claim was refuted by Justice Wallace, since most of the water discounted by the 72% efficiency factor will land on ground surrounding the target area and probably infiltrate in any case. Dr. Chanasyk also assumed a 100-day irrigation schedule, instead of the 120-day irrigation schedule outlined by the plaintiff. This suggests that more water infiltrated the subsurface than predicted by Dr. Chanasyk. The efficiency factor should therefore not be taken into consideration when determining the infiltration rate at the surface. Adjusting for the efficiency factor and 120-day watering schedule yields an infiltration rate due to irrigation was of 0.173 m/yr, or 17.3 % of the total water applied to the field, compared to 0.114 m/yr (or 11.4%) of the total water applied as calculated by Dr. Chanasyk.

3.2.5 Thompson River data

River flow characteristics were determined by analyzing flow rate data from monitoring station 08LF051, located at Spence's Bridge, 36 km downstream from Ashcroft. A 55-year period of record (1951-2006) is available at this flow monitoring station. Prior to 1951, flow of the Thompson River at Spence's Bridge was monitored at station 08LF022 (in the same location as 08LF051), which has a period of record from 1911 to 1950.

Flow of Thompson River is characterized by lower flow rates (between 100 and 700 m^3/s) from September to March, with elevated flows (between 1,000 and 3,200 m^3/s) occurring between May and August (Figure 3 - 3). The average monthly flow rate of Thompson River over the 55 year period of record at station 08LF051 is 778 m^3/s.

Monthly flow data for the year 2005 were analysed because this was one of the most recent years of monitored data available, and because the average monthly flow rate for 2005 was 784 m^3/s, which is very close to the average value for the period of record. Monthly flow rates for the year 2005 at station 08LF051 were converted to stage values using a rating curve that was obtained through the Water Survey of Canada and used in the transient model as discussed below (WSC, 2007).

3.3 Groundwater models

3.3.1 Reasons for modeling

The nature of groundwater flow systems in mountainous areas has been explored by Hodge and Freeze (1977). Further, the interrelation between regional groundwater flow systems and slope stability in mountain-valley systems has been investigated by Reid and Iverson (1992).

However, the hydrogeological conditions within the Thompson River Valley and the manner in which they relate to slope stability remain largely unknown, especially at the regional scale. The irrigation of upslope benchlands, and fluctuations in the stage of Thompson River have been suggested as potential contributing factors to increased pore pressures and landslide activity in the valley bottom, but neither has been quantified (Stanton, 1898; Porter et al., 2002; Clague and Evans, 2003). In order to determine the general effect of these parameters on regional groundwater flow systems, two models were created.

Two cross sectional groundwater flow system models of Thompson River Valley were constructed. The first cross-section (the generalized cross-section) is a non-specific interpretation of the topographic and geological composition of the valley and was selected to explore the behavior of groundwater flow dynamics in the general sense. The second cross-section (the South Slide cross-section, B-B'-B'', shown in Figure 1-1), is over 10 km in length and passes through the South Slide in its lower reaches. Although this cross-section is more encompassing than the generalized cross-section, it was selected to capture the specific behavior of regional groundwater flow within Thompson River Valley as it is based on specific topography and geology.

Both cross-sections included areas of irrigated farm fields in order to assess the effects of irrigation on the groundwater flow regime (see objectives, Chapter 1). Each groundwater flow system was tested under a variety of environmental scenarios in order to assess their response to changes in infiltration. First, the groundwater flow systems were run to steady state conditions to determine the base case scenario for each flow system neglecting the effects of irrigation. Second, infiltration due to irrigation was added and the flow systems were again run to steady state. Third, a sensitivity analysis was performed by varying the precipitation and irrigation rates

and observing changes in the pore pressure distribution generated in the flow system. Finally, a transient simulation was completed where the precipitation, irrigation, and river stage were progressively changed throughout the simulation. The simulation was carried out using HydroGeoSphere (described below).

3.3.2 Notes on HydroGeoSphere

The Thompson Valley regional groundwater flow system has several observed characteristics. First, the groundwater domain is dominated by variably-saturated flow. Second, Thompson River and several small streams are known to intersect the water table. These aid in defining boundary conditions. Third, it can be assumed that evapotranspiration is occurring, and that a fraction of the precipitation and irrigation water will not infiltrate. Finally, several seepage faces are observed where the water table intersects the ground surface. Water discharging from a seepage face will ultimately recharge at a downstream location after briefly ponding on the ground surface. The need to model groundwater-surface water interaction to conserve water mass motivates the use of HydroGeoSphere (Therrien et al., 2005).

Cross-sectional flow system models of the Thompson River Valley were constructed using HydroGeoSphere, a three-dimensional, variably saturated, fully coupled surface-subsurface water flow and transport model (Therrien et al., 2005). HydroGeoSphere has been used on many occasions to successfully simulate large-scale flow problems where surface-subsurface fluid interaction is an important consideration (e.g., Panday and Huyakorn, 2004, Sudicky et al., 2005; Li et al., 2008). Key components of the hydrologic cycle in Thompson River Valley as simulated within HydroGeoSphere are:

$$P \times A = (Q_{S2} - Q_{S1}) + (Q_{G2} - Q_{G1}) + (E_T)A + (\Delta S_S + \Delta S_G)\Delta t \quad (3\text{–}1)$$

where P is the net precipitation [L/T], A is the top surface area of the cross-section [L^2], Q_{S1} and Q_{S2} are the surface water inflow and outflow [L^3/T], Q_{G1} and Q_{G2} are the groundwater inflow and outflow [L^3/T], ET is the evapotranspiration from the soil surface and through plant transpiration [L/T], ΔS_S and ΔS_G are changes in surface water and groundwater storage [L3], and Δt is the increment of time [T].

In summary, Richards' equation is used to determine two-diemensional flow of groundwater in the saturated and unsaturated zones. Surface water flow is represented by the two-dimensional depth—averaged Saint Venant equation, with the interaction between groundwater and surface water regimes fully-integrated using physically-based exchange flux relationships (Li et al., 2008). Detailed formulation of these mechanisms is included in Appendix C.

3.4 Generalized cross-section hydrogeological model

3.4.1 Overview

To gain a general understanding of the groundwater flow regime a cross-section of the Thompson River Valley was constructed for use in the HydroGeoSphere groundwater model (Figure 3 - 4). The cross-section was based on a nonspecific geological interpretation of the Ashcroft area outlined by Ryder (1976), with some slight modification. The cross-section is approximately 2.7 km in length, and runs from the centre of the Thompson River (280 mASL) to the benched terraces to an elevation of 776 mASL. Depth of the cross-section ranges from approximately 47 m at its shallowest point, to 180 m at its deepest point (Figure 3 - 4).

The generalized cross-section incorporates 11 different geological materials, including: competent bedrock, fractured bedrock, pre-Fraser glaciolacustrine clay and silt (unit 2), pre-Fraser till (unit 3), glaciolacustrine silt (unit 3), fluvial gravels (unit 4), Fraser till (unit 5), gravel outwash, glaciolacustrine silt and sand (unit 7), terrace gravels (unit 8), and postglacial alluvial fans. Units with associated numbers are described in detail in Chapter Two (see Figure 2 - 1). Those units listed without numbers (gravel outwash and postglacial alluvial fans) are found in Thompson River Valley (Ryder (1976)), but are not defined in the Clague and Evans (2003) geological succession. Units, 1 (early Pleistocene glacial till) and 6 (matrix-supported diamicton) were not included in the generalized cross-section because they do not appear in the Ryder (1976) cross-section.

3.4.2 Hydrogeological parameter selection

The hydrogeological parameters used in the generalized cross-sectional flow model were selected based on previous discussion. A complete list of hydrogeological parameters used as input to the HydroGeoSphere model is provided in Table 3 - 2.

3.4.3 Boundary conditions for steady state (base case) analysis

The generalized cross-section model was first run to a steady state flow condition, considering only infiltration from precipitation and neglecting additional input from irrigation. This was achieved using a critical depth boundary condition for model nodes at the river level (282 mASL, the mean water level at Spences Bridge monitoring station 08LF052, for January 2005), and an

assumed infiltration rate of 0.04 m/yr over the surface nodes of the model (about 17% of the mean annual rainfall of 232 mm/yr).

After the steady state pressure heads were first established, the HydroGeoSphere model was run to a steady state flow condition using additional infiltration from irrigation. A value of 0.173 m/yr (17% of the total irrigation water applied throughout the year) was applied over a 377m length of nodes in the valley-scale groundwater model cross section (Figure 3 - 4).

3.4.4 Boundary conditions for transient analysis

It has been suggested that fluctuation in the stage of Thompson River has a negative impact on the stability of landslides in the area (Porter et al., 2002, Eshraghian et al., 2006). In order to evaluate the effects of variable river stage on the pore pressure distribution near Thompson River a fluctuation of the Thompson River stage was applied to the groundwater model in a transient manner. River fluctuation was determined by analyzing flow rate data from monitoring station 08LF051, located at Spences Bridge 36 km downstream from Ashcroft (Environment Canada, 2008).

Mean monthly rainfall data from Environment Canada monitoring station #1167637 at Spence's Bridge for the year 2005 were used to determine the precipitation applied at the surface boundary of the transient simulation. 2005 data were chosen to be consistent with the river level boundary condition. The infiltration rate applied to the upper boundary of the groundwater model was assumed to be approximately 17% of the total precipitation, which accounts for losses attributed to evapotranspiration. Monthly infiltration rates were applied to the transient simulation in eight steps, reflecting significant changes in precipitation rates that can be observed in the data. Figure

3 - 5 shows the annual variation in infiltration rate used at the surface boundary of the transient simulation.

Infiltration rates due to irrigation were calculated assuming the 1981 and 1982 estimations of daily evapotranspiration are similar to those in 2005. Losses associated with runoff were neglected, since it is assumed that any water subject to runoff from the field after irrigation would be unable to escape the greater surface water flow regime before infiltrating or evaporating. The watering schedule outlined in Table 3 - 4 was followed in the transient analysis.

3.5 South Slide (regional scale) hydrogeological model

3.5.1 Reasons for selection

Using the generalized cross-section we were able to develop a sense of the regional groundwater behaviour in Thompson River Valley at the slope scale. We felt it was important to refine those results with an additional flow model based on an actual cross-section. Currently the prevailing slope stability problems in Thompson River Valley occur at the Goddard, North, South, and Ripley slides (Chris Bunce, CP, personal communication, 2007). Of these areas the South Slide was the only location where any piezometric data was available, and as such it was chosen as the location for the slide-specific model.

3.5.2 Cross-section

Surface topography for the South Slide cross-section was created using a 30m digital elevation model of Thompson River Valley (Figure 3 - 6). The cross-section is 10.7 km in length,

extending eastward from river level (272 mASL based on DEM data) through the southern portion of the slide to the top of Glossy Mountain (1828 mASL), a local peak assumed to be a groundwater divide (B-B', Figure 1 - 1). The cross-section was extended deep in order to capture regional flow fields. Thickness varied from over 1.7 km at the peak of Glossy Mountain, to just over 200 m at river level.

Limited borehole information provided by BGC (2005) was used to interpret the geology of the westernmost 300m of the cross-section, and the remaining 10.4 km were interpreted using surficial mapping of the area completed by Ryder (1976) (Figure 3 - 6). Descriptions of geological units in the South Slide cross-section were adapted from Ryder (1976). The cross-section incorporates six different geological units, all of which were previously defined: bedrock, fractured bedrock, diamicton till blanket (unit 6), glaciolacustrine interbedded silt and clay (unit 2), fluvial gravel (unit 4), gravelly till drift blanket (similar to unit 6) (Figure 2 - 1).

3.5.3 Hydrogeological parameter selection

Hydrogeological parameters were chosen to closely resemble those parameters used in the generalized cross-section. Initial simulations of the South Slide cross-sectional flow model showed unrealistic surface ponding when using the same hydraulic parameters for the generalized flow model. Hydraulic conductivity of the competent bedrock, fractured bedrock, and glaciolacustrine silt and clay was increased slightly compared to the generalized cross-section, to promote surface drainage within the simulation. All other hydraulic parameters remained constant between the generalized and South Slide models. The diamicton till blanket and gravelly till blanket units, equivalent to unit 6, were not included in the generalized cross-

section model. The hydraulic properties of these units were based on those of units 3 and 7, which are very similar. Hydrogeological parameters used in the South Slide model are listed in Table 3 - 5.

Table 3 - 5. South Slide cross-section hydraulic parameters.

					Van Genuchten Parameters		
Unit Description	Equivalent Unit Number	Porosity*	Specific Storage [1/m]*	Hydraulic conductivity (m/s)	α [m^{-1}] **	β **	Residual Sat. S_r **
Fluvial gravels	4	0.33	2.40E-06	1.00E-05	3.52	3.2	0.01
Gravelly till drift blanket	6*	0.4	9.80E-04	3.00E-06	0.506	1.7	0.065
Till (diamicton) blanket	6	0.4	9.80E-04	3.20E-07	0.506	1.7	0.065
Interbedded silt and clay	2	0.45	7.80E-02	3.40E-08	1.62	1.3	0.111
Fractured bedrock	-	0.1	1.40E-06	1.50E-06	1	3	0.01
Competent bedrock	-	0.05	9.90E-06	5.00E-07	1	3	0.05

*similar to unit 6, with inclusions of stratified drift and colluvium.
Van Genuchten Parameters are defined in Appendix C

3.5.4 Boundary conditions

As in the case of the generalized cross-section model, the South Slide model was run to steady state conditions considering only infiltration from precipitation over the top surface boundary, resulting in the base case simulation. Compared to the generalized cross-section a greater portion of the South Slide model surface is sloped, and more runoff is expected to occur. For this reason the rate of infiltration due to precipitation for the South Slide flow system model was 35 mm/yr (15% of the average annual precipitation), slightly less than what was assumed for the generalized cross section (40 mm/yr, 17% annual average).

A constant head boundary condition of 348 mASL was created at the location shown in Figure 3 - 6 to represent the lower of two points where Barnard Creek intersects the cross-section. Critical depth nodes were placed at Thompson River level to control flow out of the flow system model, as was the case with the generalized cross-section. An infiltration rate of 0.173 mm/yr was used in the steady state simulation to represent irrigation on surface nodes between horizontal points 8000m and 8900m (Figure 3 - 6).

3.6 Results

3.6.1 Overview

Both cross-sections were simulated to steady state conditions using two infiltration scenarios. In the first scenario only infiltration due to precipitation was considered, yielding the base case results, and in the second scenario infiltration due to irrigation was applied in addition to precipitation. Further, both models were tested for sensitivity to input variables where rates of rainfall and irrigation were varied and the simulation response was compared. Additionally, a transient simulation of the generalized cross section was completed where seasonal variations in river level, precipitation and irrigation were investigated. Results from this simulation negated the need for a transient simulation of the South Slide. In all simulations the resulting pressure head and saturation distributions are obtained for comparison.

3.6.2 Generalized cross-section, steady state simulations

Figure 3 - 7 shows the saturation conditions for the steady state simulation neglecting irrigation (the base case). Figure 3 - 8 shows the saturation condition for the steady state simulation

including irrigation. Differences between panels in Figure 3 - 7 and Figure 3 - 8 are difficult to observe graphically. However, increased saturation of the geological units is clearly visible in the unsaturated zone beneath the irrigated field in panel d of Figure 3 - 8. The area of increased saturation appears to be confined to this region only, indicating that irrigation of the benchland has limited influence within the unsaturated zone.

Depth of the saturated zone varies within the groundwater flow simulations (Figure 3 - 7 and Figure 3 - 8). Towards the upslope side the water table generally follows the upper surface of the bedrock. Moving closer to the river level the water table levels out, following the surface of the silt and clay unit. Several seepage faces are predicted on the surface near the toe of benched scarps (Figure 3 - 7 and Figure 3 - 8). These features are clearly visible amongst the sagebush scrublands found in Thompson River Valley as isolated areas of lush vegetation, and occasional stands of trees at low elevation. Figure 3 - 9 is a photograph of one of the many seepage faces found in Thompson River Valley.

The presence of seepage faces in Thompson River Valley was interpreted as support for the selection of the rate of infiltration applied at the surface boundary of the cross-section. As previously discussed, a rate of infiltration of 17% of the mean annual precipitation was used along the surface boundary. This number, which was determined through discussion in the 1986 court case (Wallace, 1987), accurately predicts the locations of seepage faces in the valley. In the sensitivity analysis presented in a later section the infiltration rate is increased and decreased, resulting in an inaccurate representation of the seepage faces in the valley. This supports the rate of infiltration determined in the court case (Wallace, 1987) and provides justification for use of this value in the groundwater simulation.

The pressure head distributions predicted by the groundwater simulation for the steady state simulation neglecting irrigation is provided in Figure 3 - 10. This figure demonstrates the presence of elevated pore pressures below the surface at the base of the valley. In the downslope region of the cross-section pressures are found to significantly exceed the ground surface elevation at depth, indicating the presence of strong artesian conditions. Within the lower glaciolacustrine silt and clay (unit 2) at the interface with fractured bedrock artesian conditions reach a maximum of 68 m above ground surface. This value decreases upwards through the silt and clay unit. The pressure head distribution for the case where irrigation is included is not shown because no graphical differences are observed between the two scenarios.

Artesian pressures in Thompson River Valley may not be this high in reality. Flowing wells were drilled at the base of the valley (BGC, 2005). Calculation of the artesian pressure at these wells is dependent upon the hydraulic properties of the soil, the length of the well screen (if any). In most cases the artesian conditions were noted during drilling, and these parameters are not known. We cannot calculate an exact artesian pressure with such limited information. Instead, the groundwater flow model should be taken as an approximation of the groundwater conditions in Thompson River Valley based on a balance of probabilities approach.

3.6.3 Generalized cross-section, transient simulation

The steady-state simulation does not provide an indication of the simulated flow system response to variable boundary conditions. Although only slight differences could be found between the steady state simulations, variability in boundary conditions may have a greater impact on flow system dynamics. For this reason a 20-year transient simulation was completed where the

HydroGeoSphere model was run with fluctuating boundary conditions (precipitation, infiltration, river level) as described previously. The base case simulation results neglecting irrigation were used as an initial condition for the transient simulation. Saturation distributions from various output times during the transient simulation are displayed in Figure 3 - 11. Almost no observable change in saturation occurs over the progression of the transient analysis, except in the unsaturated zone directly beneath the irrigated field. The same can be said for the pressure head distribution over the cross-section.

No visible change in saturation occurs within in the glaciolacustrine silt and clay despite variation in the river level over the course of the transient simulation. This is likely attributed to the fact that these materials are so impermeable that they remain uninfluenced by seasonal fluctuations in the river stage. Very slight numerical differences between the hydraulic head distribution at river level for the base case and the transient simulation are observed.

The relation between hydraulic head and depth was explored for a slice directly adjacent to the river (x = 2675, shown in Figure 3 - 4) in the generalized groundwater simulation at various times in the transient analysis and for the base case. The vertical pressure profile is shown for various times in the transient simulation in Figure 3 - 12. In the figure negative values indicate a reduction in pore pressure between the base case and the transient simulation, and positive values indicate areas where pore pressures have increased in the transient simulation compared to the base case.

In contrast to the findings of Eshraghian et al. (2005) these results show that variability in river stage has no significant affect on pore pressures within the glaciolacustrine silt and clay after 20 years of transient fluctuation. In the silt and clay unit maximum deviation from the base case

that was noted in the transient simulation amounted to an increase in head of less than one centimeter. This was only noted within the area of the subsurface directly adjacent to the river. The influence of the river boundary sharply decreases from this point, with almost no change occurring in the glaciolacustrine silt and clay unit. The transient simulation has a greater, although still negligible, impact on the fractured bedrock and intact units. In these units the maximum change (reduction) in pore pressure was less than 6 cm.

Results also show that the transient response of the model is felt greater at depth (i.e. within the bedrock), indicating that the transient application of precipitation has a greater impact on the pore pressure distribution compared to irrigation or variation in river stage.

3.6.4 Generalized flow system cross-section, sensitivity analysis

Future climate change in the Thompson Valley area may influence regional groundwater flow characteristics by changes in precipitation and temperature, which may affect landslide activity. Similarly, current farming practices on the benchlands above Thompson River may change in the future. For these reasons it is prudent to test the sensitivity of the groundwater flow system against scenarios involving alternate rates of infiltration. Four additional scenarios that considered variable rates of precipitation and irrigation were tested, and ran to steady-state conditions. Details regarding the various infiltration scenarios are provided in Table 3 - 6.

Table 3 - 6. Infiltration scenarios for generalized cross-section.

	Rate of Infiltration (m/yr)	
	Precipitation	**Irrigation**
No irrigation steady-state	0.04	0
Irrigation steady-state	0.04	0.173
Scenario I	0.02	0
Scenario II	0.08	0
Scenario III	0.04	0.0865
Scenario IV	0.04	0.346

The first infiltration scenario (scenario I) involved decreasing the infiltration due to precipitation from 0.04 m/yr to 0.02 m/yr (a 50% reduction). The second infiltration scenario (scenario II) involved increasing the precipitation from 0.04 m/yr to 0.08 m/yr (a 100% increase). Infiltration due to irrigation was not considered in scenarios I and II in order to monitor the degree to which precipitation affects the steady-state model conditions. The third scenario (scenario III) involved decreasing the infiltration due to irrigation from 0.173 m/yr to 0.0865 m/yr (a 50% decrease). The fourth scenario (scenario IV) involved increasing the infiltration due to irrigation from 0.173 m/yr to 0.346 m/yr (a 100% increase). For scenarios III and IV, the rate of infiltration due to precipitation was kept constant at 0.04 m/yr.

Saturation profiles for the four scenarios are provided in Figure 3 - 11. Examining the saturation profiles it is apparent that the four scenarios have varying degrees of influence on the unsaturated zone, and a marked change on the height of the water table and location of seepage faces. Scenario I is clearly the driest of all scenarios. In the uppermost surface till zone, for example, the saturation has been reduced approximately 12% compared to the base case. Additionally, scenario I shows the disappearance of the uppermost seepage face and draining of the bedrock at higher elevations, indicating a general lowering of the water table. Conversely, scenario II

shows the wettest conditions observed in the sensitivity analysis. Thickening of the seepage faces is pronounced to the point where the lower reaches of the model are almost near complete saturation and the overall height of the water table is visibly greater than the base case. Scenarios III and IV, measuring irrigation sensitivity, demonstrate less deviation from the base case over most of the flow system domain. Saturation is slightly elevated in the region directly below the zone of irrigation. The water table has been slightly elevated in this area, especially in scenario IV.

The model response to changes in irrigation and precipitation was expected. Increasing the precipitation by a factor of two results in a greater volume of water being applied compared to increasing the irrigation by the same multiplier, resulting in overall greater saturation. As such, it is essential to normalize the results for comparative purposes.

In order to normalize the analysis of model results three points within the flow system cross-section were selected and their pressure heads were compared. These points are located within the saturated zone upslope (Point 1, horizontal 1250 m, elevation 440 m), directly beneath (Point 2, horizontal 1950 m, elevation 350 m), and downslope (Point 3, horizontal 2400 m, elevation 280 m) of the zone of irrigation (shown in Figure 3 - 4).

Normalized sensitivity coefficients at these locations were calculated by the following formula (Dr. Neil Thompson, University of Waterloo, personal communication):

$$S_n = \frac{dP}{d\alpha} \cdot \frac{\alpha}{P} \qquad (3-2)$$

where P represents the pressure head at a given location, dP represents the change in observed pressure head between the base case and a given scenario at the same location, α represents the

perturbed parameter (either rainfall or irrigation), and $d\alpha$ represents the change in the perturbed parameter compared to the base case.

Results of the sensitivity analysis are shown in Table 3 - 7. Pressure heads were generally most sensitive to changes in precipitation especially in upslope regions. Irrigation had very little impact over the flow system domain except where irrigation was being applied. Pressure heads in the downslope region appear to be insensitive to both changes in precipitation and irrigation. This is likely a result of the low permeability of the glaciolacustrine silt and clay, which was fully saturated in the base case. Additional water may run off the surface or find a lower flow path when it encounters an impermeable unit such as the silt and clay.

The concept of water finding a lower flow path is intriguing because forcing additional water underneath the impermeable unit may lower the effective stress state of the slope, affecting slope stability. An area of higher pressure may be generated by the presence of the impermeable unit, leading to upward groundwater flow through this unit. The resulting increase in the groundwater pore pressure lowers the effective stress state of the slope. This is discussed further in Chapter Four.

To determine the path of water in the flow system, particle tracking was used. Figure 3 - 8 shows the local groundwater flow paths for the simulation where irrigation was considered. In this case all irrigation water traveling through the unsaturated zone ultimately discharges through the uppermost seepage face. What is not shown by the flow lines is the reentry of water at the seepage faces. This behaviour is shown in the plot of flux along the surface boundary (panel b of Figure 3 - 8). In this figure seepage faces appear as a red line indicating strong discharge directly above a blue line indicating strong recharge. Surface water depths are also shown in Figure 3 - 8 (panel a). No significant ponding occurs, except within the Thompson River area.

Table 3 - 7. Normalized model sensitivity to precipitation and irrigation.

	Approx. Normalized Sensitivity Coefficient		
	Beneath zone of irrigation	Upslope of irrigation	Downslope of irrigation
Precipitation only			
Scenario I	0.133	0.383	0.009
Scenario II	0.1	0.716	-0.008
Irrigation			
Scenario III	0.002	0	0
Scenario IV	0.136	0	-0.003

3.6.5 South Slide model, steady-state simulations

Figure 3 - 13 and Figure 3 - 14 show the saturation distribution for the base case South Slide steady state simulations. At first glance one may notice the jagged appearance of the interface between saturated and unsaturated regions in the deep bedrock. This phenomenon is a relic of the coarse grid discretization that was specified for this area during construction of the model flow system. A constant number of vertical divisions is kept for the rectangular elements in the bedrock. As the bedrock thickness decreases towards the slide area the grid spacing decreases, refining the grid. Coarse discretization in the deep bedrock is not anticipated to impact the overall results. It should also be noted that vertical exaggeration of this figure amplifies the appearance of coarse grid discretization.

The saturated zone ranges considerably in depth along this cross section. Towards the peak of Glossy Mountain the water table is over 1.2 km deep and gradually slopes towards Thompson River. Thick unsaturated zones as predicted by the model are characteristic of flow regimes in semi-arid mountain areas, such as those found at Yucca Mountain (Wang and Bovardsson, 2003;

McLaren et al., 2000). Several seepage faces are again produced in the lower region of the model domain where almost all subsurface materials are fully saturated.

Pressure head distribution for the base case South Slide simulation is shown in Figure 3 - 15. As was the case with the generic cross-section, elevated pore pressures are predicted at the depth within the glaciolacustrine clay, fractured bedrock, and bedrock units, near Thompson River in the lower region of the South Slide cross-section. This indicates the presence of artesian conditions in this area. Within the glaciolacustrine silt at the interface with the fractured bedrock artesian conditions reach a maximum of 34 m above ground surface. This value decreases upwards through the silt and clay unit.

3.6.6 South Slide model sensitivity analysis

The various infiltration scenarios used in the sensitivity analysis of the generalized cross-section were repeated for the South Slide cross-section (Table 3 - 8). Results for the South Slide area show similar trends to the generalized cross section. Pressure head was measured at three observation points and was again considered for the South Slide sensitivity analysis. These are located just beneath the saturated zone upslope (Point 1 in Figure 3 - 6), directly underneath (Point 2 in Figure 3 - 6) and downslope (Point 3 in Figure 3 - 6) of the zone where irrigation was applied. The first two observation points are situated within the bedrock unit, and the downslope observation point is located in the glaciolacustrine silt and clay. Results from the sensitivity analysis are provided in Table 3 - 9. The flow system pressure head was again more sensitive to precipitation compared to irrigation. In the areas beneath the zone of irrigation and upslope of

irrigation (i.e. – in the bedrock) pressure heads were much more sensitive to precipitation, with most areas showing near double sensitivity to the parameter compared to irrigation.

Similarities exist between sensitivity scenarios III and IV, where irrigation was considered. The area where pressure head was most sensitive to changes in irrigation was located directly beneath the zone of irrigation. This was consistently more than twice as sensitive to changes in irrigation compared to the upslope observation location (Point 1), which in turn was more than twice as sensitive to the downslope observation location (Point 3).

Patterns emerging from the sensitivity analysis can be explained in geological terms. The downslope observation point (Point 3) was located within the less permeable glaciolacustrine silt and clay, whereas the other two observation points were located within the more permeable bedrock. Comparing the two observation points located in bedrock (Points 1 and 2), the observation point directly beneath the source of irrigation (Point 2) was obviously more sensitive than the upslope location (Point 1) due to its location with respect to the irrigated field.

Table 3 - 8. Infiltration scenarios for South Slide.

	Rate of Infiltration (m/yr)	
	Precipitation	**Irrigation**
No irrigation steady-state	0.035	0
Irrigation steady-state	0.035	0.173
Scenario I	0.0175	0
Scenario II	0.07	0
Scenario III	0.035	0.0865
Scenario IV	0.035	0.346

Table 3 - 9. Results of pressure head sensitivity analysis.

	Approx. Normalized Sensitivity Coefficient		
	Beneath zone of irrigation	Upslope of irrigation	Downslope of irrigation
Precipitation only			
Scenario I	1.576	1.284	0.202
Scenario II	0.728	0.702	0.093
Irrigation			
Scenario III	0.165	0.049	0.026
Scenario IV	0.462	0.122	0.108

Saturation distributions for all cases are shown in Figure 3 - 16. The saturation distribution for the scenario I where precipitation was halved showed significantly drier conditions. The water table is lowered considerably over the model domain, and is prevented from continuing further by the constant head condition at Barnard creek. The uppermost seepage face has disappeared and the saturation of the silt and clay unit has reduced in its upper regions compared to the base case.

Conversely, for the case where precipitation was doubled (scenario II) the resulting saturation distribution was noticeably wetter and the water table significantly elevated throughout the model domain. Infiltration pathways through the unsaturated zone have become visible in scenario II, as indicated by streaks of increased saturation (Figure 3 - 16). Seepage faces in this scenario are markedly thicker. The surface of the saturated zone is obviously influenced by irrigation in scenarios III and IV. Significant water table mounding and increased saturation in the unsaturated zone are noted beneath the zone of irrigation in these scenarios, especially in scenario IV.

As with the steady state pressure-head distribution (Figure 3 - 15), changes between the various scenarios are not possible to discern visually. Based on the results of the sensitivity analysis the pressure head is expected to increase with the addition of water to the model domain. The relative change in pressure head would be greater over most of the cross-section domain for the addition of precipitation compared to irrigation.

Regional paths for the South Slide cross-section are given in Figure 3 - 13 and Figure 3 - 14. Slope-scale flow paths for the South Slide cross-section are given in Figure 3 - 17. Similar behaviour to the generalized cross-section is noted in the flow patterns observed in the South Slide area. Water that infiltrates in the upper reaches of Glossy Mountain is channelled directly downward, through the bedrock, ultimately discharging at one of the seepage faces, or beneath Thompson River. Water that is originally applied at the zone of irrigation migrates downward through the bedrock, then horizontally across the top of the less permeable glaciolacustrine silt and clay before discharging at the constant head boundary representing Barnard Creek. Figure 3 - 13 and Figure 3 - 14 also show the surface water depths and exchange fluxes. Some slight ponding is shown in one of the downslope seepage faces, as well as within Thompson River.

3.7 Discussion and conclusions

Groundwater flow fields play an important role in controlling slope stability problems by influencing effective stresses in a slope (Reid and Iverson, 1992). The geological setting is an important consideration in slope stability problems, not only from the perspective of relative shear strength of the materials involved, but also because it can strongly influence regional groundwater flow fields (Hodge and Freeze, 1977). The landslides south of Ashcroft, British

Columbia are believed to be strongly related to pore pressures generated by local groundwater flow fields; however very little data exists to either support or contest this idea (Porter et al, 2002). In the absence of groundwater data we rely on two-dimensional flow models based on two well defined geological cross-sections to explore the influence of local and regional groundwater flow on slope stability. Several conclusions can be made that apply to both the generalized and South Slide cross-sections.

(1) The glaciolacustrine silt and clay unit (unit 2) found near the valley bottom is important in controlling groundwater flow patterns. Based on particle tracks preferential flow paths are developed that channel water in two directions around this unit, likely due to its low permeability and interbedded nature. As water infiltrating from directly above encounters unit 2 it is redirected horizontally towards the slope, reinforcing seepage faces on the surface. Water that originates further upslope is channelled underneath unit 2, through either the bedrock or more permeable fractured bedrock, and migrates upwards to the surface closer to river level. Both of these mechanisms are anticipated to have a negative impact on slope stability by increasing pressure heads, thereby lowering effective stresses in the slope.

(2) The regional flow regime is capable of generating elevated pore pressures in the glaciolacustrine silt and clay, fractured bedrock, and bedrock units in the lower region of the valley near Thompson River. Hydraulic heads in these areas in both models were elevated above ground surface. The generalized cross-section simulations showed maximum artesian conditions in the glaciolacustrine silt and clay (unit 2) of 68 m above ground surface. The South Slide cross-section simulation showed maximum artesian conditions in the glaciolacustrine silt and clay (unit 2) of 34 m above ground surface. In both cases the maximum value was in the lower portion of unit 2 near the interface with fractured bedrock. This simulated finding

corresponds with the flowing artesian conditions known to occur in the area (BGC, 2005). Further, this agrees with the groundwater flow fields in mountainous areas simulated by Hodge and Freeze (1977). Artesian pressures in Thompson River Valley may not be exactly as predicted by the groundwater simulations. However, the results indicate the presence of artesian pressures, as suggested by limited field observations, and are thought to demonstrate the behaviour of groundwater flow fields.

(3) The effect of irrigation is minimal in terms of pressure head sensitivity. However, this does not directly translate to slope stability. As shown in conclusion (1), additional infiltration from directly above the slope is channelled outwards to the seepage face, contributing to increased groundwater flow in this part of the slope. In a fragile system such as Thompson River Valley where slopes are continuously on the verge of failure small additions to the groundwater system may be enough to increase pressure heads enough to trigger slope movement.

(4) Pore pressures within the glaciolacustrine silt and clay are not significantly affected by fluctuation of the Thompson River stage. Maximum change in pressure head observed throughout the simulation within this unit was less than one centimetre.

(5) Climate change within Thompson River Valley may have a significant impact on the local groundwater flow regime. Pressure heads were shown to be sensitive to changes in precipitation. In an area where slopes are intrinsically unstable small increases in precipitation may have a negative consequence on slope stability. Conversely, should the future climate of Thompson River Valley become drier this would result in more stable conditions. Although a slight increasing trend in precipitation has been noted for the nearby Kamloops area over the past century this has not been correlated to slope movement activity (Porter et al, 2002). In

addition to considering long-term trends in precipitation it would also be useful to consider changes in precipitation characteristics in terms of intensity and duration.

In the next chapter we attempt to bridge the gap between the results of groundwater modeling and slope stability analysis.

Figure 3 - 1. Photograph taken from atop the North Slide (shown in Figure 1-1). Hummocky terrain of the north slide debris is visible in the foreground. The Goddard (1982) landslide is outlined in the dashed line. Directly opposite Thompson River from the Goddard slide is the Ashcroft (CN 53.4) slide.

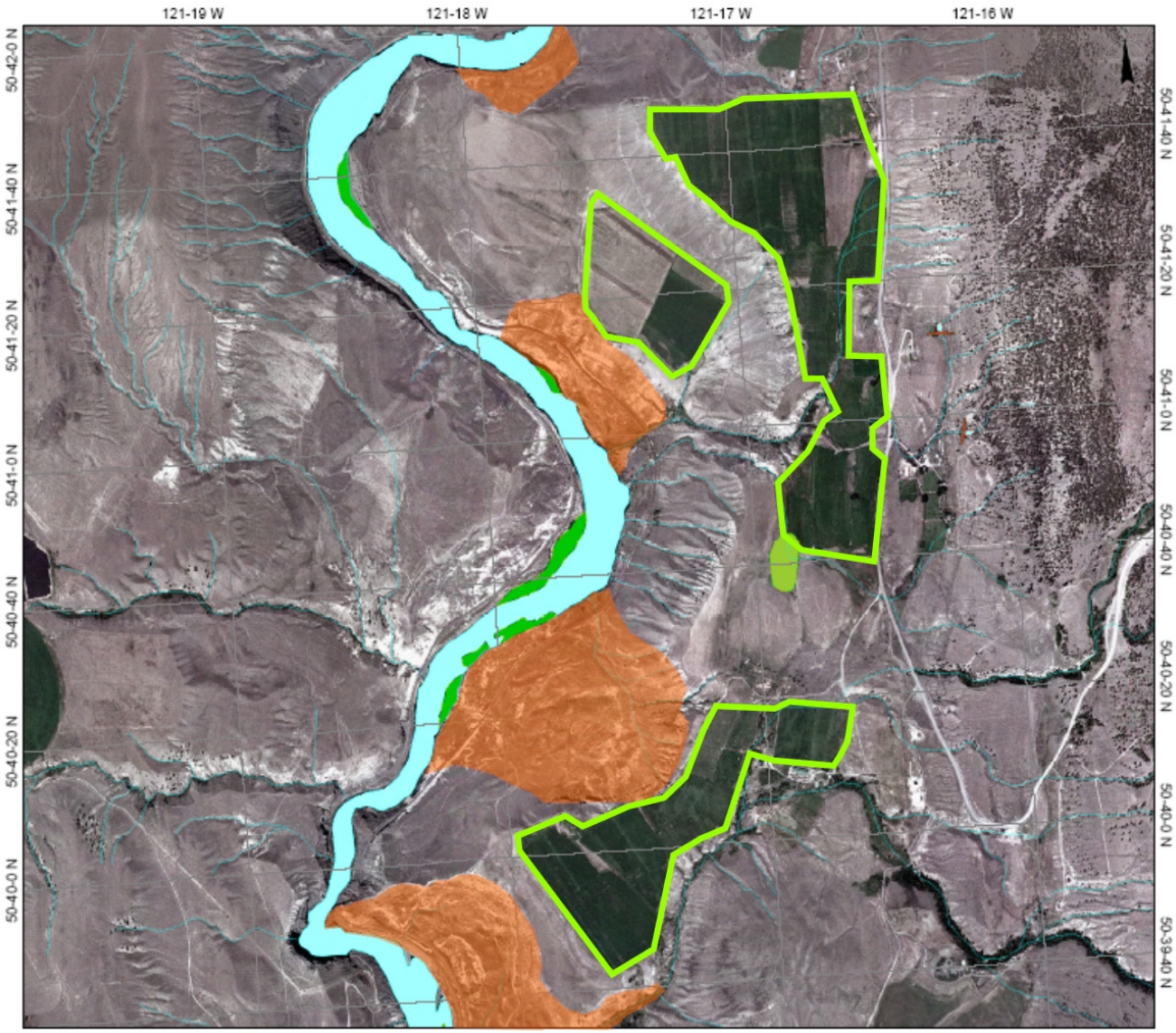

Figure 3 - 2. Aerial photograph showing physical setting of landslides and irrigated fields. Location of this photo is shown in the dashed box in Figure 1-1. Landslides are shaded in orange, irrigated fields are outlined in green.

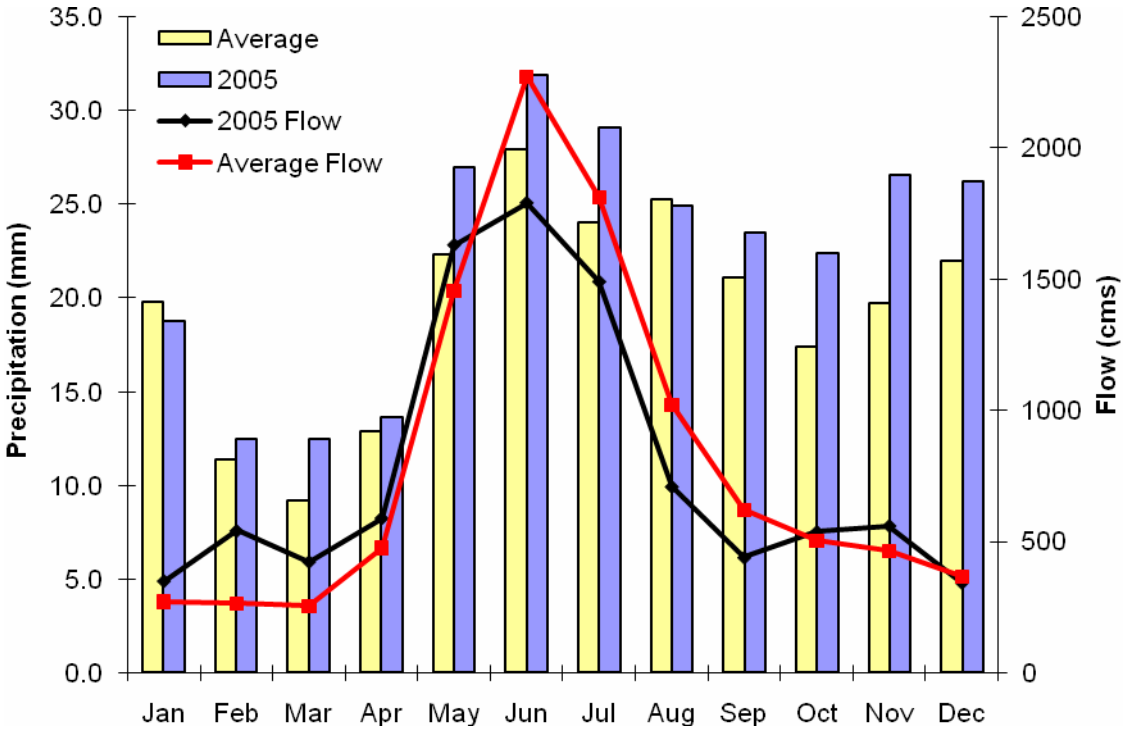

Figure 3 - 3. Average monthly precipitation and Thompson River flow compared to 2005 values. These data are based on Environment Canada monitoring stations listed in Table 3 - 3.

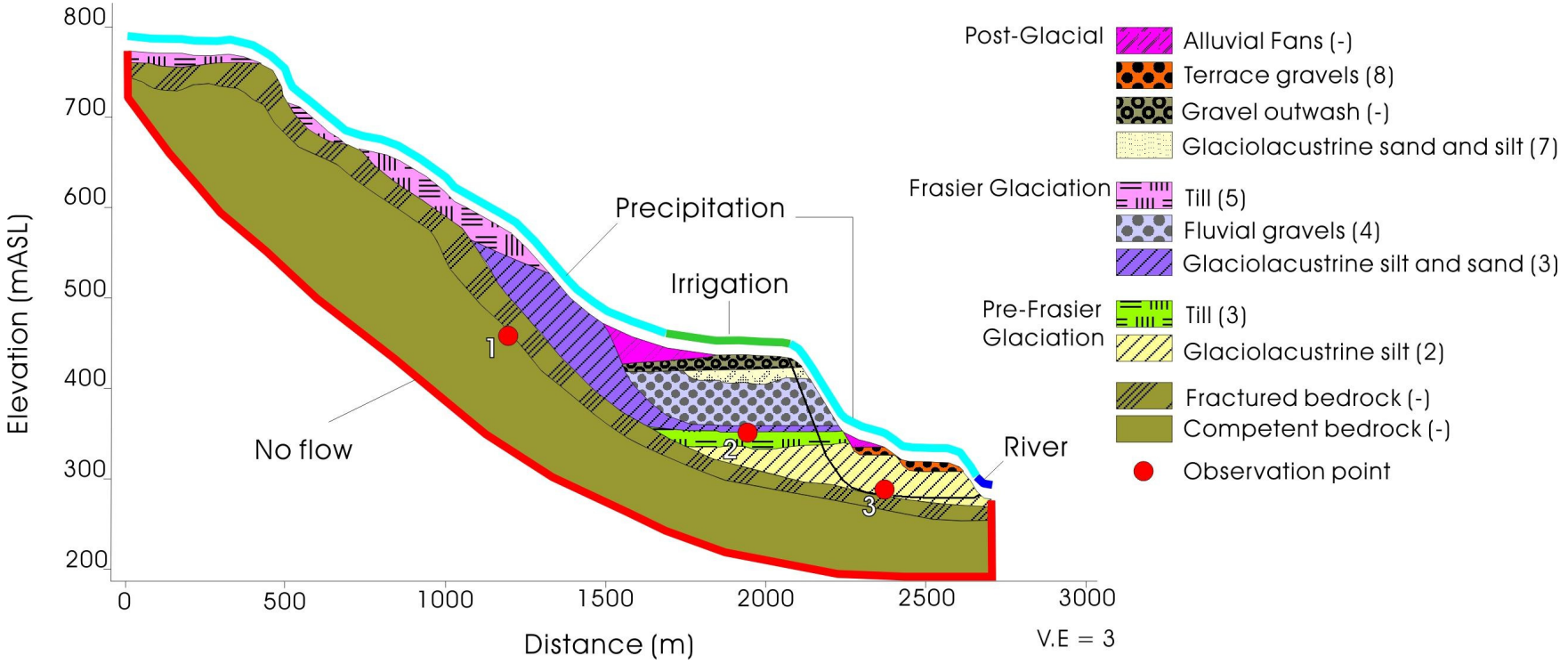

Figure 3 - 4. Generalized cross-section of Thompson River Valley used in HydroGeoSphere model. Boundary conditions and observation locations for sensitivity analysis are shown. A typical failure surface (black line) is shown. Geology based on Ryder (1976, Figure 11)

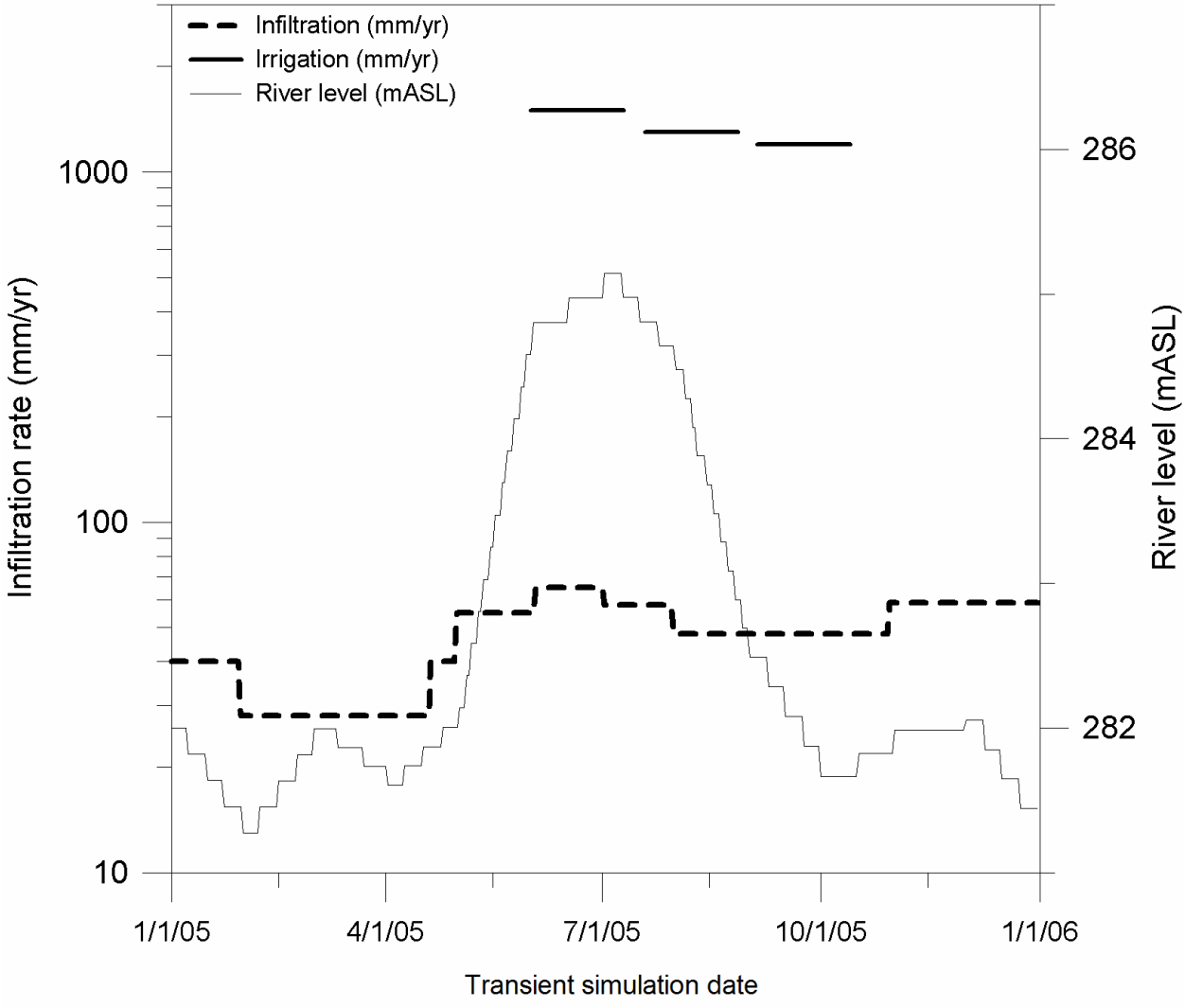

Figure 3 - 5. Annual variation in river level, infiltration, and irrigation used in the transient simulation.

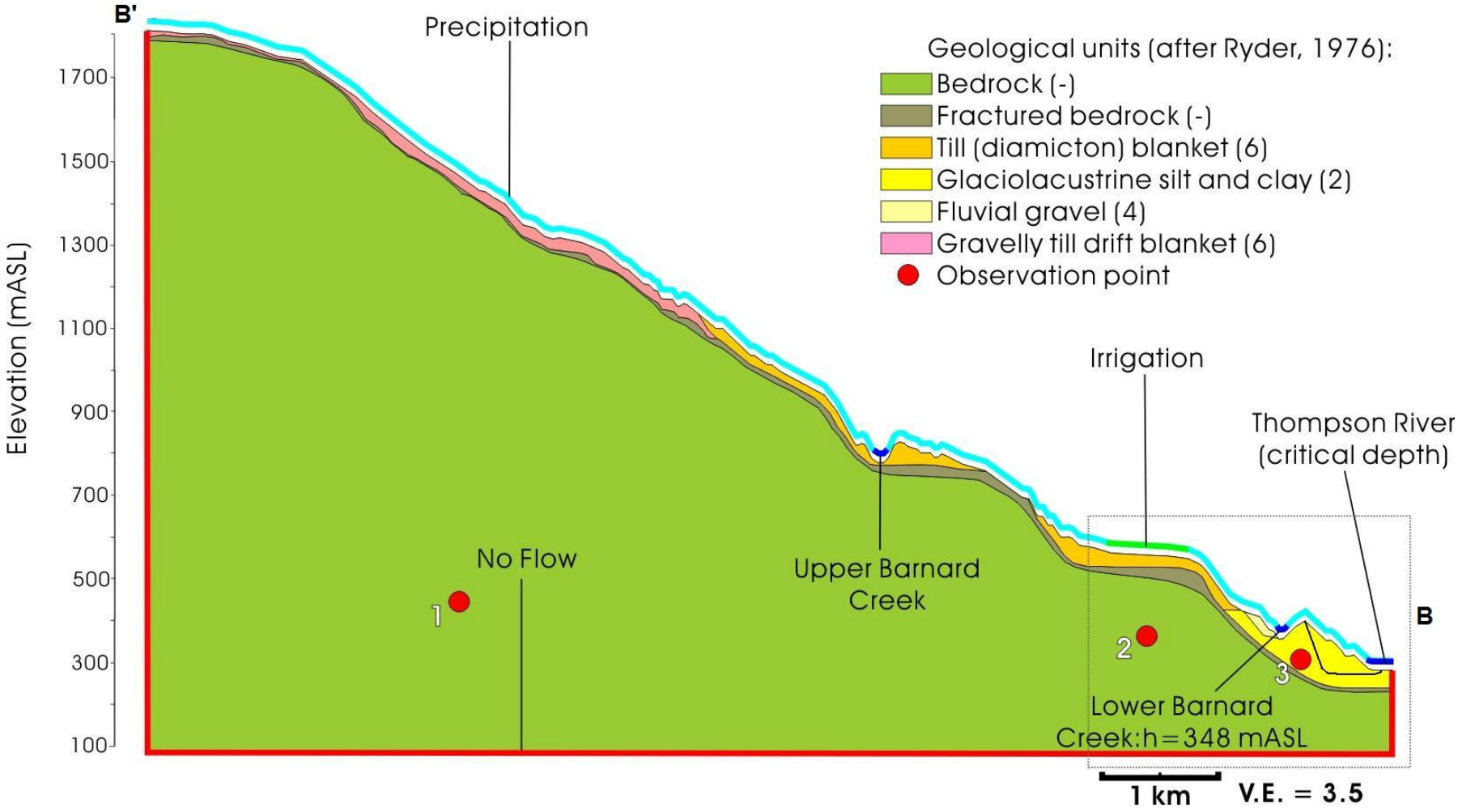

Figure 3 - 6. Geological cross-section of South Slide. Boundary conditions and observation locations used in the sensitivity analysis are shown.

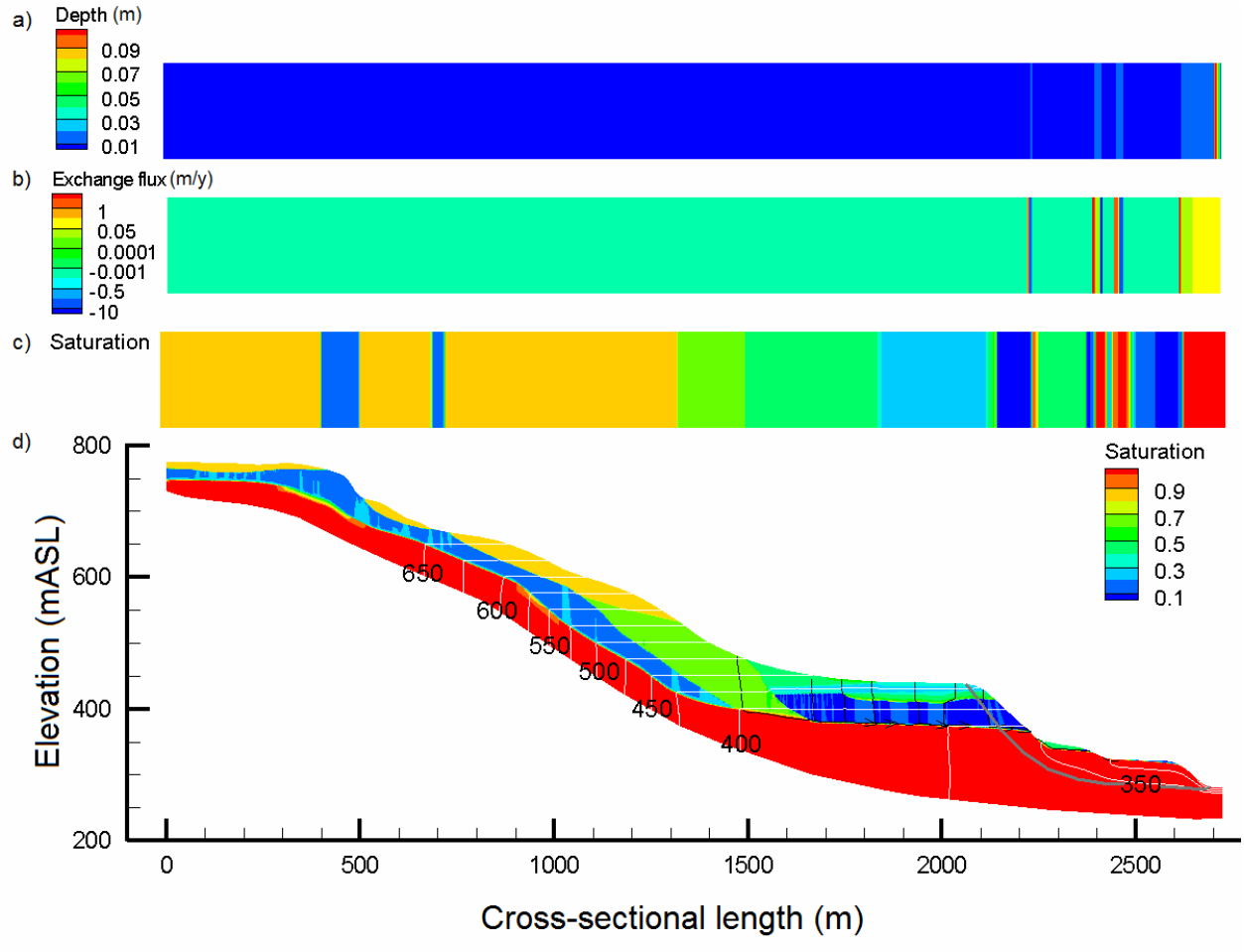

Figure 3 - 7. Steady state saturation distribution of the generalized cross-section neglecting irrigation. The red areas indicate full saturation. (d) Particle tracks (black lines) showing the generalized cross-sectional groundwater flow regime. White lines are the total hydraulic head contours labelled in 50 m intervals. The failure surface is shown (grey line). Top-view sections showing a) water depth; b) surface exchange flux; and c) saturation. Note the exchange flux in panel b showing the outflow (red bands) and immediate inflow (blue bands) of the seepage faces. Vertical exaggeration of panel d is 1.7.

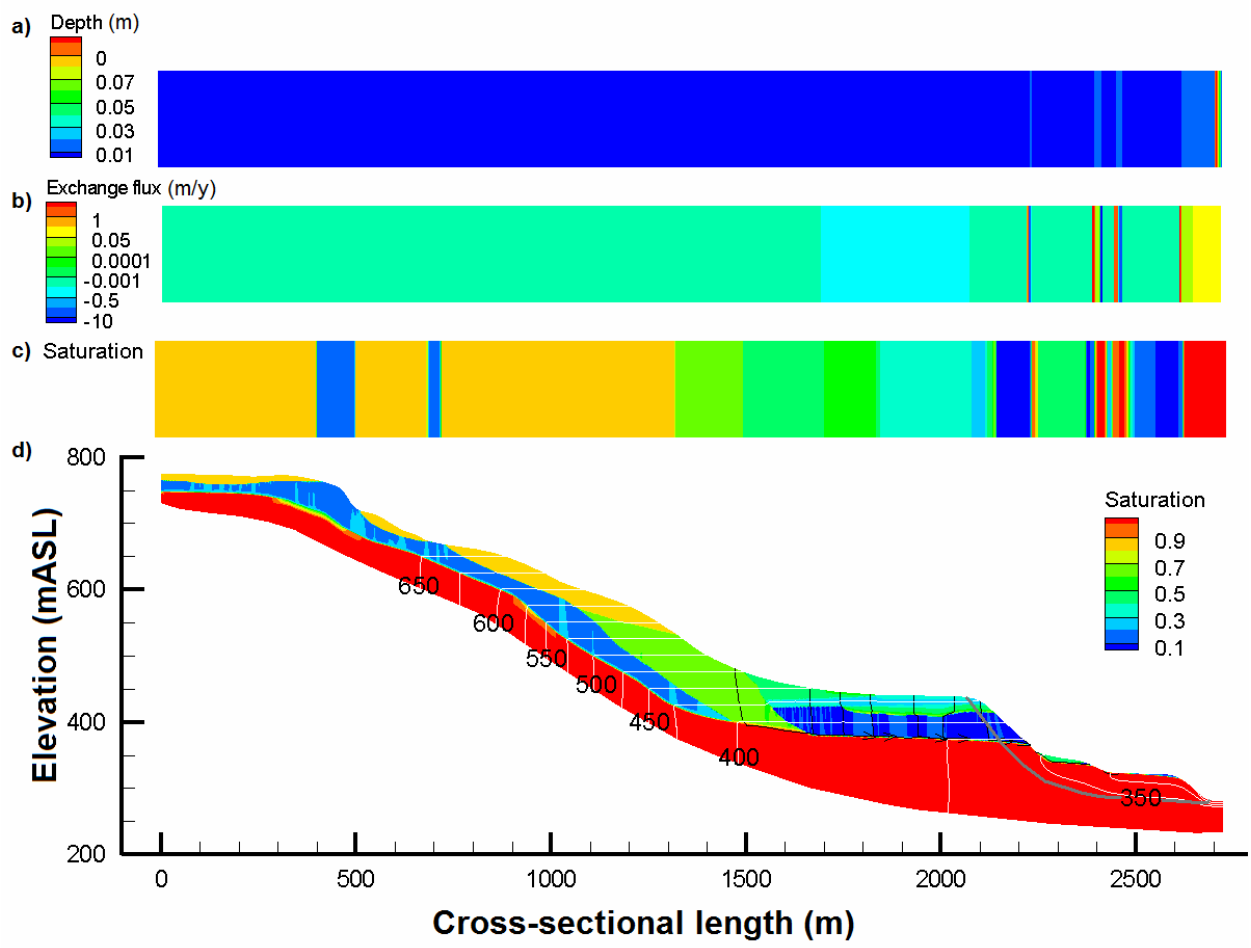

Figure 3 - 8. Steady state saturation distribution of the generalized cross-section including irrigation. The red areas indicate full saturation. (d) Particle tracks (black lines) showing the generalized cross-sectional groundwater flow regime. White lines are the total hydraulic head contours labelled in 50 m intervals. The failure surface is shown (grey line). Top-view sections showing a) water depth; b) surface exchange flux; and c) saturation. Note the exchange flux in panel b showing the outflow (red bands) and immediate inflow (blue bands) of the seepage faces. Vertical exaggeration of panel d is 1.7.

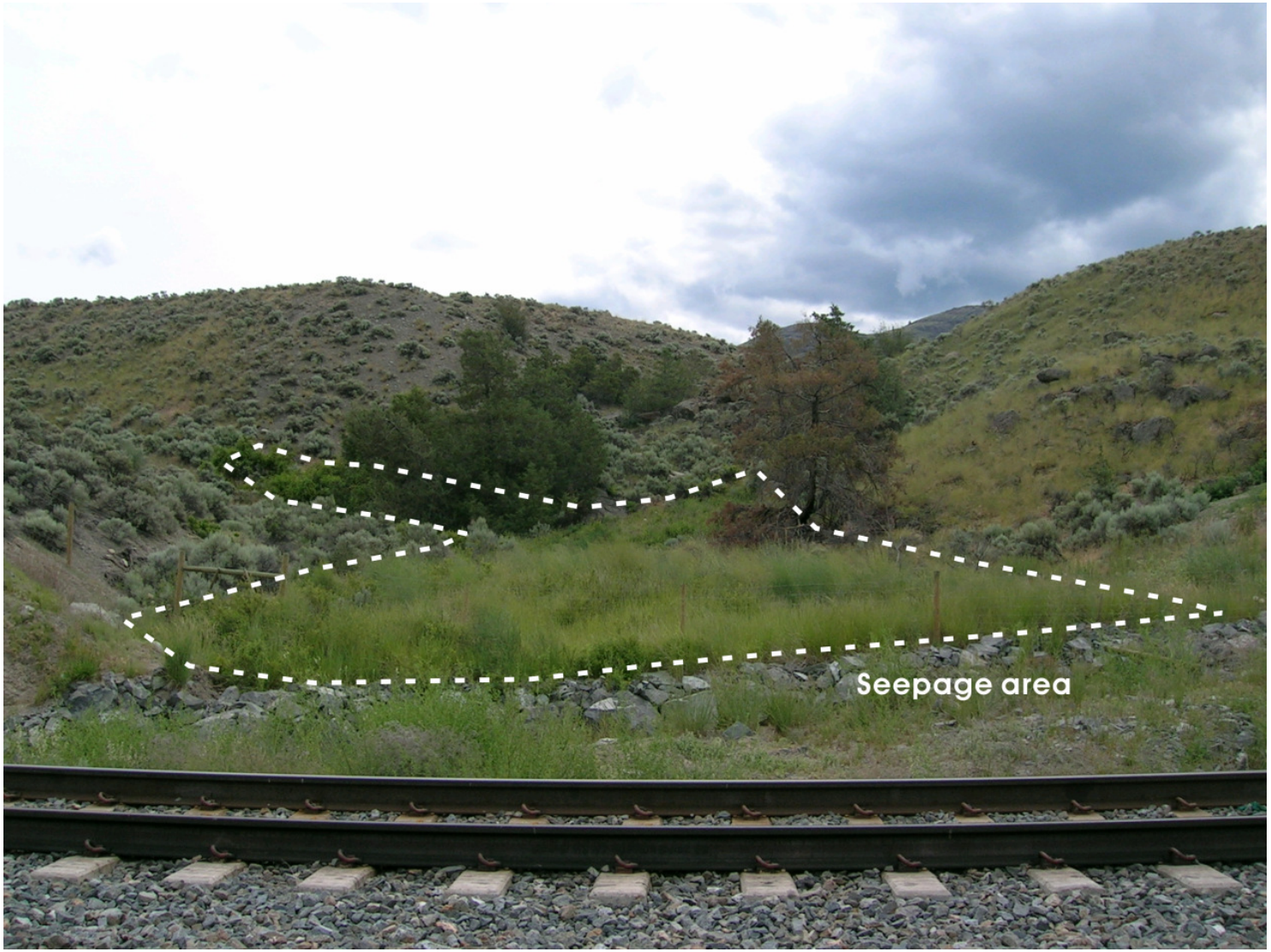

Figure 3 - 9. Seepage face in Thompson valley, June, 2007.

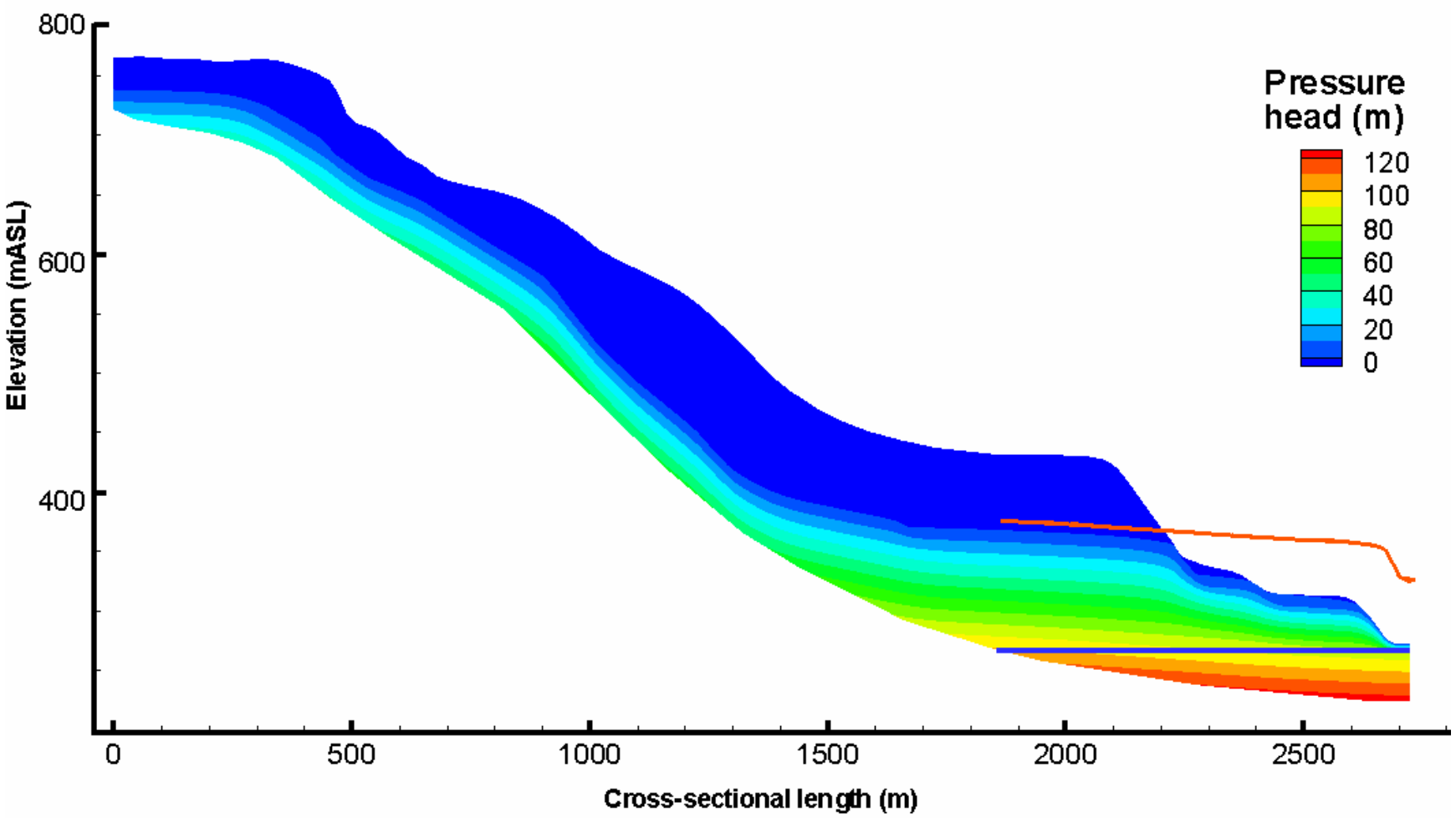

Figure 3 - 10. Pressure head distribuation of the slope scale generalized cross-section for a) the case where irrigation was neglected (base case). Results for the case where irrigation was included are identical in appearance at this resolution. The red line shows the potentiometric surface given along the horizontal (dark blue) line at Z=277m, roughly the elevation of the bottom of the silt and clay unit. Note that the red line is well above ground surface for the lower part of the cross section, indicating artesian conditions. Vertical exaggeration is 2.5.

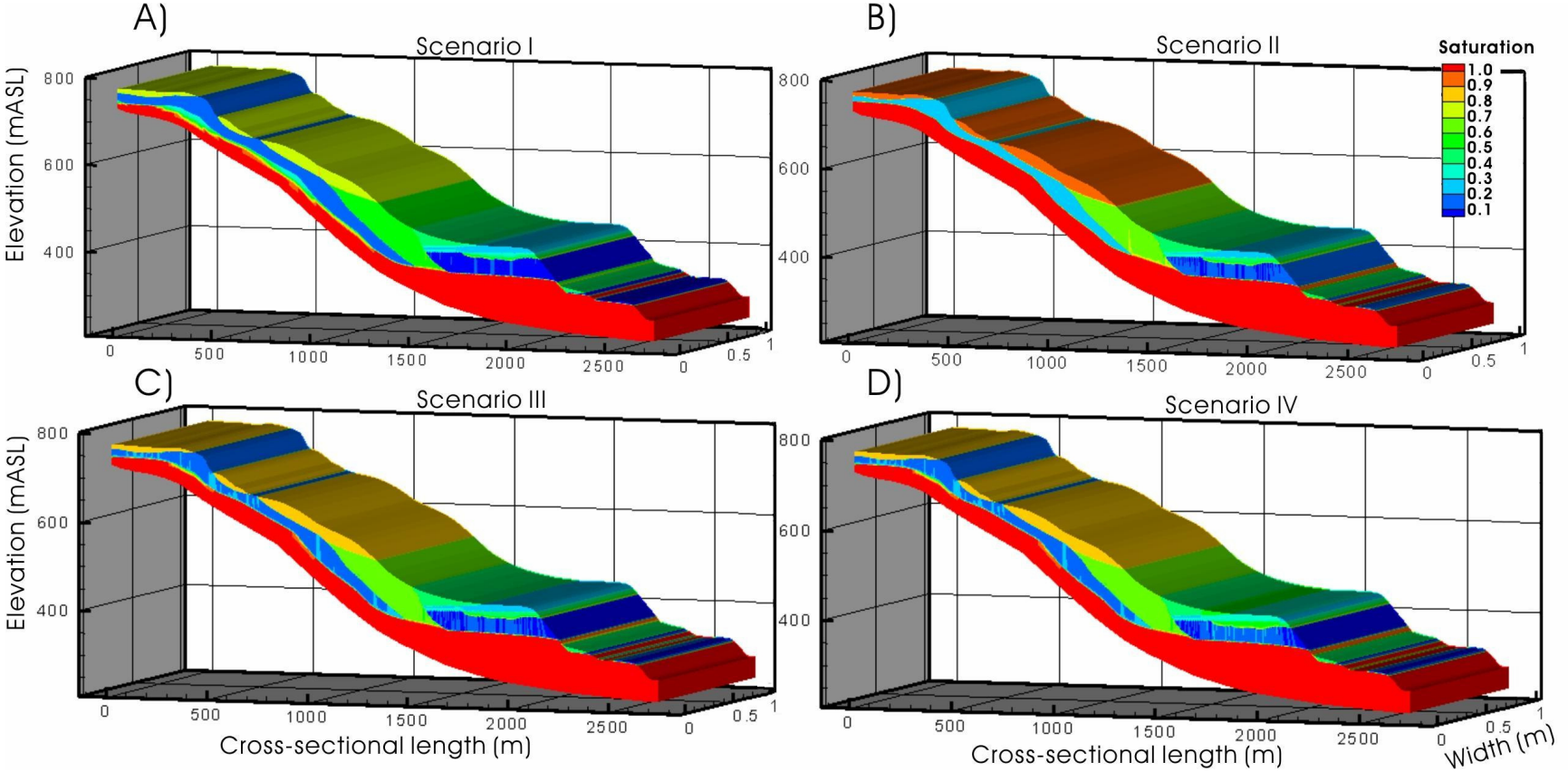

Figure 3 - 11. Saturation profiles of the generalized cross-section for various precipitation and irrigation scenarios. A) Scenario I: half precipitation, B) Scenario II: double precipitation, C) Scenario III: half irrigation, and D), double irrigation.

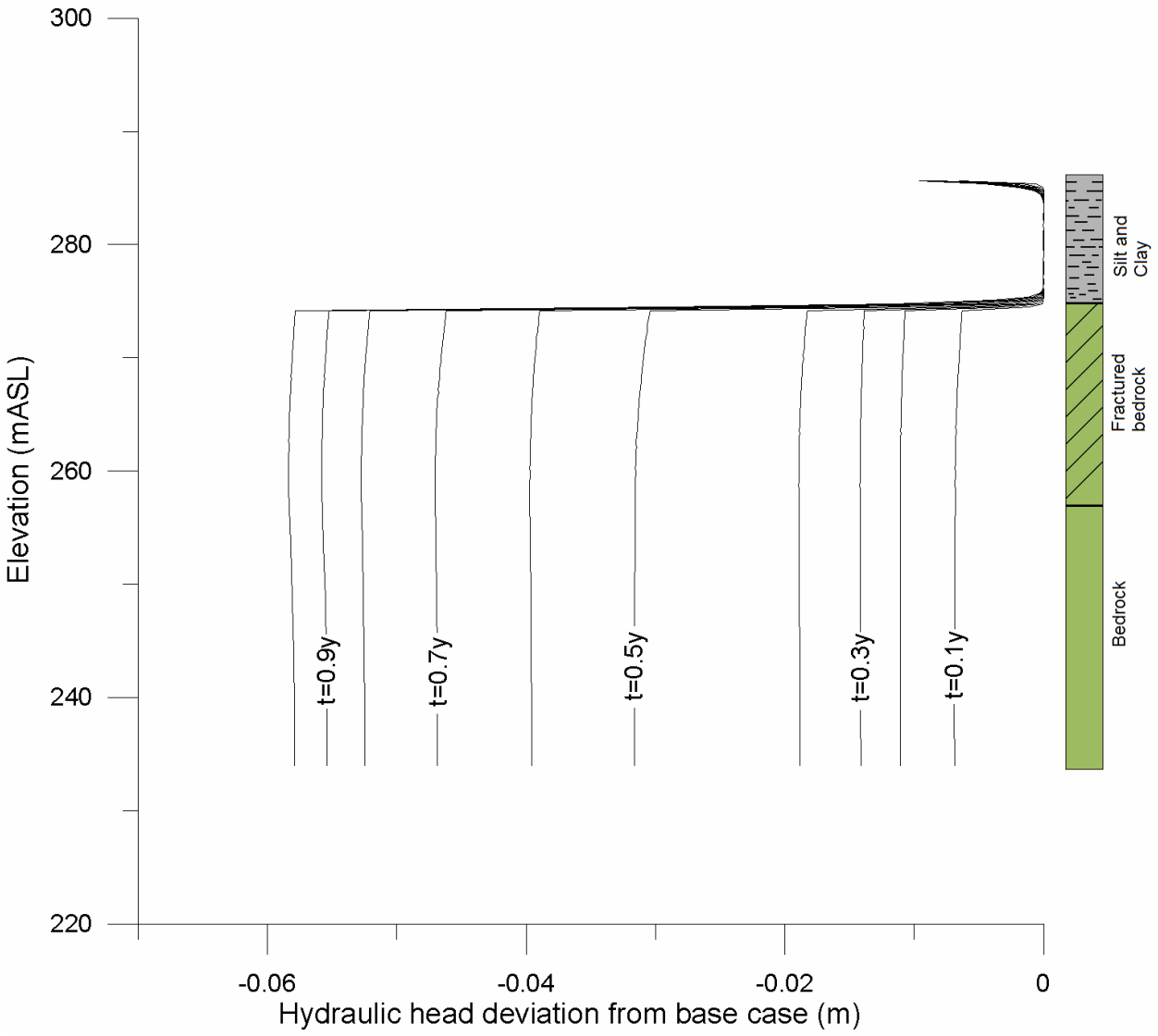

Figure 3 - 12. Progression of pressure head differences between the transient simulation and the base case along a slice taken adjacent Thompson River throughout a one year simulation. The uppermost region shows change in the pressure head within the glaciolacustrine silt and clay (approx. 275-285mASL), the mid section (approx. 260-275 mASL) shows the change in the pressure head in the fractured bedrock, and the lower section (approx. 234-260 mASL) shows the change in the pressure head in the bedrock. Labels indicate the position in time where the profile was observed.

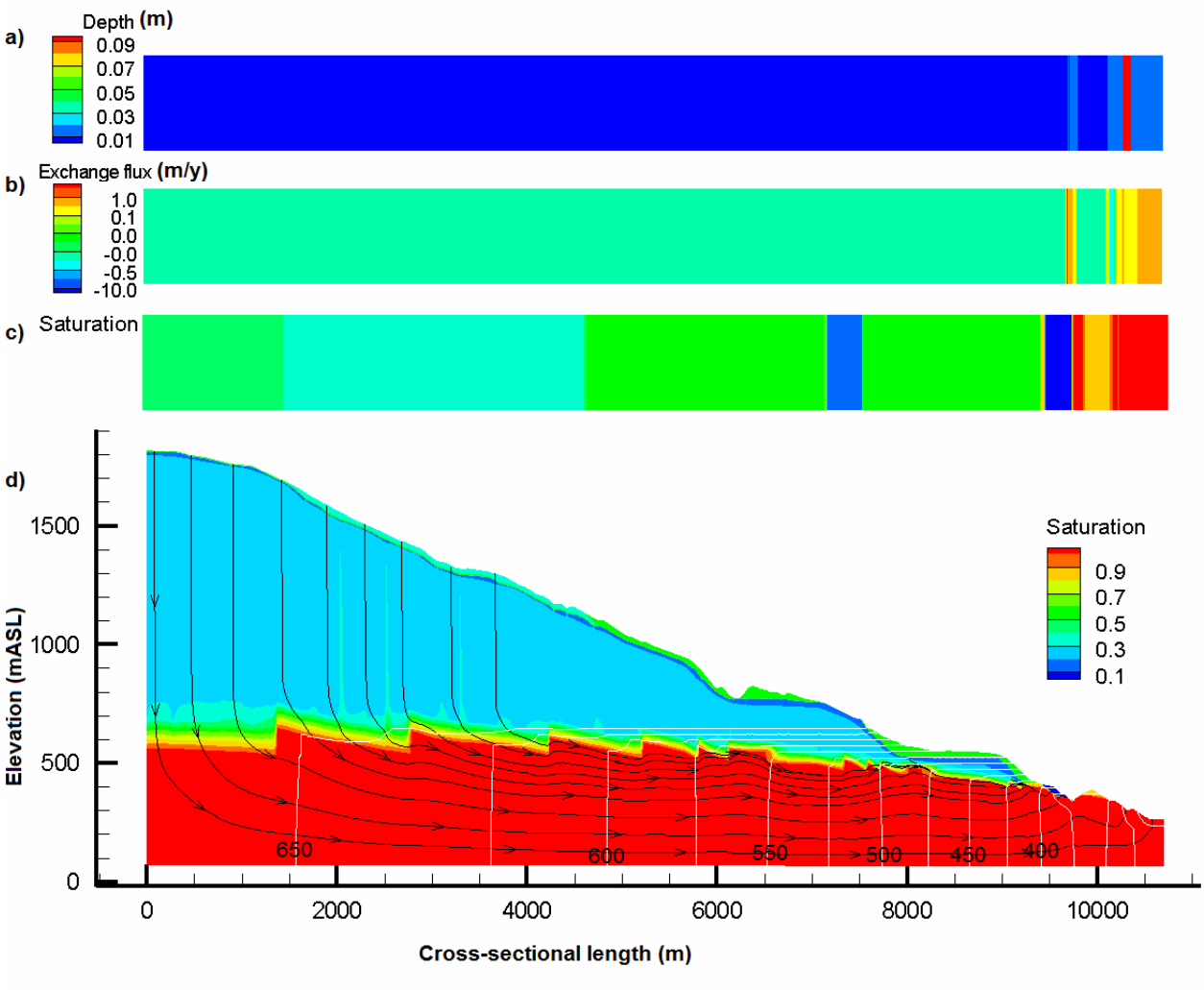

Figure 3 - 13. Steady state saturation distribution of the South Slide cross-section neglecting irrigation. (d) Particle tracks (black lines) showing the regional groundwater flow regime. White lines are the total hydraulic head contours labelled in 50 m intervals. Top-view sections showing a) water depth; b) surface exchange flux; and c) saturation. Vertical exaggeration of panel d is 2.5.

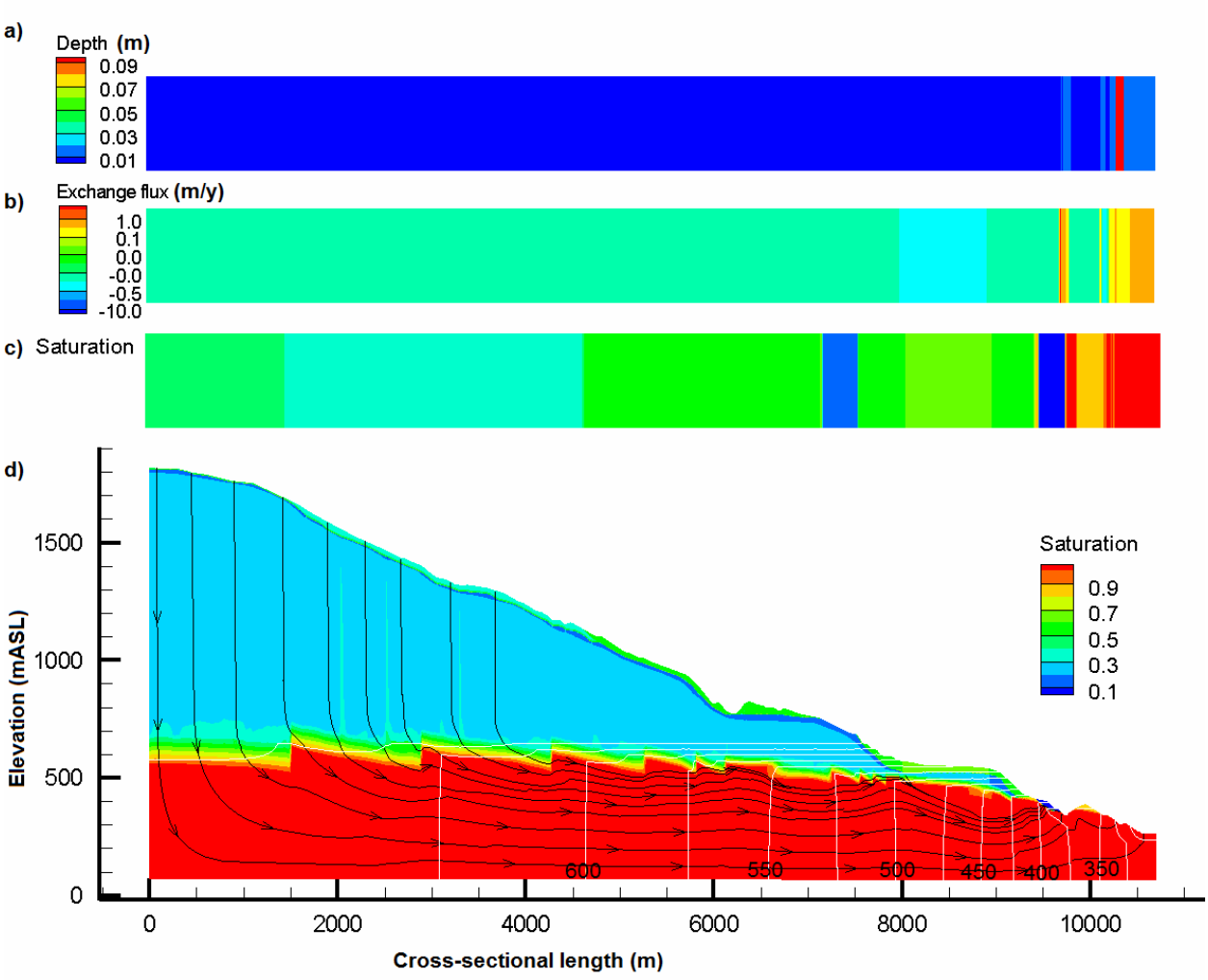

Figure 3 - 14. Steady state saturation distribution of the South Slide cross-section including irrigation. (d) Particle tracks (black lines) showing the regional groundwater flow regime. White lines are the total hydraulic head contours labelled in 50 m intervals. Top-view sections showing a) water depth; b) surface exchange flux; and c) saturation. Vertical exaggeration of panel d is 2.5.

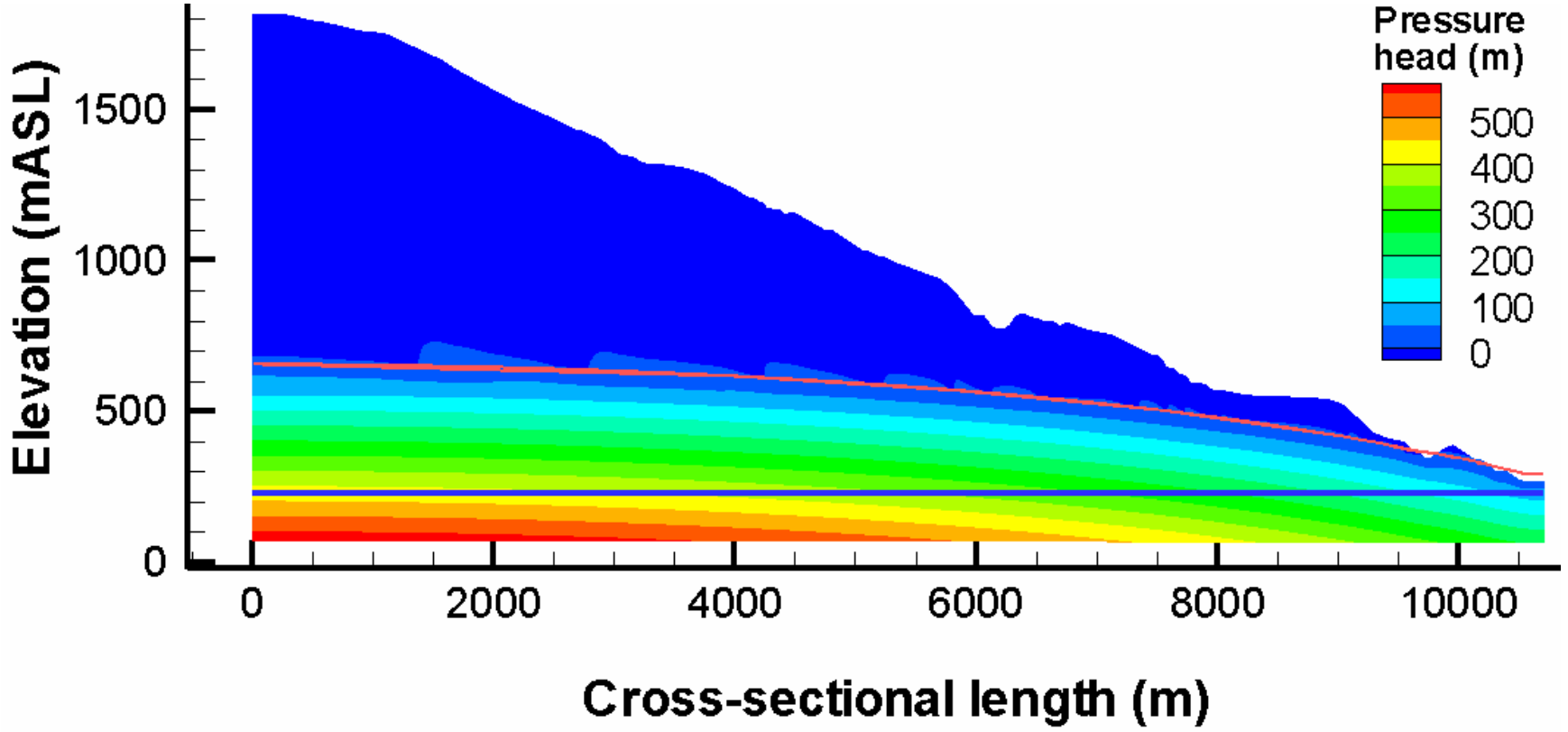

Figure 3 - 15. Steady state pressure head conditions at South Slide for the case neglecting irrigation. The red line shows the potentiometric surface given along the horizontal (dark blue) line at Z=235m, roughly the elevation of the bottom of the silt and clay unit. Note that the red line is above ground surface close to the river. Vertical exaggeration is 2.5.

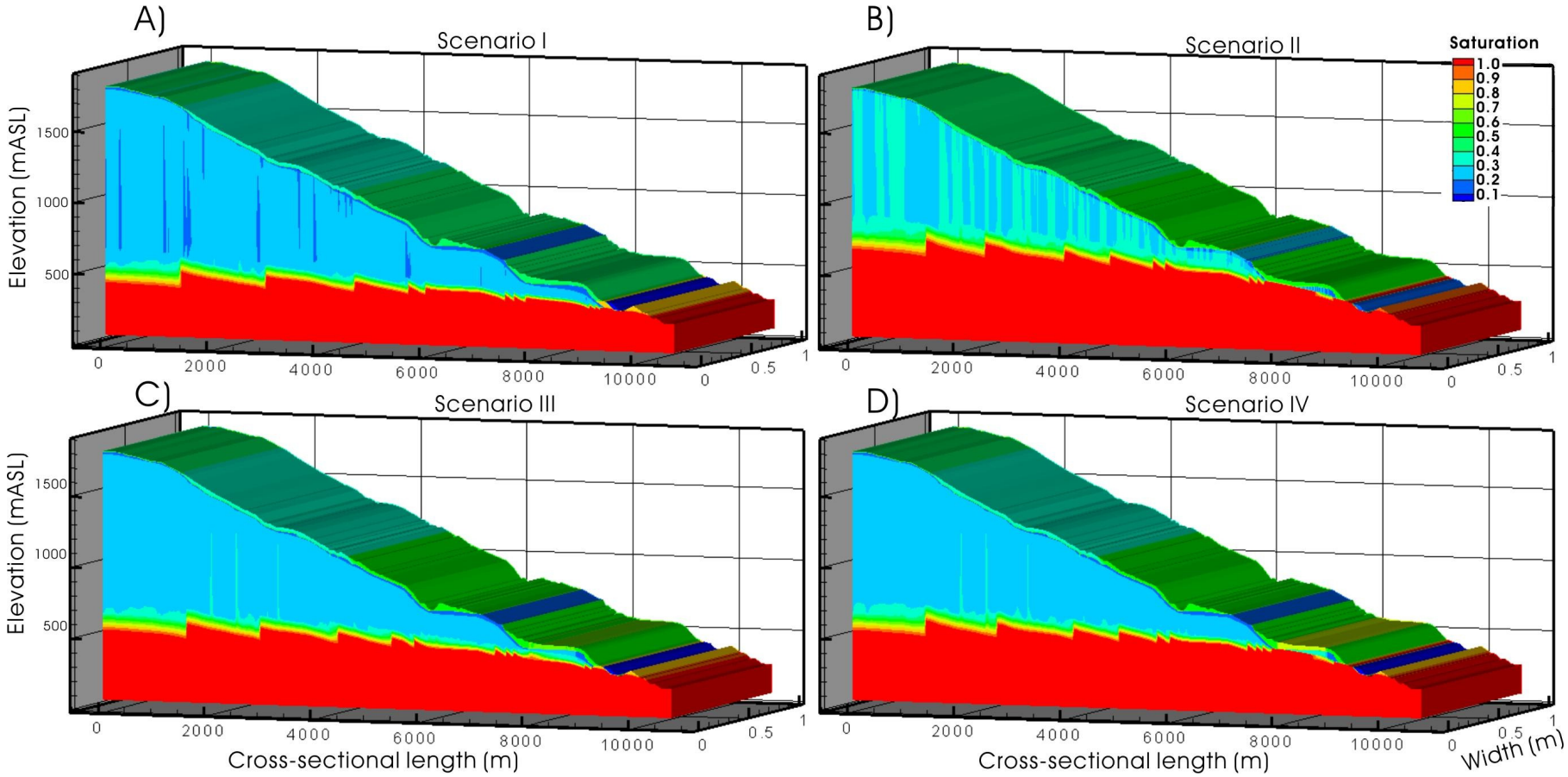

Figure 3 - 16. Saturation distribution for South Slide sensitivity scenarios.

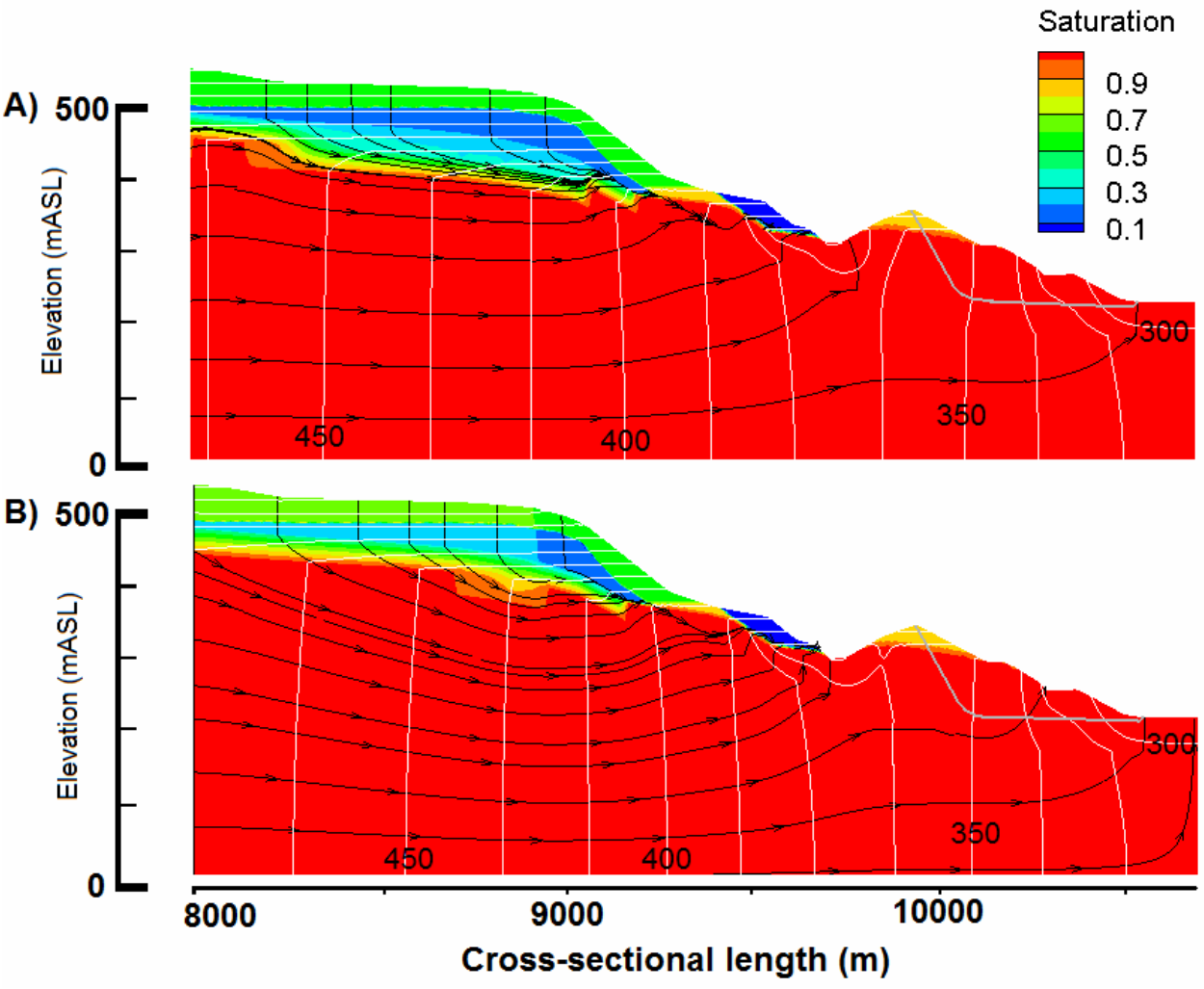

Figure 3 - 17. Slope-scale groundwater flow paths (black lines) where irrigation was neglected (A, above), and where irrigation was included (B, below). Hydraulic head contours are shown (white lines) as is the failure surface (grey line). Location of enlarged portion shown in Figure 3 - 6. Vertical exaggeration of the cross-sections is 2.5.

Chapter 4

Slope stability analysis

4.1 Introduction

Groundwater flow fields have been shown to play an important role in controlling the slope stability of areas with hillslope topography (Hodge and Freeze, 1977; Reid and Iverson, 1992). The connection between groundwater flow and slope stability in fully saturated soils can be demonstrated through the use of the effective stress equation (Craig, 1974):

$$\sigma' = \sigma - u \qquad (4\text{-}1)$$

where σ' is the effective stress, u is porewater pressure, and σ is the normal stress. The shear stress, a material property, is defined by:

$$\tau = c + \sigma' \tan \phi' \qquad (4\text{-}2)$$

where c is the cohesive strength of the material, and ϕ' is the effective friction angle. From equation (4-2) it is apparent that shear strength expressed in terms of effective stress is dependent on both the geotechnical properties of the soil (c, ϕ'), and the porewater pressure condition of the soil (u) (Hodge and Freeze, 1977). Specifically, within Thompson River Valley, the two controls on slope stability are (1) the very low residual shear strength of the highly plastic glaciolacustrine silt and clay basal unit, and (2) the elevated pore pressures within the glaciolacustrine silt and clay.

In the previous chapter it was demonstrated through the use of groundwater models that elevated porewater pressures generated by the regional groundwater flow regime can occur in the valley

fills south of Ashcroft, British Columbia. The effects of changing rates of precipitation and irrigation were tested to define the regional groundwater conditions that consider data uncertainty and future agricultural management practices. Artesian pressures found at the valley bottom suggest that the current regional groundwater flow regime in Thompson River Valley is linked to slope stability. However, the degree to which slopes are being affected by groundwater conditions cannot be assessed through the use of groundwater modeling alone. Results from groundwater modeling will now be linked directly to slope stability analysis in order to explore the role of flowing groundwater on slope stability in Thompson River Valley. SEEP/W was used to replicate the results from the HydroGeoSphere model, and SLOPE/W was used to analyze slope stability (Geo-Slope International, 2007).

4.2 Stability analysis setup

4.2.1 Notes on SEEP/W and SLOPE/W

SEEP/W and SLOPE/W are software packages produced by GEO-SLOPE International Ltd., which are commonly used to analyze slope stability problems that take the flow of groundwater into consideration as a part of the analysis (Geo-Slope, 2007). SEEP/W is a finite element, numerical model capable of predicting groundwater movement in saturated and unsaturated flow regimes. This can be coupled with SLOPE/W, software used for the analysis of slope stability.

4.2.2 Cross-sections

The two cross-sections used for the groundwater simulations described in Chapter 3 were originally constructed to represent the regional scale behaviour of the Thompson River Valley

groundwater flow system, and as such they encompassed a large area. However, slope stability problems within the valley generally occur close to Thompson River (Clague and Evans, 2003; Porter et al., 2002). The cross-sections used in slope stability analyses were directly taken from those used in the groundwater models, but only the area close to the river was used in the analysis.

One cross-section is intended to be a generalized representation of the geology encountered within Thompson River Valley, as mapped by Ryder (1976) (Figure 4 - 1). The generalized geology and topography used in this cross-section is characteristic of the pre-failure configuration of the slope.

The second cross-section was constructed to represent a 1000m section of the South Slide, where initial catastrophic failure occurred sometime between 1865 and 1877 (BGC, 2005) and involved a volume of approximately 3 Mm^3 (Figure 4 - 2). Subsequent reactivation of the inner part of the slide was noted during the winter of 1977 and fall of 1997 (BGC, 2007). Although the South Slide cross-section represents post-catastrophic failure geometry it should be noted that gradual, continuous movement in places along the South Slide failure surface has occurred at a rate of 3.4 mm/yr between 1998 and 2003 (BGC, 2003). Recently, slope inclinometers have measured movement rates between 8 and 10 mm/yr along deep failure surfaces (BGC 2005). The South Slide alone accounts for approximately $10,000 worth of track maintenance each year for Canadian Pacific (Chris Bunce, personal communication, 2008). Surface topography of the cross-section was obtained using a 30m DEM of Thompson River Valley.

In contrast to the generalized cross-section, geology was kept simple for the South Slide representation, including only four units: bedrock, fractured bedrock, undisturbed

glaciolacustrine silt and clay, disturbed glaciolacustrine silt and clay. Geology of this cross-section was constructed based on surficial mapping by Ryder (1976).

Additional geological information was estimated from a variety of sources. Four piezometers were advanced in the South Slide area by BGC (2005) (location given in Figure 1-1). Borehole logs from these piezometers were used to interpret the depth to bedrock and the undisturbed glaciolacustrine clay unit as well as the failure surface location. Several sand seams that were found in the glaciolacustrine silt and clay unit were omitted from the cross-section. These are neither extensive nor continuous and are therefore not anticipated to affect the overall regional groundwater flow or slope stability.

4.2.3 Geotechnical material properties

Considerable attention has been given to the valley fill materials within Thompson River Valley and surrounding areas, however most of the available information focuses on the lower glaciolacustrine silt and clay unit, as this is the weakest unit in the sequence (Clague and Evans, 2003). Eshraghian et al. (2006) provide some geotechnical properties of this unit. Residual friction angle values used by Eshraghian et al. (2006) were estimated based on Stark and Eid's (1994) relationhip. Miedema et al (1981) examined a similar geological formation in the Columbia River Valley near Grand Coulee, WA. Lum (1979) provides an analysis of some of the upper silt units found close to Kamloops, BC. Evans and Buchanan (1977) collected and tested many samples of South Thompson silt. Extensive testing and analysis of the silt and clay found in Thompson River Valley was previously compiled by Bishop et al. (2008).

SLOPE/W requires unit weight, cohesion, and friction angle as input to any Mohr-Coulomb material model. Unit weights of the glaciolacustrine silt and clay of the Grand Coulee area (analogous to unit 2) were provided by Meidema et al (1981), and applied to the stability analysis. Unit weights of Fraser glaciolacustrine silt and sand were calculated based on void ratio and specific gravity data provided by Evans and Buchanan (1977). Cohesion for all units was specified as zero because it was assumed that slope failure is occurring along pre-sheared surfaces caused by either glacial overriding or prehistoric landsliding, and that the strength of these materials must therefore be at residual values (Clague and Evans, 2003). Bishop et al (2008) provide residual friction angle data for both the silt and clay components of unit 2.

Two residual friction angles were used for unit 2, reflecting the composite failure surface geometry of the landslides in Thompson River Valley (Figure 4 - 1, Figure 4 - 2). In the lower, horizontal component of the failure surface, where the weaker clay layers are more important in controlling failure, a residual friction angle closer to that of the clay was selected ($\phi_r = 17^o$). For the backslope component of the failure surface, where the stronger and thicker silt layers are more important, a higher residual friction angle was selected ($\phi_r = 25^o$). Slope stability analysis parameters are provided in Table 4 - 1.

Tills, gravels and diamicton units found in the area are largely unrepresented in the geotechnical literature. Unit weights, cohesion, and friction angles of these materials were estimated for the slope stability analysis of the generalized cross section. This approach is not expected to affect overall results, as the failure surface in the analysis is defined mostly through the glaciolacustrine silt and clay unit with only a lesser fraction through the five of the remaining units.

Table 4 - 1. Slope stability analysis parameters for various units.

Unit Number	Unit Description	Unit Weight (kN/m^3)	Cohesion (kPa)	Friction angle (^{o})
-	Alluvial fans	20	0	35
7	Postglacial silt and sand	20	0	32
-	Gravel outwash	20	0	35
4	Fluvial gravels	20	0	35
3	Fraser glaciolacustrine silt and sand	18	0	30
3	Pre-Fraser till	18	0	30
2	Upper glaciolacustrine silt and clay (unit 2)	17.5	0	25
2	Lower glaciolacustrine silt and clay (unit 2)	17.5	0	17

4.2.5 Other considerations

Failure surfaces defined in the generalized and South Slide stability analyses were specified based on the dimensions and shape of failure surfaces that are currently known within the valley (Figure 4 - 1, Figure 4 - 2). These are often composite in nature, with pronounced vertical and horizontal components (BGC Engineering, 2005). The failure surfaces extend from the first break in benched terrace slopes (elevation 400 - 460 mASL) to river level (elevation 280 mASL). The horizontal distance of the failure surface is approximately 600 m.

A static uniform load was applied to the toe of the failure surface in order to account for the pressure exerted in this area by Thompson River water. In places Thompson River can be quite deep, and where lower failure surfaces outcrop within the river channel the additional weight of water may significantly improve the stability of the slope.

4.3 Results

4.3.1 Overview

Data limitations contribute to a degree of uncertainty that can be associated with the generalized and South Slide cross-sections. Although information is available, the geological conditions, climatic conditions, hydraulic material properties, and geotechnical material properties cannot be fully delineated. Further to this, additional uncertainty in the local future climate of the Ashcroft area must also be considered. For these reasons both the generalized and South Slide cross-sections were tested under various infiltration scenarios by varying rates of precipitation and irrigation. The various scenarios are provided in Table 3 - 6 and Table 3 – 8.

Two qualitative observations relating to stability of the Thompson Valley slopes can be made based on the results of the HydroGeoSphere groundwater models. First, several seepage faces appear on the slope surface for both cross-sections (Figure 3 - 13 and Figure 3 - 14). The presence of seepage faces on vertical valley walls indicates a horizontal groundwater flow component, which was confirmed by stream traces. This may contribute to instability by decreasing effective stress on the upper failure surface. Second, strong upward groundwater flow is noted in the lower regions of each cross section, as indicated by the closely-spaced head contours (Figure 3 - 17). Again, this is detrimental to slope stability by contributing to elevated pore pressures close to the failure surface.

Pore pressures along identical failure surfaces are compared for each simulation scenario in Figure 4 - 3. Little change is observed between the pressure profile of each scenario along the generalized failure surface, with only a slight reduction in pressure being shown in the lower part of the failure surface for the scenario where precipitation was halved. Slightly more change in

pressure is observed along the South Slide failure surface. Again, most of the pressure change between scenarios was shown in the case where precipitation was halved. A slight increase in pressure was visible in the case where precipitation was doubled.

4.3.2 SLOPE/W results

The Factor of Safety was calculated for each of the precipitation and irrigation scenarios described previously for the generalized and South Slide cross-sections. All results were achieved using only one specified failure surface for each cross-section, which was analysed for all infiltration scenarios. This approach was taken to ensure consistency between scenarios. Results are given for both the Bishop and Morgenstern-Price methods of stability analysis and are summarized in Table 4 - 2 for the generalized cross section, and Table 4 - 3 for the South Slide cross-section.

The Factor of Safety calculated for the base case scenario was close to unity for both cross-sections. This result indicates that the slopes are naturally unstable under ordinary groundwater conditions (as predicted by the groundwater simulations) due to the presence of weak materials at residual strength (as measured in the laboratory). Since no external influences (e.g., river level or irrigation) are required to reduce the Factor of Safety to unity it can be concluded that the presence of landslides in Thompson River Valley can be explained by regional groundwater flow dynamics and weak material properties alone.

Table 4 - 2 and Table 4 - 3 give Factors of Safety in absolute terms for the various scenarios in addition to relative percent change in factor of safety compared to the base case (highlighted). The scenario having the greatest overall impact on slope stability is scenario I, where

precipitation was halved. This scenario resulted in an increase in factor of safety between 4% and 8% for the generalized cross-section, and between 9% and 11% for the South Slide cross-section.

Two scenarios, double rainfall (scenario II) and double irrigation (scenario IV), produced very similar reductions in the factor of safety, having the greatest negative impact of all scenarios. Scenario II resulted in a reduction in factor of safety between 0.5% and 0.9% for the generalized cross-section, and between 4.4% and 4.9% for the South Slide. Scenario IV resulted in a reduction in factor of safety between 0.5% and 0.8% for the generalized cross-section, and 4.0% and 4.7% for the South Slide cross-section. Differences in factor of safety between the two baseline scenarios were minimal. For the generalized cross-section the Bishop method of stability analysis resulted in a reduction of 0.1%, and the Morganstern-Price method did not change the factor of safety.

For the South Slide cross-section the base case with irrigation reduced the factor of safety by 0.2% to 0.4%. Perhaps the only unexpected result was found at the South Slide for scenario III, where irrigation was halved. It was expected that this scenario would yield an overall reduction in factor of safety compared to the base case, however, the factor of safety actually increased between 1.2% and 1.6%. Reasons for this result are unknown. It is possible that the difference is so slight that it remains within the realm of uncertainty inherent to the modeling process.

Table 4 - 2. Factors of safety and relative percent changes in relation to the base case from SLOPE/W analysis for generalized cross-section for all scenarios.

Morganstern-Price Method

	Base		Double		Half	
Precipitation	1.07		1.07	-0.0047	1.12	-3.91%
Irrigation	1.07	0.00%	1.06	-0.0047	1.07	-0.0009

Bishop Method

	Base		Double		Half	
Precipitation	1.04		1.03	-0.0086	1.13	-7.96%
Irrigation	1.04	-0.001	1.02	-0.0077	1.04	-0.001

Table 4 - 3. Factors of safety and relative percent changes in relation to the base case from SLOPE/W analysis for South Slide cross-section for all scenarios.

Morganstern-Price Method

	Base case		Double		Half	
Precipitation	1.05		1.00	-0.0485	1.17	-10.74%
Irrigation	1.05	-0.0019	1.01	-0.0467	1.07	-1.62%

Bishop Method

	Base case		Double		Half	
Precipitation	1.26		1.21	-0.0437	1.38	-9.13%
Irrigation	1.26	-0.004	1.22	-0.0398	1.28	-1.19%

4.4 Discussion and conclusions

Several conclusions can be made based on the results of this stability analysis:

(1) The use of residual shear strength parameters is critical to evaluating the stability of the Thompson River Valley landslides. The use of residual shear strength parameters is necessitated by the presence of pre-sheared surfaces in the valley fill material caused by historical landsliding and glacial overriding.

(2) The weaker clay interbeds within the glaciolacustrine silt and clay are very important in controlling slope instability, and they are most influential in doing so along the horizontal component of the failure surface. Conversely, the stronger silt interbeds control the stability of the vertical component of the failure surface.

(3) Slopes are unstable under natural conditions; the factor of safety for the South Slide base case was close to unity (1.05). As such, a slight reduction in the factor of safety may be sufficient to trigger landslide movement.

(4) Given the dimensions of a typical hayfield in Thompson River Valley (31 Ha), and the addition of irrigation water at the rate of infiltration specified in the 1986 court case (0.17m/yr) the resulting change in pore pressure along the failure surface was not sufficient to significantly reduce the factor of safety of the slope. Therefore it is concluded that the effects of irrigation are minimal in controlling slope failure. Historical irrigation techniques, such as the ditch-irrigation systems used in Stanton's (1898) time, would likely contribute much greater volumes of irrigation water to the subsurface compared to modern sprinkler irrigation systems. This perhaps explains the observation that many of the landslide movements in Thompson River Valley occurred prior to the advent of modern irrigation techniques (circa 1940), as noted in Table 1-1.

(5) Of the scenarios evaluated using slope stability analysis coupled with groundwater modeling it was found that decreased precipitation leads to the greatest increase in the Factor of Safety. The increased factor of safety was expected. It was noted during the groundwater modeling exercises that this scenario resulted in significantly drier conditions and reduced pore pressures.

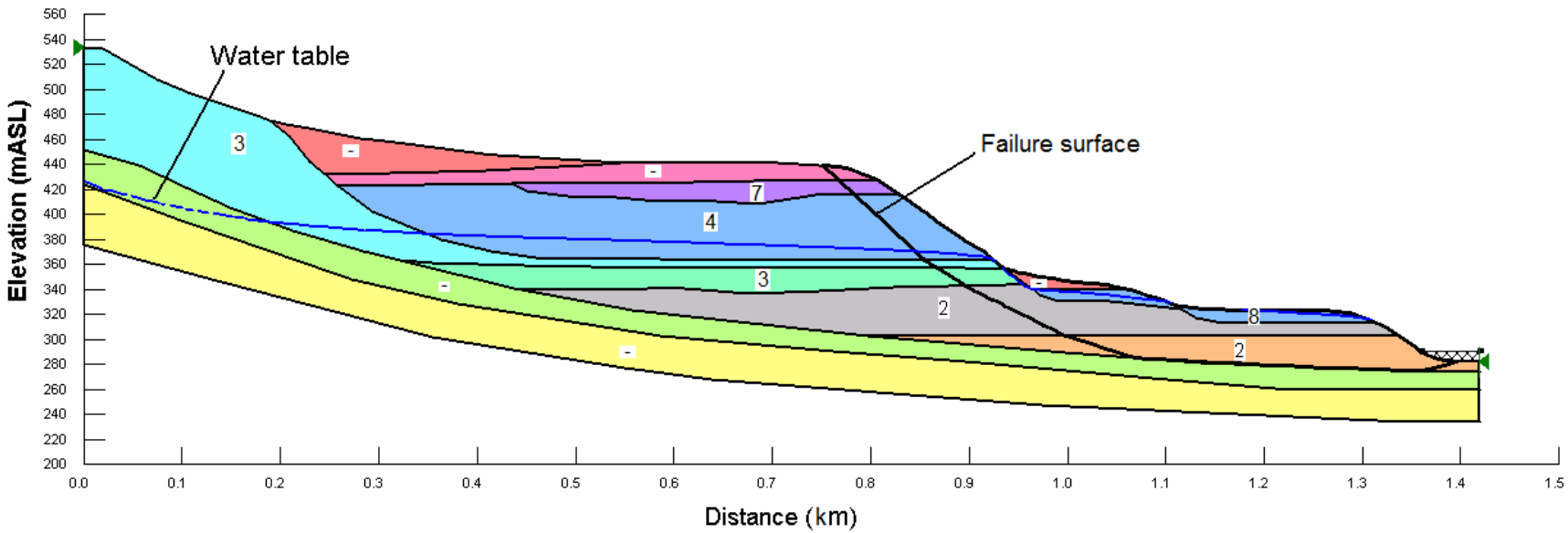

Figure 4 - 1. Generalized (Ryder, 1976) cross-section used in slope stability analysis. Numbered geologic units correspond to those listed in Chapter 2. Unlabled units are described in Figure 3-4.

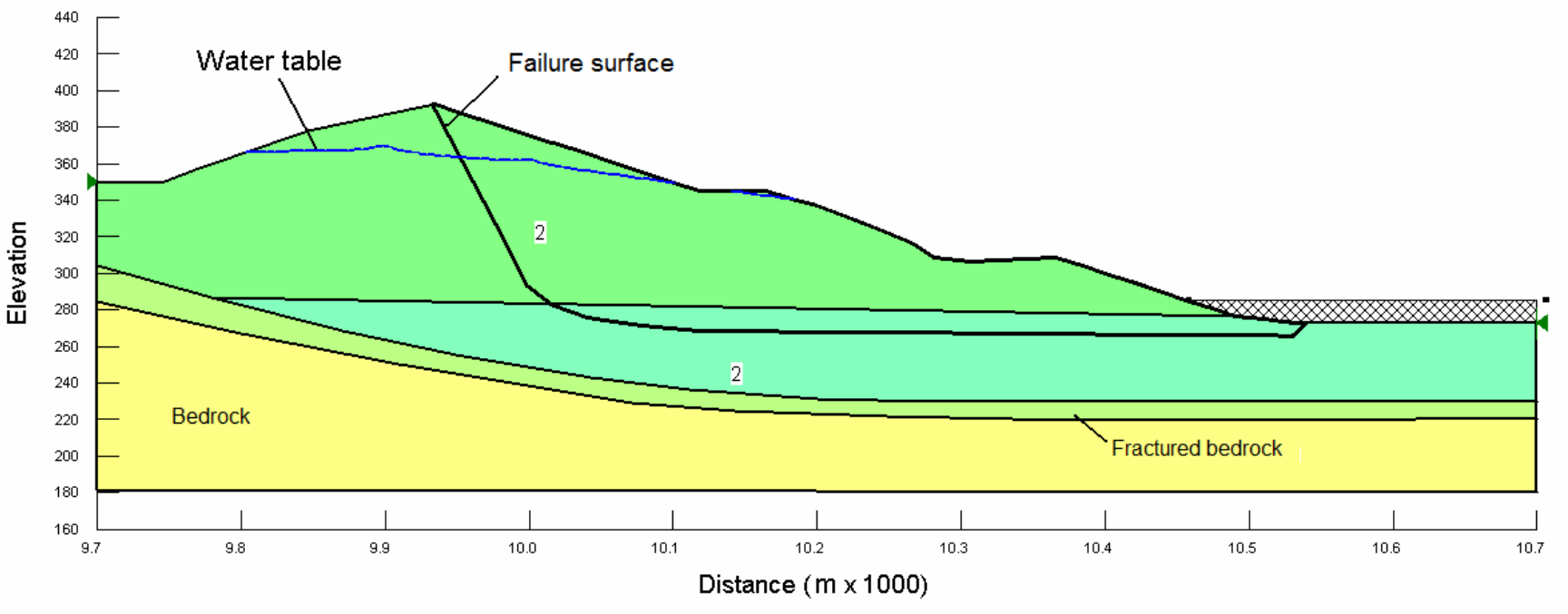

Figure 4 - 2. South slide cross-section as used in the slope stability analysis. Transect A'-A'' is shown in Figure 1-1. Geologic unit number (unit 2) corresponds to that unit described in Chapter 2. The lower unit represents the disturbed portion of unit 2, and the upper unit represents the less disturbed portion of unit 2.

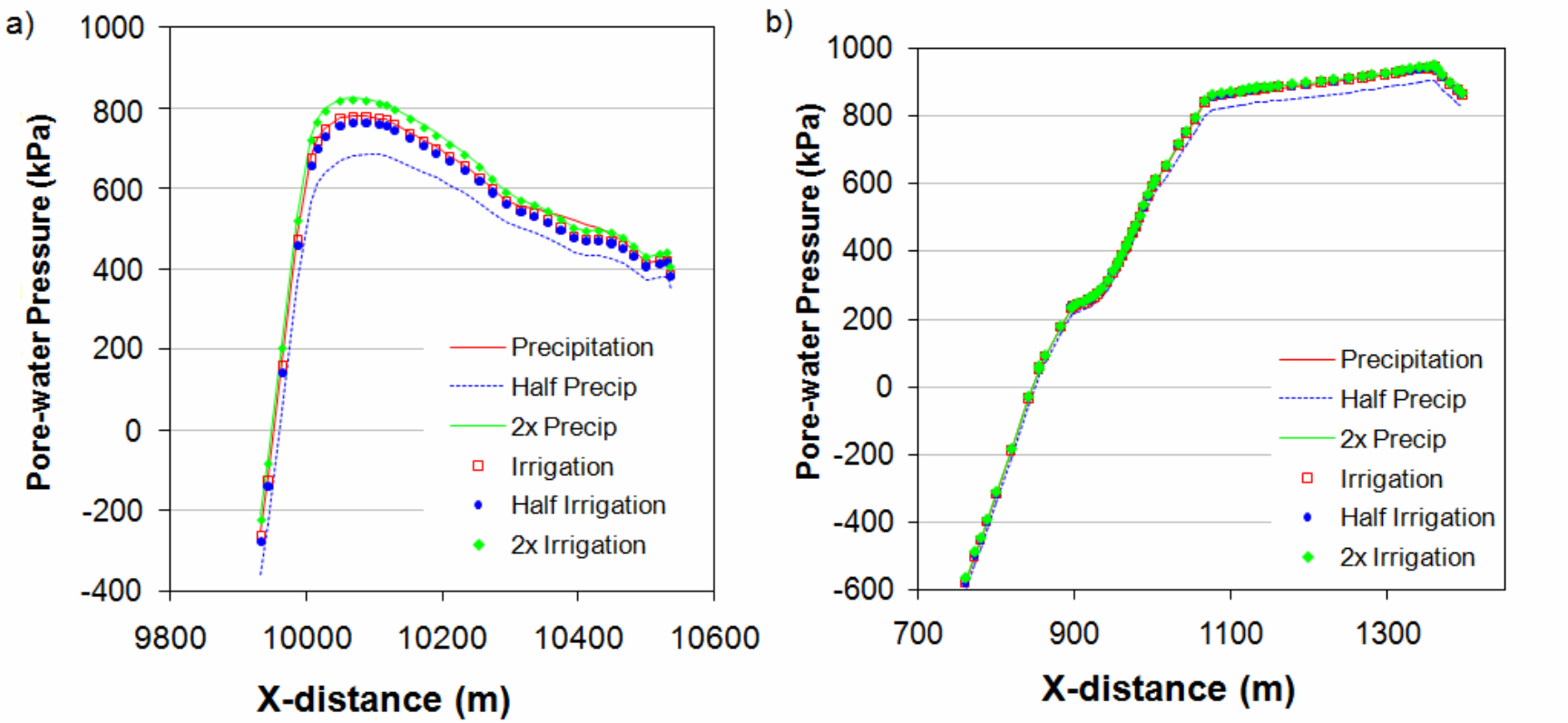

Figure 4 - 3. Pore pressures along the South Slide (a) and generalized (b) cross-section failure surfaces for all scenarios.

Chapter 5

Summary and discussion

In Chapter One we defined five thesis objectives. These were to 1) establish the geotechnical properties of key units within the valley fill materials, 2) establish the groundwater flow regimes within Thompson River Valley at the slope scale and regional scale, 3) determine the degree to which irrigation of upslope benchlands contributes to increased pore pressure along the failure surface, 4) evaluate the pore pressure effects of variable Thompson River levels, and 5) explore the role of the groundwater flow systems on slope stability. Our objectives were met by constructing two groundwater models to simulate the behavior of local and regional groundwater flow fields, and coupling these models with slope stability analyses. The sensitivity of the groundwater flow system pore pressures was analyzed by varying the amounts of precipitation and irrigation applied at the boundary conditions. This work contributes to the understanding of the regional flow dynamics within Thompson River Valley, as well as mountainous semi-arid areas in general, and explains how these are influenced by dynamic anthropogenic and climactic factors. Further, the interaction between groundwater and slope stability was explored, with emphasis on the material properties of valley fill sediments found in the study area.

Groundwater model results show that pore pressures generated by regional flow fields in addition to the presence of weak pre-sheared materials explain the formation of landslides in Thompson River Valley. The regional model shows groundwater infiltrating from nearby peaks travels vertically through the unsaturated zone until it reaches the saturated zone deep within the bedrock, where it then travels horizontally until encountering valley fill, where it travels along any number of flow paths to discharge at one of the seepage faces, or within Thompson River.

Due to its low permeability and interbedded nature, the glaciolacustrine silt and clay (unit 2) is critical in determining the terminal path taken by groundwater, and is therefore a key element towards the development of the elevated pore pressures that occur in the valley bottom.

Glacial overriding and historical landsliding have created pre-sheared surfaces within the lower valley fill materials. The importance of pre-sheared surfaces in Thompson River Valley cannot be understated. As a result of these features the valley fill materials are reduced to residual strengths. Highly plastic clay beds within Unit 2 possess very low residual friction angles, usually between 10^{o} and 15^{o}. Therefore, Unit 2 is not only critical in controlling the regional hydrogeology within Thompson River Valley, but also in controlling slope stability.

Slopes in Thompson River Valley can be viewed as naturally unstable due to the combination of elevated pore pressures generated by a regional groundwater flow system and the presence of weak valley fill materials at residual strength. This is affirmed by the fact that gradual, continuous slope movement is currently observed at a number of locations in the area: North, South, Goddard, and Ripley landslides. Slope stability analyses indicate that the Factor of Safety of the slopes in their natural state is just over unity (1.04 to 1.26).

The addition of excess infiltration due to irrigation of upslope farmlands at the rate described in the 1986 court case (0.17 m/yr) had minimal impact on the Factor of Safety. Original observations citing irrigation as a contributing factor to landslide activity apply to historical irrigation techniques, which were less efficient and would have supplied much greater volumes of water to the subsurface.

Fluctuations in the stage of Thompson River were simulated using transient boundary conditions in the flow system model. The resulting maximum change in pore pressure within the glaciolacustrine silt and clay adjacent to the river amounted to an increase of less than one centimeter. The effects of the dynamic stage of the river are therefore not expected to affect the stability of slopes in Thompson River Valley.

Although irrigation and river stage were not shown to greatly influence the stability of slopes in the Thompson River Valley, the groundwater flow regime is more sensitive to climatic changes. In the sensitivity analysis we tested scenarios where precipitation was doubled and halved. Years where annual precipitation was double the normal value are observed in historical data. However, unless highly elevated rates of precipitation occur over extended periods of time they are not anticipated to have an adverse impact on slope stability.

It was not the objective of this study to design or evaluate stabilization options for application to the landslides in Thompson River Valley. However, some implications that arise from a study of the behaviour slope stability with variable pore pressures show that draining the slopes would likely be highly beneficial in terms of improving stability. In practice, achieving this result would be difficult and expensive given the low permeability of the glaciolacustrine silt and clay materials and the depths of lower, more permeable units. Thus, the next logical step in following the work presented in this study is to evaluate various slope stabilization options. This topic continuously arises as a part of the management strategy adopted by the railways. The cost of stabilizing large landslides often does not outweigh the benefit. As a result, sections of railway that experience continuous problems are often not preventively maintained, but allowed to fail and be fixed as required. From the railway's perspective this method of coping with the problem is giving way to a monitoring-intensive approach to alleviate risk.

References

BGC Engineering Inc. 1998. 1998 slope instrumentation at South Slide. Project No. 0034-175-02. BGC Engineering Inc., Vancouver, British Columbia.

BGC Engineering Inc. 2003. CN Nepa / South Slide monitoring. Project memorandum 0034-175-10, April 8, 2003. BGC Engineering Inc. Kamloops BC.

BGC Engineering Inc. 2005. THOM 052.80 WESTCAP Geotechnical Investigation Project No. 0087-032-09. BGC Engineering Inc., Vancouver, British Columbia.

BGC Engineering Inc. 2007. Site Visit of 28 & 29 March 2007, Mile 54.4 Thompson Subdivision. Project No. 0087-039-02. BGC Engineering Inc., Vancouver, British Columbia.

Bishop, A.W. 1971. Shear strength parameters for undisturbed and remolded soil specimens. *In* Proceedings of the Roscoe Memorial Symposium, Cambridge, Mass., p. 3-58.

Bishop, N.F., Evans, S.G., Petley, D.J., Unger, A.J.A. 2008. The geotechnics of glaciolacustrine sediments and associated landslides near Ashcroft (British Columba) and Grand Coulee Dam (Washington). *In* Proceedings of 4th Geohazards conference, May 20-24, Quebec City, PQ.

Bouwer, H. 1989. The Bouwer and Rice slug test – an update. Ground Water 27, 12-9 – 12-14.

Bradbury, K.R.; Muldoon, M.A. 1989. Hydraulic conductivity determinations in unlithified glacial and fluvial materials. ASTM technical publication 1053. pp 138-151.

Bradley, R.S. 1999. Paleoclimatology: Reconstructing Climates of the Quaternary (second ed.), Academic Press, New York.

British Columbia Ministry of Water Land and Air Protection (BCMWLAP). 2008. Water Stewardship Division; Wells. [online]. Available from www.env.gov.bc.ca/wsd/plan_protect_sustain/groundwater/wells.html. [cited 24 June, 2008].

Chanasyk, D.S., Mapfumo, E., Chaikowsky, C.L.A. 2006. Estimating actual evapotranspiration using water budget and soil water reduction methods. Canadian Journal of Soil Science 86, 757-766.

Clague, J.J. 1991. Quaternary glaciation and sedimentation, Chapter 12 *in* Geology of the Cordilleran Orogen in Canada. *Edited by* H. Gabreilse; C.J. Yorath. Geological Survey of Canada, Geology of Canada, no. 4, p. 419-434.

Clague, J.J., Evans, S.G. 2003. Geologic framework of large historic landslides in Thompson River Valley, British Columbia. Environmental and Engineering Geoscience, 9, 201-212.

Craig, R. F. 1978. Soil mechanics. Van Nostrand Reinhold, United Kingdom (GBR).

Droogers, P. 2000. Estimating actual evapotranspiration using a detailed agro-hydrological model. Journal of Hydrology 229, 50-58.

EBA Engineering Consultants Ltd. 1983. Geotechnical evaluation of the Goddard Landslide. Report 302-950. Report to Canadian Pacific Railway, Vancouver Division, Thompson Subdivision. EBA Engineering Consultants Ltd.

Environment Canada. 2008. Environment Canada National Climate Archive. [online]. Available from climate.weatheroffice.ec.gc.ca. [cited 24 June 2008].

Eshraghian, A. 2007. Hazard analysis of reactivated earth slides in the Thompson River Valley, Ashcroft, British Columbia. Ph.D. thesis. Department of Civil and Environmental Engineering, University of Alberta, Edmonton, Alberta.

Eshraghian, A., Martin, C.D., Cruden, D.M. 2005. Landslides in the Thompson River Valley between Ashcroft and Spences Bridge, British Columbia. *In* Landslide Risk Management. *Edited by* Hungr;Fell;Couture;Eberhard. Taylor & Francis Group London. pp. 437-446.

Eshraghian, A., Martin, C.D., Morgenstern, N.R., Cruden, D.M. 2006. Groundwater movements of earth slides in the Thompson River Valley. *In* proceedings of the Sea to sky geotechnique, 59th Canadian geotechnical conference. October 1-4, 2006. Vancouver, B.C.

Eshraghian, A., Martin, C.D., Cruden, D.M. 2007. Complex earth slides in the Thompson River Valley, Ashcroft, British Columbia. Environmental & Engineering Geoscience 13(2), 161-181.

Eshraghian, A., Martin, C.D., Morgenstern, N.R. 2008. Hazard analysis of an active slide in the Thompson River Valley, Ashcroft, British Columbia, Canada. Canadian Geotechnical Journal. 45, 297-373.

Evans, S.G. 1982. Landslides in surficial deposits in urban areas of British Columbia: a review. Canadian Geotechnical Journal 19, 269-288.

Evans, S.G. 1984. The 1880 landslide dam on Thompson River, near Ashcroft, British Columbia. Current Research, Part A, Geological Survey of Canada Paper 84-1A. p. 655-658.

Evans, S.G., Buchanan, R. G. 1976. Some aspects of natural slope stability in silt deposits near Kamloops, British Columbia. *In* proceedings of Slope stability 29th Canadian geotechnical conference. October 13-16, 1976. Vancouver, B.C.

Fleischer, S. 1972. Scherbruch und Schergleitfestigkeit von bindigen Erdstoffen. Neue Bergbautechnik, 2, 98-99.

Flint, R.F., Irwin, W.H. 1939. Glacial history of Grand Coulee dam, Washington. Geological Society of America Bulletin 50(5), 661-680.

Freeze, R.A., Cherry, J.A. 1979. Groundwater. Prentice Hall, NJ.

Fulton, R.J. 1965. Silt deposition in late-glacial lakes of southern British Columbia. American Journal of Science, 263(7), 553-570.

Fulton, R.J. 1975. Quaternary geology and geomorphology, Nicola-Vernon area, British Columbia. Geological Survey of Canada, Memoir 380, 50 pp.

Geological Survey of Canada (GSC). 1989. Map 42 – 1989, Sheet 1. Geology, Ashcroft, British Columbia. Geological Survey of Canada Cartographic Information and Distribution Centre, Ottawa, ON.

George, H. 1986. Characteristics of varved clays of the Elk Valley, British Columbia, Canada. Engineering Geology 23, 59-74.

Geo-Slope International, 2007. Stability Modeling with SLOPE/W 2007. Geo-Slope International Ltd, Calgary, Alberta.

Golder Associates. 1999. Assessment of resource potential, Ashcroft Ranch, Ashcroft, B.C. 992-1892. Golder Associates, Burnaby, British Columbia.

Golder Associates. 2004. Ashcroft Ranch landfill project. 03-1411-100.9000.9500. Golder Associates, Burnaby, British Columbia.

Government of Canada (1982). History of Irrigation in Western Canada. Prairie Farm Rehabilitation Administration, Government of Canada.

Haefeli, R. 1951. Investigation and measurements of the shear strength of saturated cohesive soils. Geotechnique, 2, 186-187.

Hodge, R. A. L., Freeze, R. A. 1977. Groundwater flow systems and slope stability. Canadian Geotechnical Journal 14, 466-476.

Hvorslev, M.J. 1951. Time lag and soil permeability in groundwater observations. U.S. Army Corps of Engineers, Waterways Experiment Station Bulletin No. 36. Vicksburg, Mississippi.

Johnsen, T.F., Brennand, T.A. 2004. Late-glacial lakes in the Thompson Basin, British Columbia: paleogeography and evolution. Canadian Journal of Earth Sciences 41, 1367-1383.

Jones, F.O., Embody, D.R., Peterson, W.L, Hazlewood, R.M.. 1961. Landslides along the Columbia River Valley northeastern Washington. Geological Survey Professional Paper 367. United States Government Printing Office, Washington.

Kenney, T.C. 1977. Residual strength of mineral mixtures. *In* Proceedings of the 9th International Conference on Soil Mechanics, Tokyo, Vol. 1, p. 155-160.

Ladd, J. H. 1977. Cache Creek-Nicola contact, Ashcroft area; 92 1/11 W. Department of Geological Sciences, Cornell University, Ithaca, NY.

Lambe, R.W. 1985. Amuay landslide. *In* Proceedings of the 6th International Conference of Soil Mechanics and Foundation Engineering, San Francisco.

Li, Q., Unger, A.J.A., Sudicky, E.A., Kassenaar, D., Wexler, E.J., Shikaze, S. 2008. Simulationg the multi-seasonal response of a large-scale watershed with 3D physically-based hydrologic model. Journal of Hydrology, doi: 10.1016/j.aaen.2005.05.001.

Lum, K.K.Y. 1979. Stability of the Kamloops Silt Bluffs. M.A. Sc. Thesis, University of British Columbia, Vancouver, BC

Lupini, J.F., Skinner, A.E., Vaughan, P.R. 1981. The drained residual strength of the cohesive soils. Geotechnique 31, 181-213.

McLaren, R.G., Forsyth, P.A., Sudicky, E.A., VanderKwaak, J.E., Schwartz, F.W., Kessler, J.H. 2000. Flow and transport in fractured tuff at Yucca Mountain: numerical experiments on fast preferential flow mechanisms. Journal of Contaminant Hydrology 43, 211-238.

Mesri, G., Cepeda-Diaz, A.F. 1986. Residual shear strength of clays and shales. Geotechnique 36, 269-273.

Miedema, D., Byers, J., McNearny, R. 1981. Residual shear strength determination of overconsolidated Nespelem clay. Laboratory Shear Strength of Soil, ASTM STP 740, R.N. Yong and F.C. Townsend, Eds., American Society for Testing and Materials, pp. 594-609.

Milligan, V. Soderman, L.G., Rutka, A. 1962. Experience with Canadian varved clays. Journal of the Soil Mechanics and Foundations Division, Proceedings of the American Society of Civil Engineers 88(SM4), 31-67.

Mitchell, J.K. 1976. Fundamentals of Soil Behaviour, Wiley, New York.

Monger, J. W. H., McMillan, W. J. 1982. Geology, Ashcroft, British Columbia; map, charts and notes. Geological Survey of Canada, map sheet 1, scale 1:250,000.

Monger, J. W. H., Price, R. A . 2000. A transect of the southern Canadian Cordillera from Vancouver to Calgary. Open-File Report. Geological Survey of Canada.

Owsiacki, G. 1999. Report on Map 092INW. Government of British Columbia, Ministry of Energy, Mines and Petroleum Resources, Victoria, BC.

Panday, S., Huyakorn, P.S., 2004. A fully coupled physically-based spatially-distributed model for evaluation of surface/subsurface flow. Advances in Water Resources 27, 361-382.

Pauls, G.J., Sauer, E.K., Christiansen, E.A., Widger, R.A. 1999. A transient analysis of slope stability following drawdown after flooding of a highly plastic clay. Canadian Geotechnical Journal 36, 1151-1171.

Porter M.J., Savigny K.W., Keegan T.R., Bunce C.M., MacKay C. 2002. Controls on stability of the Thompson River landslides. *In* Proceedings of the 55th Canadian Geotechnical Conference, Niagara Falls. Southern Ontario Section of the Canadian Geotechnical Society. p. 1393-1499.

Reid, M.E., Iverson, R.M. 1992 Gravity-driven groundwater flow and slope failure potential; 2, Effects of slope morphology, material properties, and hydraulic heterogeneity. Water Resources Research 28, 939-950.

Ryder, J. M. 1976. Terrain inventory and Quaternary geology, Ashcroft, British Columbia. Geological Survey of Canada Paper no.74-49, 17 pp.

Skempton, A.W. 1964. Long-term stability of clay slopes. Geotechnique 14, 77-102.

Stanton, R.B. 1898. The great land-slides on the Canadian Pacific Railway in British Columbia. *In* Institution of Civil Engineers, Session 1897-1898, Vol. 132, Part II, Section 1, Minutes of Proceedings, pp. 1-46.

Stark, T.D., Eid, H.T. 1994. Drained residual shear strength of residual soils. Journal of Geotechnical and Geoenvironmental Engineering 120, 269-273.

Sudicky, E.A., Therrien, R., Park, Y.J., McLaren, R.G., Jones, J.P., Lemieux, J.M., Brookfield, A.E., Colautti, D., Panday, S., Guvanasen, V. 2005. On the challenge of integrated surface-subsurface flow and transport modelling at multiple catchment scales. Abstracts with programs, Geological Society of America, 2005 annual meeting, Salt Lake City, UT, United States, Oct 16-19, 2005.

Therrien, R., McLaren, R.G., Sudicky, E.A., Panday, S.M. March 8, 2005. HydroSphere – a three-dimensional numerical model describing fully-integrated subsurface and surface flow and solute transport. Groundwater simulations group software manual.

Thomson, S., Mekechuk, J. 1982. A landslide in glacial lake clays in central British Columbia. Canadian Geotechnical Journal 19, 296-306.

Tiwari, B., Marui, H. 2005. A new method for the correlation of residual shear strength of the soil with mineralogical composition. Journal of Geotechnical and Geoenvironmental Engineering 131, 1139-1150.

United States Department of Agriculture. 2005. ROSETTA class average hydraulic parameters. [Online]. Available: http://www.ars.usda.gov/Services/docs.htm?docid=8955, November 6, 2007.

United States Bureau of Reclamation. 1983. Columbia basin project Grand Coulee riverbank stabilization program. U.S.B.R. Division of Designs Branch technical memorandum No. GC-III 222FA-4. February, 1983.

Van Genuchten, M.T., 1980. A closed-form equation for predicting the hydraulic conductivity of unsaturated soil. Soil Science Society of America Journal 44, 892-898.

Voight, B. 1973. Correlation between Atterberg plasticity limits and residual shear strength of natural soils. Geotechnique 23, 265-267.

Wallace, J. 1987. Reasons for judgement of the honourable Mr. Justice Wallace, in the Supreme Court of British Columbia. Canadian Pacific Limited vs. Highland Valley Cattle Co. Ltd. Vancouver regestry No. C841694.

Wang, J.S.Y., Bovardsson, G.S. 2003. Evolution of the unsaturated zone testing at Yucca Mountain. Journal of Contaminant Hydrology 63, 337-360.

Water Survey of Canada. 2007. Real-time Hydrometric Data for Thompson River near Spences Bridge (08LF051). [Online]. Available: http://scitech.pyr.ec.gc.ca/waterweb/fullgraph.asp, November 7, 2007.

Appendix A: Summary of geotechnical analysis of Ashcroft silt and clay.

Sample	Field Description	Liquid Limit %	Plastic Limit %	Plasticity Index %	Clay Fraction %	Ring Shear Cohesion kN/m^2	Ring Shear Residual Strength ^{o}
Goddard Slide							
17AU-1A	Clay varve	84	24	60	34	-	-
17AU-1B	Clay varve	72	34	38	75	-	-
17AU-1D	Clay rich slickenside	76	32	44	59	-	-
17AU-1E	Clay rich slickenside	53	24	29	41	-	-
17AU-1F	Clay rich slickenside	81	33	48	34	0	33
17AU-1F	Clay rich slickenside	42	22	20	17	-	-
17AU-1G	Silt block	40	33	7	20	-	-
17AU-1H	Silt block	37	20	17	21	-	-
17AU-1I	Silt block	41	21	20	-	-	-
17AU-1L	Silt block	76	31	45	46	-	-
17AU-1L	Silt block	47	22	25	24	10	26
17AU-1M	Clay from shear zone	79	36	43	33	-	-
17AU-1N	Clay block from shear zone	58	25	33	31	-	-
17AU-1O	Clay	56	24	32	47	-	-
17AU-1O	Clay (for x-ray analysis)	66	28	38	-	3	15
North Slide							
17AU-2A	Clay	85	21	64	43	-	-
17AU-2B	Silt	38	26	12	17	-	-
17AU-2C	Silt	40	33	7	8	-	-
17AU-2D	Clay	80	37	43	45	-	-
South Slide							
17AU-3A	Clay	78	35	43	30	-	-
17AU-3B	Silt	37	24	13	11	-	-
17AU-3C	Silt	38	25	13	10	-	-
Ashcroft (CN 53.4) Slide							
18AU-1A	Silt block	39	23	16	27	-	-
18AU-1B	Silt block	36	24	12	20	-	-
18AU-1C	Silt block	34	25	9	13	-	-
18AU-1D	Silt block	41	24	17	20	-	-
18AU-1E	Clay	53	24	29	61	-	-
18AU-1F	Silt block	38	24	14	-	0	29
Mile 54 Slide							
18AU-2B	Clay	85	39	46	-	0	10
18AU-3B	Silt block	35	22	13	12	0	32
18AU-3E	Clay	63	35	28	-	0	11
1905 Spences Bridge Slide							
18AU-4A	Clay block (with silt?)	49	23	26	-	15	24
18AU-4C	Clay block (with silt?)	45	22	23	-	0	25

Sample	Grain Diameter (mm)	% Passing
17AU-1A	0.0704	100
	0.0497	99
	0.0352	99
	0.0249	99
	0.0176	99
	0.0128	97
	0.0092	95
	0.0065	92
	0.0046	92
	0.0014	5.3
17AU-1B	0.0679	100
	0.0480	100
	0.0339	100
	0.0240	100
	0.0170	99
	0.0125	99
	0.0090	98
	0.0063	94
	0.0045	90
	0.0013	66
17AU-1D	0.0704	100
	0.0497	100
	0.0352	100
	0.0249	100
	0.0176	100
	0.0128	96
	0.0092	94
	0.0065	92
	0.0046	87
	0.0013	42.3
17AU-1E	0.0695	100
	0.0492	100
	0.0348	99
	0.0246	97
	0.0176	92
	0.0128	87
	0.0091	79.1
	0.0065	71.1
	0.0046	61.1
	0.0013	32.2

Sample	Grain Diameter (mm)	% Passing
17AU-1F	0.0704	100
	0.0497	100
	0.0352	99
	0.0249	97.1
	0.0178	94.1
	0.013	93.1
	0.0092	90.1
	0.0065	86.1
	0.0046	83.2
	0.0014	9.7
17AU-1G	0.0679	100
	0.0480	97
	0.0343	96
	0.0243	89
	0.0172	80
	0.0127	70
	0.009	59
	0.0064	48
	0.0045	36
	0.0014	14
17AU-1H	0.0704	99.9
	0.0497	97.9
	0.0352	94.9
	0.0249	88.9
	0.0176	79.9
	0.0128	70.9
	0.0092	60
	0.0065	46
	0.0046	38
	0.0014	14
17AU-1M	0.0695	100
	0.0492	100
	0.0348	99
	0.0246	98
	0.0174	96
	0.0128	96
	0.0091	96
	0.0064	92
	0.0046	86
	0.0014	7.2

Sample	Grain Diameter (mm)	% Passing
17AU-1N	0.0687	100
	0.0486	100
	0.0343	100
	0.0243	97
	0.0172	95.1
	0.0125	90.1
	0.009	81.1
	0.0063	73.1
	0.0045	65.1
	0.0014	15.3
17AU-10	0.0704	100
	0.0497	100
	0.0352	100
	0.0249	99
	0.0176	96
	0.0128	93
	0.0092	88
	0.0065	78.1
	0.0046	70.1
	0.0013	32.1
17AU-2A	0.0695	100
	0.0492	100
	0.0348	100
	0.0246	100
	0.0174	100
	0.0128	100
	0.0091	100
	0.0064	99
	0.0046	96
	0.0014	16
17AU-2B	0.0679	100
	0.048	100
	0.0339	98
	0.024	96.1
	0.0172	92.1
	0.0125	83.1
	0.0089	70.1
	0.0063	54.2
	0.0045	38.3
	0.0014	8.4

Sample	Grain Diameter (mm)	% Passing
17AU-2C	0.0695	100
	0.0492	98
	0.0348	95.1
	0.0246	88.1
	0.0174	80.1
	0.0128	66.2
	0.0091	49.3
	0.0064	34.3
	0.0048	20.4
	0.0014	3.5
17AU-2D	0.0695	99.9
	0.0492	99.9
	0.0348	99.9
	0.0246	99.9
	0.0174	99.9
	0.0128	97.9
	0.0092	97.9
	0.0065	96.9
	0.0046	92.9
	0.0014	21
17AU-3A	0.0704	100
	0.0497	100
	0.0352	100
	0.0249	100
	0.0176	100
	0.0128	98
	0.0091	97
	0.0064	94
	0.0046	90
	0.0015	5
17AU-3B	0.0695	100
	0.0492	97
	0.0348	94.1
	0.0246	86.1
	0.0174	77.1
	0.0128	64.1
	0.0091	50.2
	0.0064	36.2
	0.0047	24.2
	0.0014	7.3

Sample	Grain Diameter (mm)	% Passing
17AU-3C	0.0695	100
	0.0492	99
	0.0348	98
	0.0246	96.1
	0.0174	90.1
	0.0128	80.1
	0.0091	67.1
	0.0064	48.2
	0.0046	30.2
	0.0014	3.3
17AU-K	0.0695	100
	0.0492	99
	0.0348	98
	0.0246	96.1
	0.0174	93.1
	0.0128	89.1
	0.0091	86.1
	0.0064	81.1
	0.0045	77.1
	0.0014	28.2
18AU-1A	0.0679	100
	0.048	99
	0.0339	98
	0.024	95
	0.017	89
	0.0125	82
	0.009	70.1
	0.0063	58.1
	0.0045	46.1
	0.0014	19.2
18AU-1B	0.0687	100
	0.0486	100
	0.0343	96
	0.0243	87
	0.0172	75
	0.0127	64.1
	0.009	52.1
	0.0064	42.1
	0.0045	32.1
	0.0014	14.2

Sample	Grain Diameter (mm)	% Passing
18AU-1C	0.0687	100
	0.0486	98
	0.0343	95
	0.0243	88
	0.0172	78
	0.0125	66.1
	0.009	47.1
	0.0064	29.1
	0.0046	24.1
	0.0014	7.2
18AU-1D	0.0679	100
	0.048	100
	0.0339	98
	0.024	95
	0.0172	90
	0.0125	83
	0.0086	68
	0.0063	52
	0.0045	37
	0.0014	12
18AU-1E	0.0695	100
	0.0492	100
	0.0348	100
	0.0246	100
	0.0174	100
	0.0127	98
	0.0091	96
	0.0064	93.1
	0.0046	91.1
	0.0013	42.1
18AU-2A	0.0679	100
	0.048	98
	0.0339	96
	0.024	91
	0.0172	83
	0.0125	74
	0.0089	63
	0.0063	52.1
	0.0045	42.1
	0.0014	19.2

Sample	Grain Diameter (mm)	% Passing
18AU-3A	0.0679	99.2
	0.048	96.2
	0.0339	88.2
	0.024	78.2
	0.0172	66.2
	0.0127	51.2
	0.009	36.2
	0.0065	26.2
	0.0047	20.2
	0.0014	11.2
18AU-4B	0.0687	94.8
	0.0486	89.9
	0.0343	85.8
	0.0243	80.8
	0.0174	75.8
	0.0128	71.8
	0.0091	65.9
	0.0064	58.9
	0.0046	51.9
	0.0013	28.9

Appendix B: Pressures calculated based on drill records of water supply wells near Ashcroft

Well tag No.	Well depth (m)	Static water depth (m)	Pressure head (m)	Bedrock depth (m)
38084	21.9	6.1	15.8	18.6
38085	13.7	1.5	12.2	11.0
41450	18.3	10.1	8.2	-
38354	31.1	22.6	8.5	-
24231	53.3	29.0	24.4	-
41958	70.1	30.5	39.6	-
51640	129.5	45.7	83.8	-
27220	64.0	32.6	31.4	-
38586	74.4	50.3	24.1	-
45135	111.9	36.6	75.3	-
16985	37.5	15.5	21.9	-
30273	38.1	4.9	33.2	36.6
29249	60.4	21.9	38.4	60.4
34441	36.0	6.4	29.6	34.7
45140	26.2	9.8	16.5	24.4
27457	52.4	33.5	18.9	-
56099	31.4	17.7	13.7	-
49712	15.8	4.3	11.6	-
43591	59.9	8.8	51.1	-
42013	31.1	14.3	16.8	-
26723	52.7	3.0	49.7	25.0
35476	22.6	3.7	18.9	-
38120	35.4	6.4	29.0	12.8
53555	129.5	4.0	125.6	9.8
76511	152.4	7.3	145.1	9.1

Appendix C: formulation of HydroGeoSphere

The model is governed by Richards' equation, using a control volume finite element method in the variably saturated subsurface domain. In HydroGeoSphere, Richards' equation is defined as (Therrien et al., 2005):

$$-\nabla \cdot (q) + \sum \Gamma_{ex} \pm Q = S_W S_S \frac{\partial \psi}{\partial t} + \frac{\partial (\phi S_w)}{\partial t} \qquad (C-1)$$

where $\nabla = (\partial / \partial x, \partial / \partial z)$, Γ_{ex} is the volumetric fluid exchange rate between the subsurface and all other domains [$L^3/L^3/T$]. For the Thompson River Valley model, a single porous medium was used with fractured bedrock defined discretely. In this case the surface represents the other domain. Q represents the fluid exchange with external sources to the model domain, such as wells. No external water sources were used in the Thompson River Valley simulation. Positive values of Γ_{ex} and Q are used to represent flow into the subsurface domain. S_W is the water saturation [-], S_S is the specific storage [L^{-1}], ψ is the pressure head [L], ϕ is the porosity [-], and q is the Darcy flux [L/T] given by:

$$q = -K \cdot k_{rw} \nabla(\psi + z) \qquad (C-2)$$

where k_{rw} is the relative permeability of the medium, which is dependent upon the degree of water saturation (S_w). The pressure and elevation heads are represented by ψ and z, respectively. K represents the hydraulic conductivity tensor, defined as (Therrien et al., 2005):

$$K = \frac{\rho g}{\mu} k \qquad (C-3)$$

where ρ is the density of water [M/L^3], g is the acceleration due to gravity[L/T^2], and μ is the viscosity of water [M/L/T], and k is the permeability tensor of the medium [L^2].

Unsaturated flow is controlled within the model using the following pressure-saturation relationship developed by Van Genuchten (1980):

$$S_w = S_{wr} + (1 - S_{wr})[1 + |\alpha\psi|^{\beta}]^{-\nu} \qquad \psi < 0 \qquad (C-4)$$

$$S_w = 1 \qquad \psi \geq 0$$

with the relative permeability given as:

$$k_r = S_e^{l_p}\left[1 - \left[1 - S_e^{1/\nu}\right]^{\nu}\right]^2 \qquad (C-5)$$

and

$$\left(\nu = 1 - \frac{1}{\beta}\right) \qquad \beta > 1 \qquad (C-6)$$

where S_{wr} is the residual water saturation, S_e = (S_w-S_{wr})/(1-S_{wr}), l_p is the pore connectivity parameter (equal to 0.5 for most soils), and α and β empirical values that fit data.

Two-dimensional overland flow along surface boundary nodes of the model is solved fully implicitly by the two-dimensional depth-averaged diffusion-wave approximation to the Saint Venant equation (Therrien et al., 2005). The equation is:

$$-\nabla \cdot (d_s q_s) - d_s \Gamma_s \pm Q_S{}^W = \frac{\partial(\phi_S h_S)}{\partial t} \qquad (C-7)$$

where d_s is the depth of surface water flow [L], h_s (=z_s + d_s) is the water surface elevation [L] and z_s is the stream bed elevation [L], Γ_s is the volumetric fluid exchange rate between the surface and all other domains within the model [$L^3/L^3/T$], ϕ_s is the surface water domain porosity [-], Q_S^W is the surface water withdraw shown in equation C-1, the right hand side of equation C-7 is equivalent of ΔS_s in equation C-1, and q_s is the flux of water given as:

$$q_s = K_s \cdot k_{rs} \nabla (d_s + z_s) \qquad (C-8)$$

where k_{rs} is the relative permeability of the surface water domain, and K_s is the conductivity which is derived using Manning's Formula:

$$K_{s_{xx}} = \frac{d_s^{2/3}}{n_{xx}} \frac{1}{(\partial h_s / \partial s)^{1/2}} \qquad K_{s_{yy}} = \frac{d_s^{2/3}}{n_{yy}} \frac{1}{(\partial h_s / \partial s)^{1/2}}$$

$$K_{s_{xy}} = K_{s_{yx}} = 0 \qquad (C-10)$$

where s is the length along the direction of maximum slope [L] and n_{xx} and n_{yy} are Manning's coefficients [$T/L^{1/3}$].

In some cases critical depth boundaries are used to represent the Thompson River along the edge of the cross-section. The advantage of this boundary condition is that it neither constrains the flow rate nor the surface water depth along the perimeter of the domain (Li et al., 2008). The boundary condition can be written as follows:

$$Q_S^W = \sqrt{g d_s^3} \qquad (C-11)$$

Hydrogeosphere has been used to support many water resource and engineering projects, however, this is the first known instance where HydroGeoSphere has been applied to a slope stability problem (e.g., Panday and Huyakorn, 2004, Sudicky et al., 2005; Li et al., 2008). For a detailed discussion of the formulation and verification of HydroGeoSphere the reader is referred to Therrien et al. (2005).